Robust Controller Design for Air Injection in the Intake Manifold of a Marine Diesel Engine

Efstathios Karlis

Diploma Thesis

School of Naval Architecture and Marine Engineering
National Technical University of Athens

Thesis Supervisor: Dr. G. Papalambrou, Lecturer
Committee Member: Professor N. Kyrtatos
Committee Member: Professor C. Frangopoulos

December 2014

Acknowledgements

This work has been carried out at the Laboratory of Marine Engineering (LME) at the School of Naval Architecture and Marine Engineering of the National Technical University of Athens, under the supervision of Dr. George Papalambrou, Lecturer in Control systems.
I would like to thank Professor Nikolaos Kyrtatos for providing the opportunity to work with the full-scale marine propulsion engine of LME, in order to evaluate experimentally the designed control system. I would also like to thank him for allowing to use the control systems room in LME and to practice on control theory on the inverted pendulum of the laboratory.
I owe my greatest appreciation to my supervisor Dr. George Papalambrou for giving me the chance to work on this thesis. Additionally, I thank him for his guidance, his willingness to provide help for any issue, his encouraging comments and his constant support.
I would also like to thank Professor Christos Frangopoulos for being a member of my supervisors committee.
I am deeply grateful to Nikolaos Vrettakos, PhD student at the LME for his helpful comments on the thesis, for handling the experimental facility of the MAN B&W marine diesel engine and his help in order to carry out the control trials.
I am also grateful to my family for their constant encouragement throughout my thesis.

Abstract

In this work the control of the intake manifold pressure of a marine CI engine is investigated. A non linear model of the diesel engine is developed and further linearization providing a frequency representation. An H_∞ robust controller is designed using the mixed sensitivity control approach. The controller is tested on a 5 cylinder marine diesel engine at LME/NTUA to validate the functionality of the controller and the results of the simulation.

Initially, the model developed was so as to simulate discrete events during an operating engine's cycle. The purpose of this model is to simulate the effect of injecting compressed air downstream of the compressor to engine parameters like cylinder pressure, temperature and their derivatives, such as the indicated effective pressure, the brake effective pressure, the amount of air induced in the cylinders, the flow of gas after the end of the combustion towards the turbine, and an approximation of the heat absorbed by the working fluid, due to combustion.

Furthermore, the implementation of engine modeling equations is described. In particular, the discrete, crank angle based events during the combustion were implemented. The modeling elements were the analogue valve for air injection, the cylinder volume, the pressure, the temperature, the intake of air, the air to fuel ratio, the net heat release, the torque, the power produced and the specific fuel consumption. For the control purposes a linear model was derived with numerical methods from the non-linear model. The linear model has the form of transfer function with the output being the intake pressure and the input being the valve position. With the linear model available, the robust controller was designed. Details from the selection of the controller parameters and their evaluation are presented. The controller was tested in simulation with both the linear and the non-linear models.

Finally, the results from the air injection experiments carried out at LME using the robust controller are presented investigating the performance of the controller. The controller functioned effectively in the nominal operating point of the engine and proved its robustness in operating points different than the nominal.

Contents

Nomenclature

ΔT_{comb} The ideal instant temperature increase at the crank angle where the combustion commences

η Index of efficiency

$\frac{dQ_{hr}}{d\theta}$ The total amount of transferred through the walls of the cylinder

$\frac{dQ_{hr}}{d\theta}$ The whole amount of heat released by the combustion of the fuel

$\frac{dQ}{d\theta}$ The change of heat offered to the system working

$\frac{dU}{d\theta}$ The change of the internal energy of the working

$\frac{dW}{d\theta}$ The change of work produced by the working fluid

λ The equivalence ratio

$\overline{PR}$ The normalized motored and loaded cycles pressure ratio

ψ The flow function

$\Sigma \frac{dH_{oi}}{d\theta}$ The sum of the heat transferred between the system and its environment

θ The crank angle

A/F Air to fuel ratio

$BMEP$ The break mean effective pressure

c_v Thermal capacity

d The disturbance signal

d When used as a subscript it indicates the trace's value downstream the reference system

e The actual error

e_m The measured error

EOC The crank angle where the combustion ends

EVO The crank angle where the exhaust valve opens

f When used as a subscript it is referring to the fuel injected

$FMEP$ The friction mean effective pressure

H_∞ Robust controller, using infinity norm

$IMEP$ The indicated mean effective pressure

IVC The crank angle where the intake valve closes

k_c The polytropic coefficient during the expansion

k_e The polytropic coefficient during the compression

KS control sensitivity function

L The open loop transfer function

m Mass flow

n The noise signal

n_c The number of revolutions per cycle

N_{eng} The rotational speed of the engine

P The generalized plant transfer function or the Mechanical Power

p_{cyl} In cylinder pressure

p_c The pressure during the compression

p_e The pressure during the expansion

PR The motored and loaded cycles pressure ratio

q_{HV} The heating value of the fuel

r The reference signal

S The sensitivity transfer function

s The position of the piston

SOC The crank angle where the combustion occurs

T The complementary sensitivity function or the engine's Torque

T_{cyl} In cylinder temperature

T_c The temperature during the compression

T_e The temperature during the expansion

u The control input

up When used as a subscript it indicates the trace's value upstream the reference system

v The sensed inputs

V_{cyl}	The in cylinder volume
w	The exogenous inputs
W_P	The performance weighting function
W_T	The closed loop weighting function
W_U	The control input weighting function
y	The actual output
y_m	The measured output
z	The exogenous outputs

Chapter 1

Introduction

1.1 Problem Description

The main purpose of this diploma thesis is the development of a robust controller, for the control of an air injection valve. A series of tests carried out in the experimental engine at the Laboratory of Marine Engineering in NTUA proved the validity of the modeling and the control approach. The objective is to augment the pressure in the intake manifold of the engine, thus inducing additional air in the engine cylinders, and eventually reaching a higher maximum in cylinder pressure per cycle.
The increase of the intake manifold pressure is regulated by the compressor. The main issue of concern is the stall phenomenon which appears when the pressure downstream of the compressor is greater than the pressure in the compressor outlet, causing instabilities in the flow direction. During experiments the stall phenomenon was investigated. As for the control method, the H_∞ robust method was adopted and investigated with direct application. In a broad sense this type of control allows to shape the transfer functions that affect behavior during disturbance rejection and command tracking and considers uncertainties in the plant. In practice, the controller is designed for a particular nominal operating point of the plant and is expected to behave acceptable in a region around the nominal plant.
For familiarization purposes a similar robust control methodology was applied to a laboratory device. Hence, an H_∞ controller was designed for the control of the inverted pendulum of LME. The control object was to maintain the rod of the pendulum in vertical position, rejecting possible external disturbances. It is an unstable system and although it posed limitations to the controller design, the proposed control method proved successful.
The mathematical representation of the specific path from the air injection valve to the intake manifold was derived in this thesis. The model calculated crank angle dependable traces such as the in cylinder pressure, the temperature and the net heat released by the combustion. The model, based on the in cylinder pressure, calculated the mean torque of each cylinder per cycle, acting upon the crank shaft of the engine. Finally, the valve injecting externally pressurized air was added. A mathematical representation in the form of a transfer function with input the displacement of the valve as a percentage of the maximum stroke and output the intake manifold pressure was acquired. Using this linear system, a robust controller was designed and tested in the Simulink non linear engine model. Finally, the controller was evaluated experimentally.

To sum up the objectives of this thesis are:

- To investigate the effect of the air injection on engine parameters like the pressure in the intake manifold, the in-cylinder pressure the fuel consumption and on the turbocharger, through simulations.
- To design a robust controller, for the control of the air injection system at the experimental engine MAN B&W L16/24 in the Laboratory.
- To validate the results from simulation through experiments in a region around the nominal operating point of the engine.

1.2 Literature Search

Papalambrou in his doctoral thesis [1] used a solenoid valve, in the same experimental facilities of LME, in order to decrease the exhaust opacity during transient.
As far as the modeling of the physical system of the engine is concerned, the work of Kyrtatos [7] and Rakopoulos [8] gave advice on various issues of internal combustion engines. The work of Guzzella [9] proved to be useful in simplifying the physical equations that describe the physical phenomenon that take place during an internal combustion engine's cycle, for the creation of a single zone physical thermodynamic models suitable for a control system design. According to the work of Guzzella, of Eriksson [10] and the work of Klein [11], the single zone cylinder pressure per crank angle model was developed.
For the mean value modelling of the airpath of turbocharged Diesel Engines Jung has published [12], while studies on modeling of the surge phenomenon and compressor instability have been published by Gravdahl and Egeland [13].
A general introduction to control issues along with specific knowledge on Robust Control and insight in linear system theory was acquired by the work of Skogestad and Postlethwaite [4] and the work of Zhou and Doyle [5]. Additional insight to robust control and especially on controller development using the Matlab environment was given by the work of Gu et al. in [6].

1.3 The Experimental Plant

The plant under examination is MAN B & W L16/24 turbocharged 5 cylinder engine, installed in the Laboratory and it is depicted in figure 1.1. It is a small size power plant, which is usually used as a gen-set in the maritime industry. The basic characteristics of the engine are presented in Table 1.1.

The controlled air injection system (900)[1] consists of an analogue valve controlled by a linear actuator, which transforms the electric control signal to a displacement of the inner-valve needle, which in turn reveals a section of the orifice of the valve, through which additional air in the engine is induced. The flow through the orifice

[1] In figure 1.2 the measuring instruments are identified. The letters define the type of the instrument, while the first digit of each number defines the part of the engine, where the instrument is installed. The following two digits define the different measuring instruments. For example PE303 is a Pressure Element, installed in the Engine Intake (300) and it is the third Pressure Element installed in this part of the engine (-03) .

Figure 1.1: The MAN B&W L16/24 experimental engine.

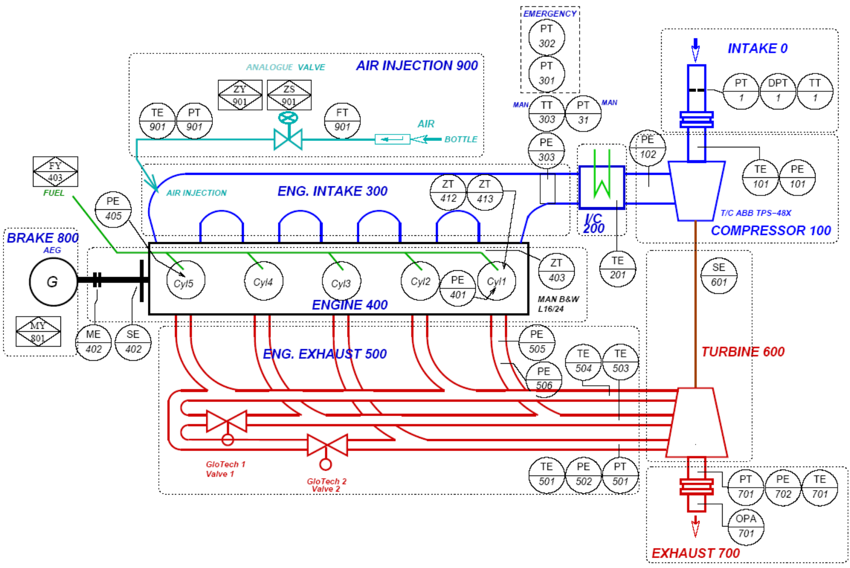

Figure 1.2: A general Scheme of the Experimental Plant.

is a function of the difference in the pressure downstream and upstream of the valve. The pressure considered upstream the valve is approximately 6 bar. The downstream pressure is approximately the one in the intake manifold (300). The flow through

Rotational Speed	RPM	1200
Power	kW	500
No. of cylinders	-	5
Bore	m	0.160
Crank Radius	m	0.240
Rod Length	m	0.474
Compression Ratio	-	15.5:1

Table 1.1: Basic Characteristics of MAN L16/24.

the valve and through the compressor are considered adiabatically and homogeneously mixed, neglecting the mixing transient length.
The control process in this thesis depends mainly on the pressure measurements in the intake manifold (PE 303), which is used to close the control loop and secondly on the pressure trace of the compressor outlet (PE 102), so as a measure of the proximity to the surge margin line to be derived. Finally, the in cylinder pressure traces of cylinders 1 and 5 (PE 401, PE 405) are acquired.

1.4 The Air Injection Valve

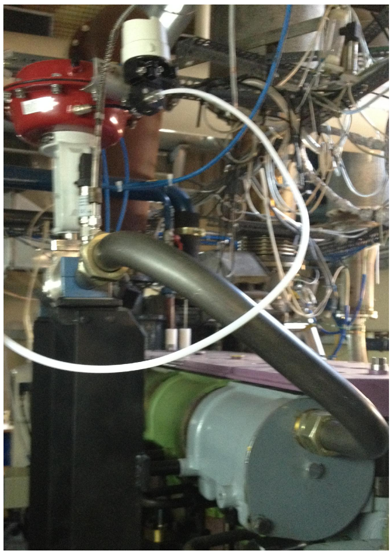

Figure 1.3: The analogue valve and the intake manifold of the experimental plant.

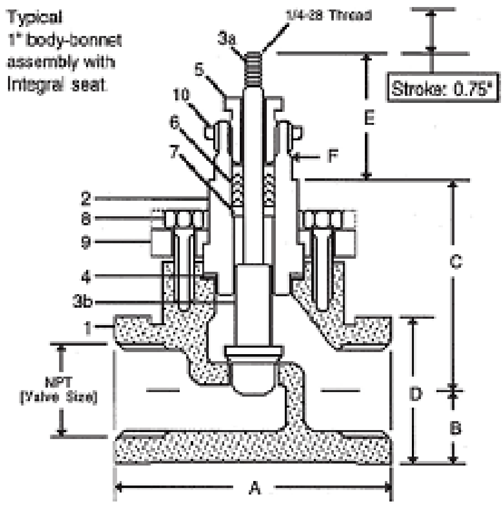

Figure 1.4: Section of the valve.

The air injection valve is RCV Model 9000, for pipe size of 5.1 cm. The actuator is linear, equipped with 6 springs in order to be able to sustain big pressure differences upstream and downstream. The maximum operational pressure difference is 10.3 bar. The orifice diameter is 3.8 cm, while the maximum stroke of the innervalve is 1.9 cm. The analogue valve and its actuator are depicted in figure 1.3. A cross section of the valve is depicted in figure 1.4 and a typical cross section of the actuator is depicted in figure 1.5. The actuator functions by increasing the pressure underneath a membrane.

Item	Description
1	Body
2	Bonnet
3a	Stemm, Innervalve
3b	Innervalve and Guide
4	Gasket
5	Packing Gland
6	Packing kit
7	Packing adapter
8	Hex screws
9	Bonnet flange
10	Yoke locknut

Table 1.2: Definition of the various parts in figure 1.4

Dimension	Value [mm]
A	124
B	44.5
C	91.2
D	92.1
E	42.7
F	28.6

Table 1.3: Dimensions of the valve in figure 1.4

The pressure times the area of the membrane produces a force that moves the membrane upwards, thus moving the innervalve. The springs produce a negative force that help the membrane maintain a steady position. The characteristics of the various parts of the valve are described in table 1.2 and the dimensions of the valve in table 1.3.

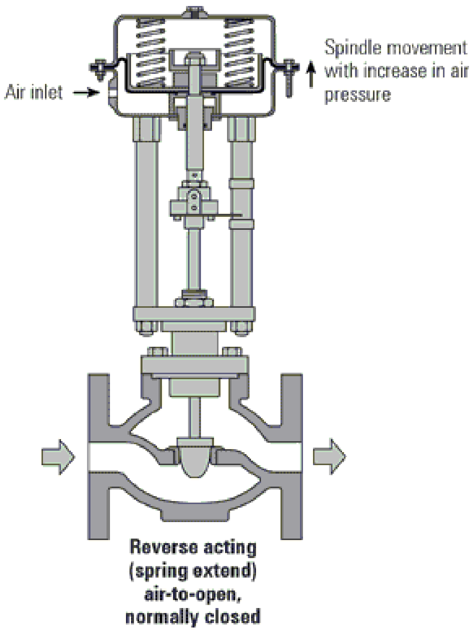

Figure 1.5: A typical cross section of an air-to-open actuator [33].

Chapter 2

Robust Control Theory

In this chapter the theory concerning the design of robust controllers is presented. Before referring directly to the robust control theory, basic concepts of control theory, such as the open and closed loop transfer functions are briefly described. Finally, the process of designing a robust controller, for a laboratory device, the inverted pendulum, is described.

2.1 Principles of Control System Design

In general the term control system design summarizes the process followed be the Control Engineer, in order to manipulate a physical system, in a manner that a predefined system behavior is achieved, without the need of the physical appearance of man during the operation. The process can be summarized in the following points [3], [4].

1. Define the control objective.

2. Obtain a mathematical description of the system and if possible simplify the model.

3. Define the model outputs, whose control will give the model the desired behaviour.

4. Decide upon the sensors and actuators that should be installed in the system. Is it possible to measure the desired output? If no can the output be estimated by other measurements?

5. Decide the type of control that will be implemented.

6. Based on the advantages of the type of control selected, the limitations imposed by the system, and the overall requirements, decide on performance specifications.

7. Design the controller.

8. Analyze the behavior of the system with the controller installed, and decide whether the result is satisfying. If not consider changes on the performance requirements, or the control method itself.

9. Implement the controller on the real plant and validate the results.

The above steps were followed and effort was put on dealing with the challenges each step posed. One of the most intriguing steps was to decide, which output would in a more direct manner be effected. The actual objective was to examine the effect of external air injection in cylinder pressure, but a direct mathematical representation of a connection between the two could not be derived, because cylinder pressure can be affected by many parameters, other than air injection. That led to the conclusion that the most directly related trace with air injection and cylinder pressure, should be the one to control. Therefore, the intake manifold pressure appeared a potential choice because the relevant mathematical model derived was simple enough, posed a few but manageable limitations, and was easy to measure.
The nature of the control objective not only defined the measured output, but it also defined the type of control problem set. Control problems are divided in two categories: regulator and servo problems. While both types refer to defining the output y by manipulating a control input u to the plant, the philosophy between them is different. In the former the controller is required to reject the effect of disturbances in the plant, while in the latter the controller is required to keep track of a given reference r. The problem examined in this thesis belongs to the servo-type of problems category, as it is required to track the reference value of the intake pressure. It is important for the measured trace to reach the desired value, without a great overshoot, allowing the plant to pass through successive states of stability.

2.2 Transfer Functions

Throughout this thesis physical systems are represented mathematically using transfer functions. The systems are considered linear, time invariant which are governed by differential equations with constant coefficients. For example consider the following set of differential equations:

$$\dot{x_1}\ (t) = a_1 x_1\ (t) + a_2 x_2\ (t) + b_1 u\ (t) \tag{2.1}$$

$$\dot{x_2}\ (t) = a_0 x_1\ (t) + b_0 u\ (t) \tag{2.2}$$

$$y\ (t) = x\ (t) \tag{2.3}$$

Here u represents the control input, x_1, x_2 represent the states and y represents the measured output. The coefficients $a_0,\ a_1,\ a_2,\ b_0,\ b_1$ are constants that are time invariant. Applying Laplace transformation to the set of equations, the following set of equations is obtained.

$$sX_1\ (s) - x_1\ (t=0) = a_1 X_1\ (s) + X_2\ (s) + b_1 U\ (s) \tag{2.4}$$

$$sX_2\ (s) - x_2\ (t=0) = a_0 X_1\ (s) + b_0 U\ (s) \tag{2.5}$$

$$Y\ (s) = X_1\ (s) \tag{2.6}$$

Y(s) denotes the Laplace transformation. Without loss of generality it is assumed $x_1(t=0)=0$ and $x_2(t=0)=0$. This yields the transfer function

$$\frac{y(s)}{u(s)} = \frac{b_1 s + b_0}{s^2 + a_1 s + a_0} \tag{2.7}$$

In general, transfer functions of the following form are used.

$$G(s) = \frac{b_m s^m + \cdots + b_1 s + b_0}{s^n + a_{n-1} s^{n-1} + \cdots + a_1 s + a0} \tag{2.8}$$

Each constant $b_i,\ a_j$ can be derived by the Laplace transformation of first principle models, or by using available measured data. In the latter case, the equation of the model is derived only for a specific point of operation and does not characterise the system thoroughly.
Transfer function representation of systems is central in control since:

- One can examine a system in the frequency domain by replacing s with $j\omega$.
- Control issues like bandwidth and peaks of magnitude of transfer functions can be examined.
- A convolution of two systems in the time domain is quite complex, however in the frequency domain the equivalent is a multiplication of the transfer functions of the systems.
- Limitations posed in control by the systems themselves can be directly detected by examining the poles and the zeros of the transfer functions.
- Representing two functions in a common frequency plot can give accurate estimations of the similarity or not of their behavior caused by the same input.

When the relations between the states of the system should be obvious in the system equations, one may choose the equivalent state-space representation in equation 2.9 and 2.10.

$$\dot{x} = Ax + Bu \tag{2.9}$$

$$y = Cx + Du \tag{2.10}$$

One can derive the transfer function from the state-space representation as follows.

$$G(s) = C(sI - A)^{-1}B + D \tag{2.11}$$

2.3 Feedback Control

In this thesis a one degree of freedom (1 DOF) feedback controller has been designed. By the term 1 DOF [1] controllers act upon a single signal the actual error e. The term feedback refers to the closing of the measurement loop, thus providing the actual value of plant in the controller. Hence, the output of the system is measured and is then compared with the reference signal, in order to produce an error signal that defines how close the system is to its reference value and based upon this, whether the controller should act upon the plant through the control signal. A classical representation of a one degree of freedom problem is presented in figure 2.1.

The controller K has as an input the signal $r - y_m$, where $y_m = y + n$ is the sensed output, which includes the noise from the measurement devices and r is the reference setpoint. The disturbances are symbolized as d and G_d is the transfer function that defines how each disturbance affects the system. The error that the controller realizes is 2.12

$$e_m = r - y_m \tag{2.12}$$

[1] In a two degree of freedom controller, the reference signal is passed through a transfer function as well.

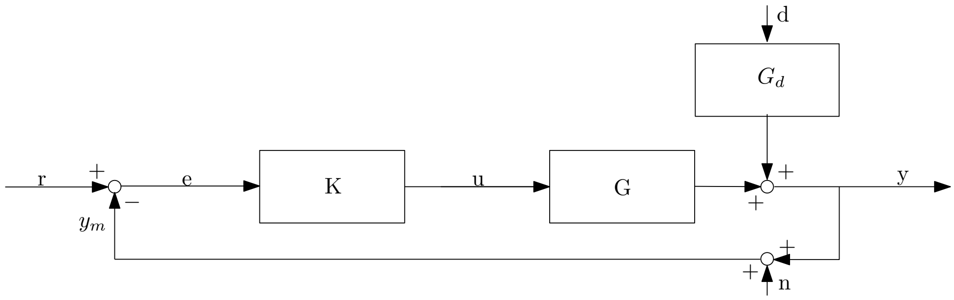

Figure 2.1: Block diagram of a one degree of freedom controller.

and the control input into the plant is 2.13

$$u = K(s)(r - y_m) = K(s)(r - y - n) \tag{2.13}$$

However the actual error and the one that is going to be used is defined as 2.14

$$e = r - y \tag{2.14}$$

So the model of the plant can be written as 2.15

$$y = G(s)u + G_d(s)d \tag{2.15}$$

and subtituting 2.13 to 2.15, 2.16 is delivered.

$$y = GK(r - y - n) + G_d d \tag{2.16}$$

or

$$(I + GK)y = GKr + G_d d - GKn \tag{2.17}$$

The closed loop response is then

$$y = \underbrace{(I + GK)^{-1}GK}_{\mathrm{T}}\, r + \underbrace{(I + GK)^{-1}}_{\mathrm{S}}\, G_d d - \underbrace{(I + GK)^{-1}GK}_{\mathrm{T}}\, n \tag{2.18}$$

We can now rewrite 2.13 and 2.14 as follows.

$$e = y - r = -Sr + SG_d d - Tn \tag{2.19}$$

and

$$u = KSr - KSG_d d - KSn \tag{2.20}$$

One should point out that *S+T=I*. The above defined transfer functions *S, T*, along with L play an important role in control theory. The following terminology is standard.

$$L = GK \quad loop\ transfer\ function \tag{2.21}$$

$$S = (I + GK)^{-1} = (1 + L)^{-1} \quad sensitivity\ function \tag{2.22}$$

$$T = (I + GK)^{-1}GK = (1 + L)^{-1}L \quad complementary\ sensitivity\ function \tag{2.23}$$

It should be noted in 2.18 that T is the transfer function relating directly the reference signal to the actual output of the system, while in 2.19 S is the transfer function relating the error signal of the controlled system to the reference. The term sensitivity derives from the fact that the magnitude of S is the one that decreases the sensitivity of the plant in disturbances of the system, as one can conclude from 2.19. L is the transfer function of the open loop system, without feedback signal and a unique input to the controller, that being the reference r.
The question that arises however is why it is advantageous to close the loop. The answer lies to the observation of the function S. By manipulating K, high gains can be implemented over certain areas of frequencies, usually the low frequency areas where errors are greater. If the gain of K is high enough then GK can force $S \approx 0$, $T \approx 1$, thus giving $y \approx r - n$ and lessening the impact of disturbances and noise measurements. So the philosophy of feedback control, which is easily implemented as will be proved later on with H_∞ controllers, is to create high feedback gains at low frequencies, while decreasing the feedback gains at higher frequencies close to the eigenfrequencies of the system where instabilities are bound to occur. The frequency that is of high importance to the behaviour of the system is the bandwidth frequency, where the magnitude of L drops below 1. Then $|S| \approx 0.5$ and $|T| \approx 0.5$ and from 2.18 it is derived that both noise signals and disturbances have high effect on the actual output.

2.3.1 Closed Loop Stability

Previously, the importance of using feedback control was stated in inducing stability in the controlled system. In general, a system can be described as being stable if and only if the input of any bounded signal or signals anywhere in the system, produces a bounded output as well. Stability should not be examined externally from one input to another, but successively within the series of signals produced. To decide whether a closed loop system is stable or not the following methods are used:

1. By defining the poles of a closed loop system, in other words by defining the roots of $1 + L(s) = 0$, which are the poles of T and S. The poles can be real or complex. The stability criterion is related with the position of poles in the plane. If there exists at least one pole that lays on the Right Half Plane (RHP), including the imaginary axis, then the closed loop response is considered unstable. The poles can also be defined by the eigenvalues of the state space matrix A of the closed loop system.

2. By plotting the Bode plot of a system, one can use the equivalent with the previous stability condition, the Bode's stability condition, which states that T is stable if and only if
$$|L| < 1$$
at the frequency where $\angle \mathrm{L}(j\omega)$ crosses -180^o for the first time.

2.3.2 Closed Loop Performance Method

While feedback control is considered a way of stabilizing an otherwise unstable system, there is always the danger of causing instabilities, mainly in high frequencies by high feedback control gains, if magnitudes of L in high frequencies do not roll-off quickly enough. However by being too conservative in order to avoid instabilities, control might

appear to tolerate higher output errors. This shows that among other objectives, in control design, a trade off should also be considered between performance and closed loop stability.
According to [4] the margin of $|L|$ from -1, mentioned in the previous subsection, is closely related to $|S|$, and since as already stated S is a means of relating the error signal to the reference signal, it is used as an indication of the performance of the system as well. The reason for giving emphasis on the relation between S and performance, is that it leads to searching for boundaries that limit the magnitude of the sensitivity function. Firstly, it is known that real plants are proper, therefore $|L| \to 0$ at high frequencies, so $S \to 0$. Furthermore, at low frequencies the sensitivity function is small, usually close to zero. However, it is not possible to keep the magnitude of the sensitivity function always between 0 and 1, for always in proper systems around the ω_{180} frequency $|L(j\omega_{180})| = 1/GM$, where GM is the gain margin of the system. However ω_{180} usually corresponds to a high frequency where the Bode diagram magnitude of L is negative as mentioned. This implies that $L(j\omega_{180}) = -\frac{1}{GM}$ and therefore $S(j\omega_{180}) = \frac{1}{1-\frac{1}{GM}}$. We see that $S > 1$ and around this frequency there is an amplification of the error signal. This proves that care should be taken so as to secure that $max|S(j\omega)| < Ms$, where M_s is a bounded number to be kept small, in the range of 1.5-2.

2.4 Robust Control

In the previous section the main reason to reach for robust control solutions was summarized in limiting M_s. It also specified that L, T and u must behave in a particular manner as well. The methodology adopted leading to robust control is referred in literature [5], [4], as *Closed Loop Shaping.* This way a thorough and strict definition of L, S, T, KS is achieved, and specific performance requirements are delivered. The shaping of those transfer functions is, defined by the selection and design of *bounds-weights* in the frequency domain. First, the control design problem will be posed so as to include the weighting transfer functions in the problem and then the weights themselves will be introduced in the control problem.
One can generally describe a closed loop feedback system as in figure 2.2.

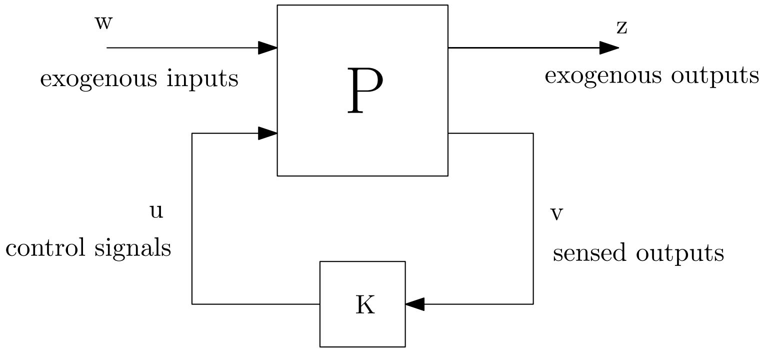

Figure 2.2: General Control Configuration.

The main control objective is to minimize the infinity norm [2] of the transfer function between w and z, by designing a controller capable of eliminating the influence of the exogenous inputs w to the exogenous outputs z, using the sensed outputs contained in v to produce the control signal u. In figure 2.2 P is the generalized plant. It integrates into the system the weighting functions, it has no feedback action, and is an open loop system.
To derive P from figure 2.1 the signals that correspond to *w, z, v and u* are identified:

1. As w we define the signals that are exogenous to the system and alter its behaviour. Those are *d,r,n*
$$w = \begin{bmatrix} w_1 \\ w_2 \\ w_3 \end{bmatrix} = \begin{bmatrix} d \\ r \\ n \end{bmatrix}$$
2. As z we consider the actual error $z{=}e$
3. As v we define the measured error $v = r - y_m$
4. Finally u is always the controller output.

The above considerations are shown in Figure 2.3.

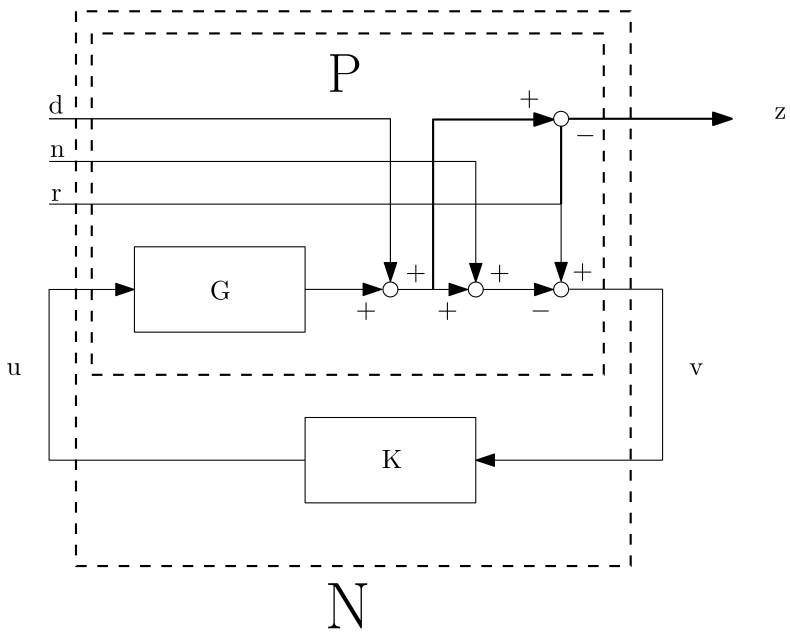

Figure 2.3: Equivalent one degree of freedom control system.

Since we have defined that z contains the real deviation from the reference setpoint, from 2.3 we consider

[2]The infinity norm of a vector x is defined as $\|x\|_\infty = max(|x_i|)$. Hence that is the maximum entries' magnitude of the vector.

$$z = y - r = Gu + d - r = Iw_1 - Iw_2 + 0w_3 + Gu \tag{2.24}$$
$$u = r - y_m = r - Gu - d - n = -Iw1 + Iw2 - Iw3 - Gu \tag{2.25}$$

and P which represents the transfer function between $\begin{bmatrix} w & u \end{bmatrix}^T$ and $\begin{bmatrix} z & v \end{bmatrix}^T$ is

$$P = \begin{bmatrix} I - I & 0 & G \\ -I & I - I - G \end{bmatrix} \tag{2.26}$$

The transfer function between the exogenous inputs and outputs, which includes the feedback subfunctions, is N. The next step is to include the weighting functions, that we want to introduce to the control design problem. We will consider the case that all three functions S, T, KS for the mentioned reasons in the previous sections are to be bounded.
Hence, we are talking about an H_∞ problem, with the objective of minimizing $|N(K)|_\infty$ by bounding the outputs of the system, with weights that are integrated into the system eventually through the stabilizing controller K.
The z vector of the system contains now traces of various points in the system that we want to manipulate. So in this case the bounded outputs are

1. $z_1 = W_u u$ (bounded control command)

2. $z_2 = W_T y$ (bounded closed loop response)

3. $z_3 = W_P(y - r)$ (bounded reference error)

The w vector can contain apart from the reference signal r, possible noise in measurements n, and the expected disturbances d. However, there are cases when one or two of them are not considered. Thus, figure 2.3 can be reconsidered with the inclusion of weights as in figure 2.4

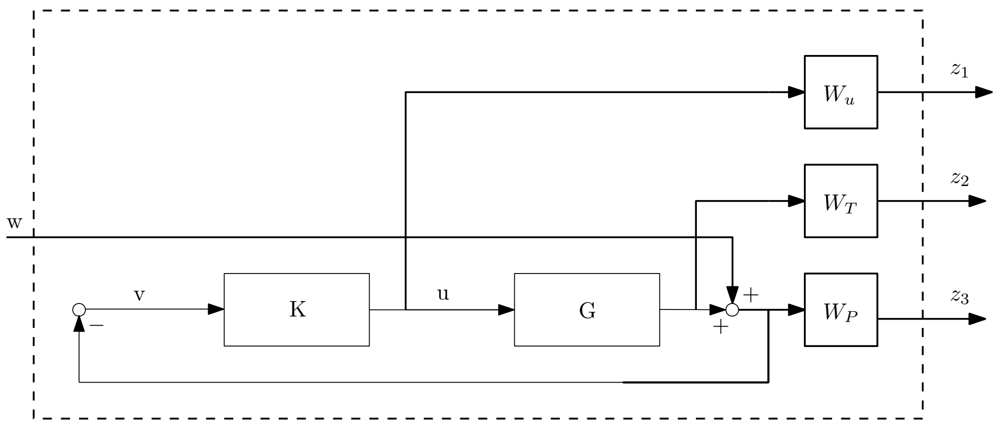

Figure 2.4: Block representation of z=Nw.

Adopting the representation in figure 2.4, N can be written as in 2.27:

$$N = \begin{bmatrix} W_u KS \\ W_T T \\ W_P S \end{bmatrix} \tag{2.27}$$

Since now we have considered more outputs from the system and not just the error signal we rewrite the equations between w and z.

$$z_1 = W_u u \tag{2.28}$$
$$z_2 = W_T G u \tag{2.29}$$
$$z_3 = W_P w + W_P G u \tag{2.30}$$
$$u = -w - Gu \tag{2.31}$$

and the generalized plant P becomes 2.32

$$\begin{bmatrix} z & v \end{bmatrix}^T = \underbrace{\begin{bmatrix} 0 \; W_u I \\ 0 \; W_T G \\ W_P I \; W_P G \\ -I \; -G \end{bmatrix}}_{\text{P}} \begin{bmatrix} w & u \end{bmatrix}^T \tag{2.32}$$

In order to see clearly how N is derived from P and K, firstly P is partitioned as 2.33 - 2.34:

$$P_{11} = \begin{bmatrix} 0 \\ 0 \\ W_P I \end{bmatrix}, \; P_{12} = \begin{bmatrix} W_u I \\ W_T G \\ W_P G \end{bmatrix} \tag{2.33}$$

$$P_{21} = I, \; P_{22} = -G \tag{2.34}$$

so it is rewritten as in 2.35

$$P = \begin{bmatrix} P_{11} \; P_{12} \\ P_{21} \; P_{22} \end{bmatrix} \tag{2.35}$$

Each of these sub matrices in 2.35 represents a certain relation between the inputs and the outputs of the open loop generalized system P:

1. P_{11} relates the exogenous outputs z with the exogenous inputs w.
2. P_{12} relates the exogenous outputs z with the sensed input u.
3. P_{21} relates the sensed outputs v with the exogenous inputs w.
4. P_{22} relates the sensed outputs v with the sensed inputs u.

So the set of equations 2.36 and 2.37 is delivered.

$$z = P_{11} w + P_{12} u \tag{2.36}$$

$$v = P_{21} w + P_{22} u \tag{2.37}$$

Now considering that the loop under P closes by 2.38

$$u = Kv \tag{2.38}$$

and eliminating u,v from equation 2.36 and 2.37 equation 2.39 is derived.

$$N = P_{11} + P_{12}K(I - P_{22}K)^{-1}P_{21} \tag{2.39}$$

Thus one can, given specific transfer functions for the controller, the system and the weights, derive from 2.39 the closed loop response of the controlled system. The methodology of integrating the weighting functions in the system to derive N has been presented. The methodology of creating the stabilizing controller K is included in the appendix chapter A, since the mathematical analysis is quite complicated and does not contribute to realizing the philosophy behind robust control.

2.5 Weight Selection

2.5.1 Weight W_P

The typical and most common bound in robust control is S, because it is related both to performance and stability. Therefore, great care is given to the design of the performance weight W_P, which apart from the other design specifications, it is supposed to be a proper function and the same goes for all types of weighting functions. In general, in terms of performance, W_P secures a minimum time of convergence (through the definition of bandwidth), sets a maximum (unavoidable as explained in subsection 2.3.2) peak magnitude M_S and keeps a maximum tracking error. All these are achieved by designing W_P in a way that

$$|W_P S(j\omega)| < 1, \forall\omega \tag{2.40}$$

or

$$|W_P S(j\omega)|_\infty < 1, \forall\omega \tag{2.41}$$

This shows that it is the inverse of $|W_P|$ that is supposed to be greater than $|S|$.
A general form of the desired weight that is imposed by the common form of the S function of real stable systems is

$$W_P(s) = \frac{(s/M^{1/n} + \omega_B)^n}{(s + \omega_B A^{1/n})^n} \tag{2.42}$$

There are four parameters $M,\ \omega_B,\ A,\ n$ in 2.42 that play a specific role in defining the behavior of $|S|$.

- M is the upper bound of S and it usually is between 1.5-3 according to how loose or tight the control is desired. Its existence is required in high frequencies around the bandwidth area.

- Bandwidth ω_B is the frequency at which $1/W_p$ crosses 1 from below. It defines the area of frequency that control has effect on the system and is related to the speed of response.

- A is the lower limit of S at low frequencies and it has a value close to zero. It is related to the steady state error requirement.

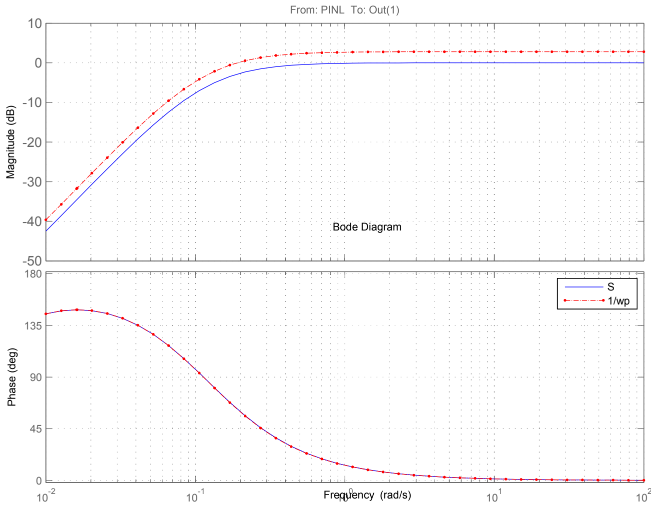

Figure 2.5: Bode diagram of S, $1/W_p$.

- The order of the weight n is selected according to the slope that $|S|$ is required to have in low frequencies. When a higher order is selected, the slope of $|S|$ is greater, so the sensitivity's function effect in y is decreased for a bigger range of frequencies.

An example of a Bode diagram of S with $1/W_P$ is given in Figure 2.5. The transfer function of the plant used in the example is 2.43, [4].

$$G(s) = \frac{200}{10s+1}\frac{1}{(0.05s+1)^2} \tag{2.43}$$

It is an example of tight control requirement since

- The maximum peak requirement is 0.1
- The bandwidth is close to 10 rad/s so control is required in this case over a wide range of frequencies
- The order of the weight is 2 because in this way the amplification of the sensitivity function stays lower than 1, over a greater range of frequencies, or in other words the slope is steeper before $|S|$ reaches 1.

2.5.2 Weight W_T

While limiting $|S|$ in low and intermediate frequencies is important, this practice alone has no actual effect on $|L|$ in higher frequencies, an area over which $|L|$ of real systems rolls off. In this frequency area, it is obvious that $|L|$ "follows" $|T|$ as they both roll off towards zero. In the Bode diagram of figure 2.6 the above statement is justified. L in frequencies above 1 rad/s is starting to roll off at the rate imposed by the weighting function $1/W_T$. A general form of a W_T weighting function is given in equation 2.44.

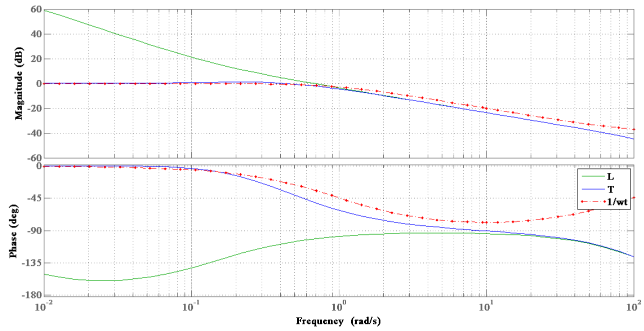

Figure 2.6: Bode diagram of L, T, $1/W_t$.

$$W_T = \frac{\left(sM_t^{1/n} + \omega_{BT}\right)^n}{\left(sAA^{1/n} + M_t\omega_{BT}\right)^n} \tag{2.44}$$

The parameters that define the form of W_T are summarized as follows:

- M_T is the maximum allowed magnitude of T in frequencies around ω_{BT} and it is required to be generally smaller than M_S because $|S|$, $|T|$ cannot differ more than 1, as around ω_{BT} measurement noise is amplified.
- Bandwidth ω_{BT} is required to be relatively large since up to this frequency the reference setpoint is traced adequately.
- n is the order of the weight. In cases where instabilities are possible to occur, in high frequencies a greater roll off rate is secured by choosing a weight of a higher order.
- AA is the upper bound of T in high frequencies.

In the Bode diagram of L, T, $1/W_T$ in Figure 2.6 these parameters can be recognized.

- M_T is required 1.
- n is 1 since L rolls off sufficiently fast already ($20dB/decade$).
- ω_{BT} is 1 rad/s .

One can see that the above design has sacrificed some performance advantages in favour of stability. The closed loop bandwidth is in general close to the performance bandwidth. Therefore ω_B is expected to be in the area of 1 rad/s. Moreover, since M_T and M_S do not differ more than one and M_T is already equal to 1, M_S is expected to be greater than 1. Hence, it is derived that performance and stability are objectives that are contradicting.

2.5.3 W_u Weight

Usually when a system has an initial state that differs quite enough from the reference set point, great errors are expected in the beginning of the control process. How much energy the control signal produced by the controller contains, can be regulated with the use of a limiting weight of the control input. This may have effects on the tracking performance but can help the system stay away from instabilities, in other words errors are tolerated for a relatively grater amount of time, to avoid a big overshoot in the time-domain, and oscillations around the reference set point. This weight is symbolized as W_U.

2.5.4 Mixed Sensitivity Design Steps

As seen in the earlier subsections, none of the weights alone can form an adequate controller, if an overall good behaviour of the system is required. This is why the Mixed Sensitivity methodology is introduced. The steps to minimize the $|N(K)|_\infty$ norm are described as follows, with the respective commands.

1. The weights W_P, W_T, W_u are designed.
2. The generalized (or augmented open loop) plant P is produced with the Matlab command $P = augw(G, wp, wu, wt)$
3. Having obtained P, the controller is obtained with command $[khinf, ghinf, gopt] = hinfsyn(P, nmeas, ncon, 0, 10, 0.1)$. The arguments in the left side of the equation are: $khinf$ is the controller obtained, $ghinf$ is the closed loop system N(P,K) and $gopt$ is the lowest upper value of $|N(P,K)|_\infty$ achieved. The arguments in the right side of the equation are P the augmented plant, $nmeas$ the number of measured traces, $ncon$ the number of the controller traces produced, 0 and 10 are the lower and upper norm margins respectively and 0.1 is the tolerance of $gopt$.
4. Next Bode diagrams of the norms of L, S, T transfer function are plotted and the closed loop behavior of the system is examined.
5. If $gopt$ is not satisfied or closed loop performance is not acceptable, the weights in step 1 are readjusted.

2.6 Design of a Robust Controller for the Inverted Pendulum

The above described methodology on the design of a robust controller, was implemented in a laboratory device, the inverted pendulum at the Laboratory of Marine Engineering.
The system consists of the inverted pendulum that is attached on a cart, which slides horizontally along two bars. The cart can be moved along the bars by a servo motor, which converts the rotational movement to transitional with the help of a timing belt. The servo motor is equipped with a rotary encoder that measures the angle displacement (θ) of the pendulum and with an encoder that measures the motor rotations that are translated to the horizontal displacement (x) of the cart. The cart is moved according to the command of the control law. A computer equipped with a Digital Signal Processor produces the control command of the controller, which is designed in Matlab/Simulink and then integrated in the Real Time Matlab environment. The

physical characteristics of the inverted pendulum are presented in table 2.1, while the free-body diagram of the cart and the rod is depicted in figure 2.7.

Parameter	Description	Units
M	Cart mass	1.096 kg
m	Pendulum mass	0.109 kg
b	Cart friction Coefficient	0.100 $\frac{N}{ms}$
l	Pendulum gravity center	0.250 m
2l	Pendulum length	0.500 m
J	Pendulum inertia	0.00034 kg m^2
θ	Pendulum angle	rad
x	Cart position	m

Table 2.1: Physical properties of the inverted pendulum

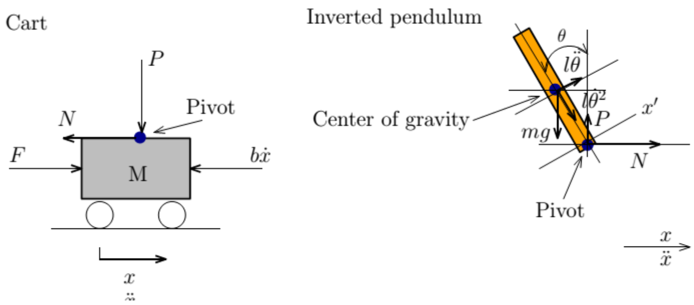

Figure 2.7: Diagram of the cart and the pendulum.

The disturbance in the system is an input that the user causes himself, by displacing the pendulum by 1 to 4 degrees from its vertical position (the system used for the controller design is a linearized one, in a range of angles between 0 and 4 degrees, where $sin(\vartheta) = \vartheta$).
The solution to stabilizing the pendulum is in general challenging, due to the RHP[3] pole of the system, which indicates instability. Here, the term instability is relative because it depends on what permanent state of the system is considered stable. In this case, the system is considered stable as long as the far end of the rod stays vertical looking upwards and this is regarded as the reference angle of stability (0^o degrees according to the manufacturer [21].

2.6.1 Mathematical Model

The designed controller was based on the transfer function between the angle displacement Θ and the cart's acceleration V. The transfer function of the system is derived by the equations, given by the manufacturer of the pendulum in [21]. The final equation is 2.45 in S.I. units

$$G(s) = \frac{\Theta}{V} = \frac{0.02725}{0.012125s^2 - 0.26705} \tag{2.45}$$

[3]RHP: Right Half Plane

or in state space form

$$\frac{d}{dt}\begin{bmatrix} x \\ \dot{x} \\ \Theta \\ \dot{\Theta} \end{bmatrix} = \begin{bmatrix} 0 & 1 & 0 & 0 \\ 0 & 0 & 0 & 0 \\ 0 & 0 & 0 & 1 \\ 0 & 0 & 29.4 & 0 \end{bmatrix}\begin{bmatrix} x \\ \dot{x} \\ \Theta \\ \dot{\Theta} \end{bmatrix} + \begin{bmatrix} 0 \\ 1 \\ 0 \\ 3 \end{bmatrix} u \tag{2.46}$$

$$y = \begin{bmatrix} x \\ \vartheta \end{bmatrix} = \begin{bmatrix} 0\,0\,0\,0 \\ 0\,0\,1\,0 \end{bmatrix}\begin{bmatrix} x \\ \dot{x} \\ \Theta \\ \dot{\Theta} \end{bmatrix} + \begin{bmatrix} 0 \\ 0 \end{bmatrix} u \tag{2.47}$$

The transfer function contains a pair of poles, one of them being quite fast as it lays in the RHP at 5.11 rad/s, causing the instability and another one which is considered stable as it lays in the LHP at -5.11 rad/s.

2.6.2 Controller Design

Based on the mathematical representation of the inverted pendulum a robust controller is designed. The weights used to form the controller are:

- For W_P a bandwidth requirement of twice the RHP pole suffices for the quick response required, so $\omega_P = 10$ rad/s. $M_P(s)$ is chosen as 0.01, indicating the requirement of disturbance rejection. In order for L to have a steeper slope below bandwidth the order of the weight is selected to be $n = 12$. The gain of the weight is chosen as 10^{-3} so as to tolerate small errors. This selection of the order of the weight is not common practice in literature. However, the requirement of both a bandwidth that is twice the RHP pole of the system, and an M_p that is small enough not to tolerate steady state errors is only achieved through a weight of a greater order. This secures that S has a steeper slope in lower frequencies, thus staying under 1 in magnitude for a greater range of frequencies.

- The closed loop transfer function T, was not bounded because of four main reasons. To start with the type of the problem is not considered as a tracking control problem where one would seek a big crossover frequency (ω_{BT}) of T with the intention of tracking r. The objective is the rejection of disturbances, which is contradicting to keeping T close to 1 for a great range of frequencies (S is complementary to T). Moreover, the need to include T in the design is diminished by the fact that in such a small scale of a plant, noise in measurements is not expected. Finally, the introduction of a W_T weight would enhance the order of the controller, giving no significant benefit to the control process.

- W_u is a constant bound of the control input. Its value is selected as 10^{-2}.

The selection of the high order performance weight, produces a controller that is eventually of a high order. This yields the necessity to simplify the controller, seeking a transfer function with the exact frequency response, but with a lower order representation. Having implemented the weighting function and after the model reduction process, the controller derived is presented in equation 2.48

$$k_{red} = 0.001005\ \frac{(s+1.646e09)\ (s+50.51)\ (s+8.419)\ (s+5.113)\ (s^2+60.91s+1496)}{(s+3633)\ (s+58)\ (s^2+50.86s+678.1)\ (s^2+60.3s+1201)} \tag{2.48}$$

In figure 2.8 the L, S, T frequency responses for the H_∞ are presented while the frequency response of the output of the controller in figure 2.9 is shown.

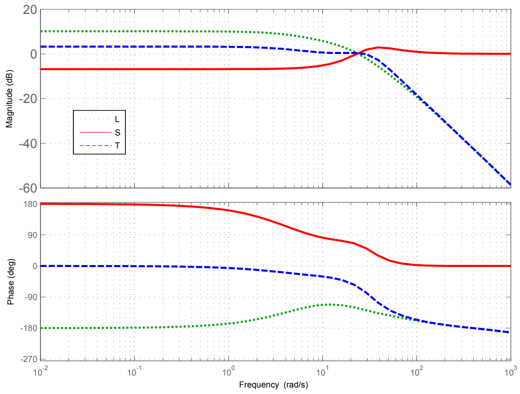

Figure 2.8: Bode diagram of L,S,T for the H_∞ controller.

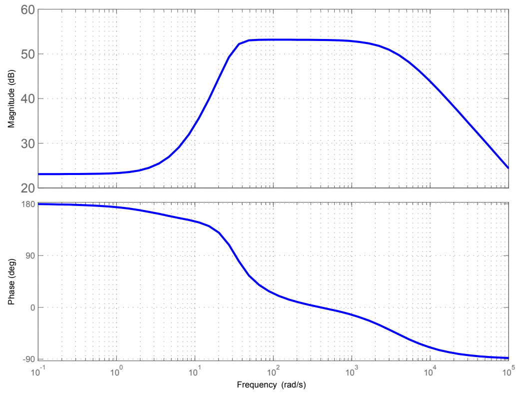

Figure 2.9: Bode diagram of KS for the H_∞ controller.

2.6.3 Control Simulation

The controller was tested in simulation in the Matlab Simulink environment. The disturbances are considered as two repeated displacements of 10 degrees in seconds 4 and 6 during the 20-seconds simulation. The time response is described in figures 2.11, 2.10.

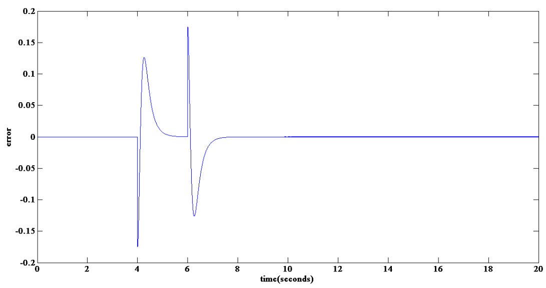

Figure 2.10: Error with H_∞ control.

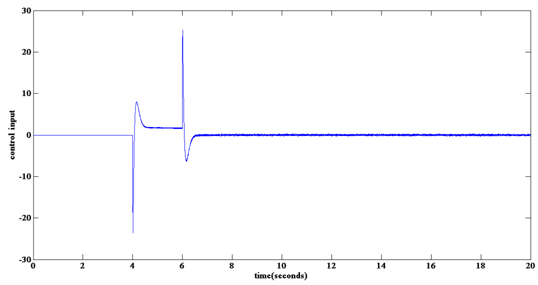

Figure 2.11: Control input of H_∞ control.

From the figures it is derived that the control input is bounded and achieves disturbance rejection with no steady state errors. The response is not oscillating heavily around the reference, but instead converges after 2 oscillations around it.

2.6.4 Controller Test on the Inverted Pendulum

$$k_{red,\ discrete} = 0.05006\frac{(z+517.1)(z-0.9248)(z^2-1.952z+0.9537)}{(z^2-1.953z+0.9536)(z^2-1.567z+0.6334)} \tag{2.49}$$

Before implementation the controller is discretized as in equation 2.49. The sampling time is 0.01 seconds, and the method used to calculate the values for each sampling period is the zero order hold[4]

[4]The Zero-Order Hold method holds its input for the sample period specified. The method accepts one input and generates one output.

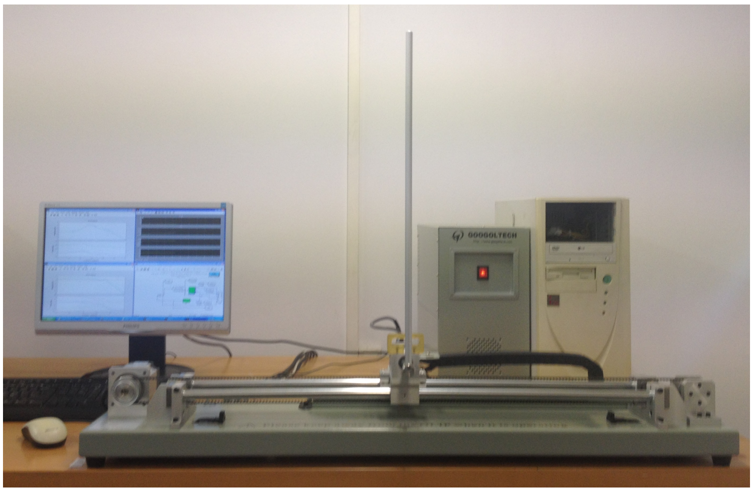

Figure 2.12: The Inverted Pendulum Experimental Device.

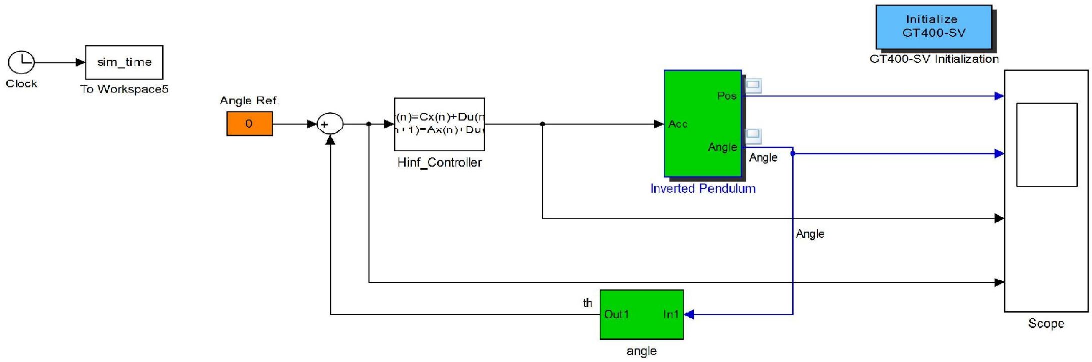

Figure 2.13: The template provided by the Laboratory to control the inverted pendulum.

The experimental device is depicted in figure 2.12, whereas the model in Simulink for the experimental test is depicted if figure 2.13. The results showed a successful operation of the controller, leading to a stable vertical position of the rod in spite of disturbances induced by the user at the far end of the rod by hand. In figure 2.14 the angle displacement of the the pendulum from the vertical position is depicted. The position of the cart upon which the rode is mounted, during the control process, is depicted in figure 2.15. The control input during the disturbance rejection process is depicted in figure 2.18. The phase diagram of the the rode angle and the rotational speed is depicted in figure 2.14, while the phase diagram of the cart position and the cart velocity is depicted in figure 2.17. Finally, the phase diagram of the cart acceleration and the cart velocity is depicted in figure 2.19.
In figures 2.14 and 2.15, it is evident that the controller, after the rejection of the imposed disturbances, achieves the retain of equilibrium. The angle is retained steadily near the vertical position (0 rad), and the cart returns to a steady position, after the disturbance rejection. The phase diagrams in figures 2.16 and 2.17 underline the above remarks. The radius of the circles formed is greater as the force of the imposed disturbances is increased. At the end of the process both the rotational speed of the rode and the cart velocity reach zero again as in the start of the process.

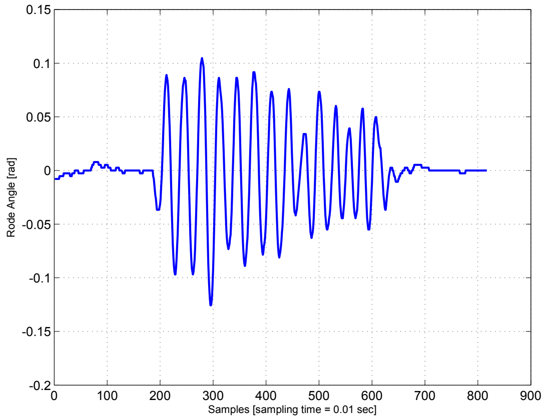

Figure 2.14: The angle displacement of the rod.

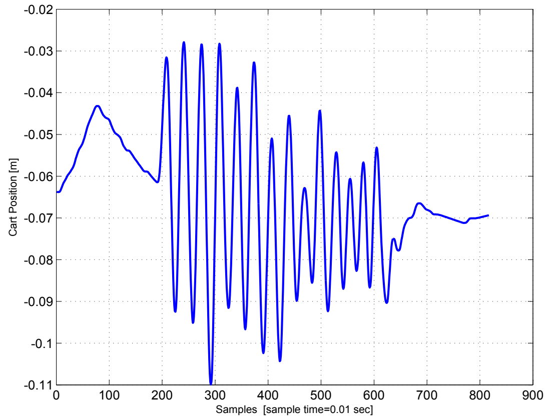

Figure 2.15: The cart position during the disturbance rejection process.

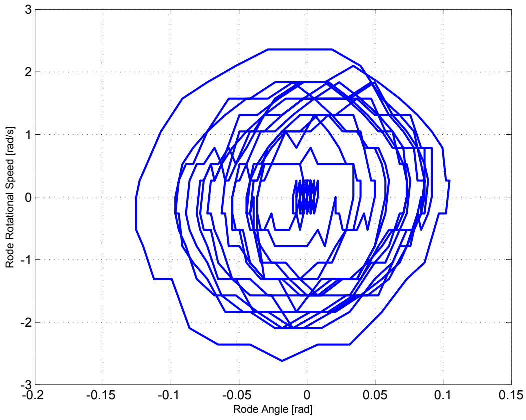

Figure 2.16: The phase diagram of the rod angle and rotational speed.

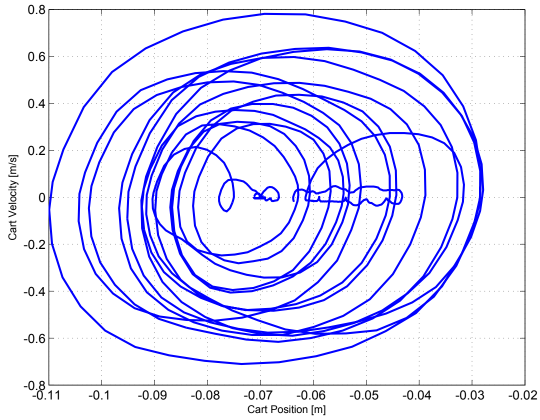

Figure 2.17: The phase diagram of the cart position and the cart velocity.

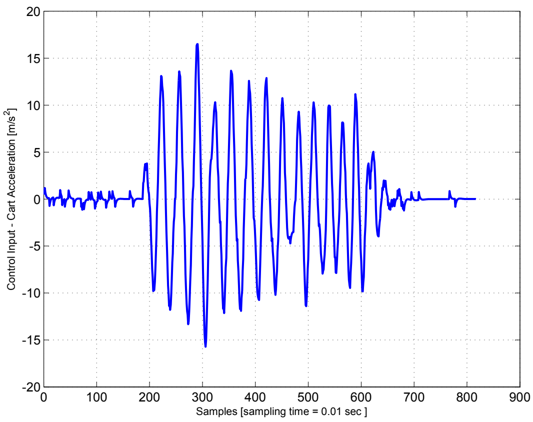

Figure 2.18: The control input of the controller.

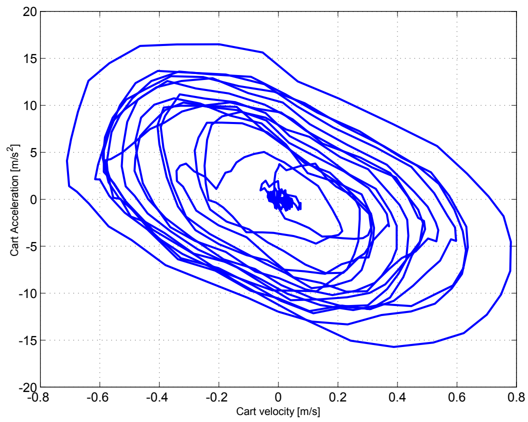

Figure 2.19: The phase diagram of the cart acceleration and the cart velocity.

Chapter 3

Crank Angle Modeling of the MAN L16/24 Engine

This chapter presents the model developed to simulate discrete events during an operating engine's cycle. The model is produced with the intention of simulating the effect of injecting compressed air downstream of the compressor to engine parameters like cylinder pressure, temperature and their derivatives, such as the indicated effective pressure, the brake effective pressure, the amount of air induced in the cylinders of the engine, the flow of gas after the end of the combustion towards the turbine, and an approximation of the heat absorbed by the working fluid, due to combustion. The model developed is a single zone model and it was based on the work of Eriksson [10]. It was then calibrated based on past experimental in cylinder pressure data. The implementation of the model and the various calibration aspects is described in chapter 4.

3.1 The Real Diesel Cycle

According to Heywood [24] and Black [17] the real diesel cycle is adequately approximated by the limited-pressure cycle (one can also find it in literature as the modified diesel cycle [8]). In the modified Diesel cycle which is the cycle presented in figure 3.1, the combustion begins in a constant-volume basis and ends on a constant-pressure basis. In other words, it is a combination of features found in both ideal Otto and Diesel cycles (in the former the combustion process is entirely isochoric). Fuel is injected at point C, while combustion is represented by the line CD. The combustion is isochoric practically for a small period of time, during which the pressure increases sharply, until the piston reaches a point slightly past TDC. Shortly the pressure trace stays in this maximum pressure area before it drops slightly, as the combustion ends at point D. Therefore, following the works of Eriksson [10], Klein [11], Guzzella [9] and Heywood [24] and our remarks on the experimental in cylinder pressure measurements, an in cylinder pressure model is derived, according to the modified Diesel engine cycle.

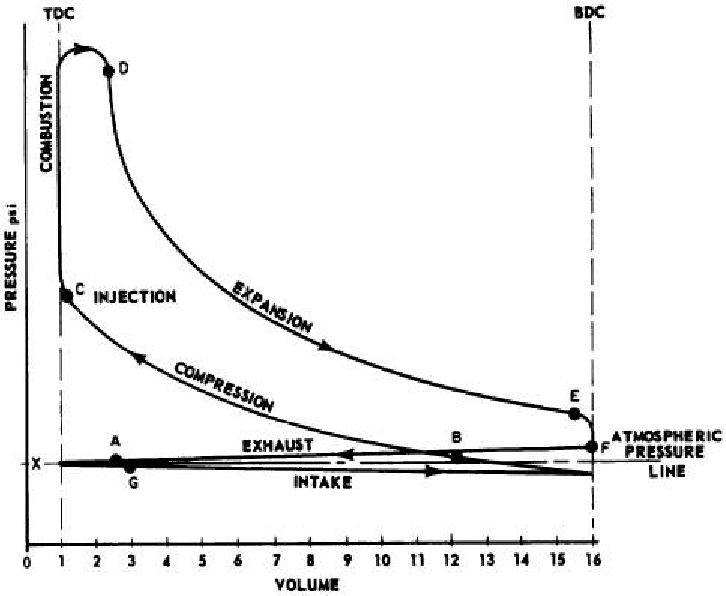

Figure 3.1: The modified Diesel cycle,[24]

3.2 Analytic Model of the Cylinder Pressure for a Four Stroke Diesel Engine

The main objective of the model is to provide an indication of the in cylinder pressure for the closed cycle, while the crank angle of the cycle develops. The method adopted is based on a parametrization of the Diesel cycle, being able to include variations in the start of combustion and in the air to fuel ratio. The main parameters that are needed as inputs to the model are the intake manifold pressure (p_{inl}) and temperature (T_{inl}), the crank angle (θ), the start and the end of the combustion (θ_{SOC} and θ_{EOC}) and the crank angles, to which the events of intake valve closing and exhaust valve opening (θ_{IVC} and θ_{EVO}) correspond.
The model is based on assumptions in order to be relatively simple and accurate. The first key assumption of the model is that both compression and expansion phases are considered as polytropic processes, therefore the pressure p and the temperature T traces in these parts of the cycle can be measured with the use of the polytropic equation 3.1 and 3.2 respectively. Considering as V_{cyl} the volume the gas takes up in the cylinder the following equations are used.

$$p \times V_{cyl}^{k} = C \tag{3.1}$$

$$T \times V_{cyl}^{k-1} = C' \tag{3.2}$$

Adopting the above method, it is assumed that because the compression and the expansion phase are short, the amount of energy exchanged with the environment is small, therefore it is fair to consider these processes as reversible adiabatic. This assumption is not entirely correct. In both processes heat is transferred between the gas and its environment, however due to the simplicity of the equation, this approximation is preferred. This approximation is proposed by Heywood as well in [24], however one should expect bigger deviations from the experimental data in the expansion stroke. As such k is equal to γ in 3.1 and 3.2, where γ is the ratio of specific heats of the working medium. To confirm that, pressure measurements are used from experiments. After plotting the pressure and volume traces in a log-log diagram the slopes of the compression and expansion asymptotes are calculated. The values obtained are then compared with theoretical ones.

The next key assumption is that the combustion is defined by a heat release analysis procedure, which is implemented through the pressure ratio management concept, described by Matekunas in [14], [15]. Matekunas observed that the S-function of the mass fraction burned is similar to the normalized pressure ratio function. The latter is derived by the ratio between a motored cycle and a firing cycle as in equation 3.3.

$$PR(\theta) = \frac{p_{firing}(\theta) - p_{motored}(\theta)}{p_{motored}(\theta)} \tag{3.3}$$

,after normalization equation 3.4 is derived.

$$\overline{PR}(\theta) = \frac{PR(\theta)}{max(PR(\theta))} \tag{3.4}$$

As stated in [16], [9] the crank angle at which the mass transfer function reaches the 50% mark, differs at most 1^o from the crank angle that $\overline{PR}(\theta) = 0.5$. In literature the mass fraction burned is usually described by the Wiebe function, which in its simplest form can be found [20] as in equation 3.5.

$$x(\theta) = 1 - e^{a\left(\frac{\theta - \theta_{SOC}}{\Delta\theta}\right)^{m+1}} \tag{3.5}$$

where $\Delta\theta$ is the duration of combustion, a and m are parameters relating to the rate of the burning of the fuel. Having defined the mass fraction burned per crank angle function, the combustion process is simulated by interpolating between the motored cycle and the ideal mixed Diesel cycle. In order to simulate the pressure asymptotes, a reference point for each one is needed, to define the constants $C_{compression}$ and $C_{expansion}$, appearing in the right side of equation 3.1.

In the following subsections the equations describing each process are described.

3.2.1 The Compression Phase

The compression part is described by a polytropic exponent k_c and a reference point. The reference point usually used in literature is the intake valve closing at θ_{ivc}. It can be assumed, to maintain simplicity, that at the end of the intake process the pressure in the cylinder has become equal to that in the intake manifold pressure.

The initial temperature is more difficult to define. The air entering the cylinders through the intake manifold is heated from T_{im} to another temperature T_a by the hot valves and the locally high heat transfer coefficients in the cylinder. However those quantities are difficult to determine using a single zone thermodynamic model, to define the amount of heat transferred to the charging air, during the intake process. Moreover, possible residual gas fraction that remain captured in the cylinder, after the exhaust process heat the fresh air as well. For the shake of simplicity, these effects are neglected and therefore the temperature at the intake valve closing crank angle is considered equal to the temperature in the intake manifold.

The pressure and temperature traces during the compression are thus calculated according to equation 3.6 and 3.7.

$$p_c(\theta) = p_{IVC}\left(\frac{V_{IVC}}{V(\theta)}\right)^{k_c} \tag{3.6}$$

$$T_c(\theta) = T_{IVC}\left(\frac{V_{IVC}}{V(\theta)}\right)^{k_c-1} \tag{3.7}$$

3.2.2 The Expansion Phase

The equations describing the asymptotic expansion process are 3.8 and 3.9.

$$p_e(\theta) = p_D\left(\frac{V_D}{V(\theta)}\right)^{k_e} \tag{3.8}$$

$$T_e(\theta) = T_D\left(\frac{V_D}{V(\theta)}\right)^{k_e-1} \tag{3.9}$$

The traces p_D, T_D, V_D refer to the state D in figure 3.1. The volume V_D is equal to the volume at the moment that the combustion ends at state D and the process in the cylinder does not include any release of heat from the oxidization of the fuel.

3.2.3 The Combustion

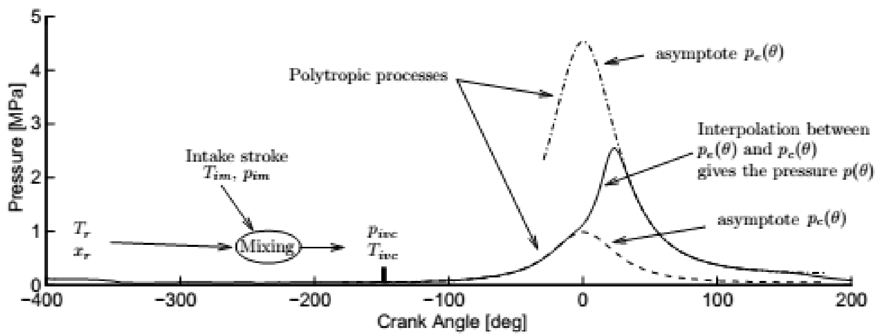

Figure 3.2: Graphical representation of the combustion approximation followed, [10].

The combustion part is approximated as follows and is based on the approaches proposed by Guzzella [9] and Eriksson [10]. An ideal instant augmentation of the temperature in the cylinder (ΔT_{comb}) is considered at the start of the combustion, which would correspond to the instant increase of the temperature in the cylinder, if it was possible for the whole amount of fuel injected, to be oxidized as soon as it entered the cylinder, instantly and not progressively as the combustion actually occurs. This theoretical temperature increase is described in equation 3.10.

$$\Delta T_{comb} = \frac{m_f q_{HV} \eta_f(\lambda)}{c_v m_{tot}} = \frac{q_{HV}\eta_f(\lambda)}{(\lambda(A/F)_s + 1)c_v} \tag{3.10}$$

where:

- q_{HV} is the lower heating value of the fuel.
- m_f is the amount of fuel injected per cycle per cylinder.
- $\eta_f(\lambda)$ is the the fuel conversion efficiency.
- c_v is the thermal capacity of the gas. It is calculated at the temperature right before the injection of fuel, at the end of the compression.
- m_{tot} is the the sum of air and the fuel injected per cycle.
- λ is the equivalence ratio.
- $(A/F)_s$ is the stoichiometric air to fuel ratio.

The ideal temperature then becomes

$$T_{max} = T_C + \Delta T_{comb} \tag{3.11}$$

and the ideal maximum temperature at the end of the isochoric combustion part is

$$p_{max} = p_C \frac{T_{max}}{T_C} \tag{3.12}$$

The pressure and temperature traces during the combustion process are then calculated as in equations 3.13 and 3.14. The interpolation scheme implemented is described in figure 3.2.

$$p(\theta) = (1 - \overline{PR}(\theta))p_c(\theta) + \overline{PR}(\theta)p_e(\theta) \tag{3.13}$$

$$T(\theta) = (1 - \overline{PR}(\theta))T_c(\theta) + \overline{PR}(\theta)T_e(\theta) \tag{3.14}$$

The terms p_c and T_c are equal to 3.15 and 3.16 respectively

$$p_c(\theta) = p_C \left(\frac{V_C}{V(\theta)}\right)^{k_c} \tag{3.15}$$

$$T_c(\theta) = T_C \left(\frac{V_C}{V(\theta)}\right)^{k_c-1} \tag{3.16}$$

,where C is defined the point at which the combustion starts in figure 3.1.
It should be noted that in 3.15 and 3.16 the exponent k_c after the TDC[1] is equal to the exponent of the expansion phase of the motored cycle and before the TDC is equal to the exponent of the firing cycle at the respective load.
The terms p_e and T_e are equal to 3.17 and 3.18 respectively,

$$p_e(\theta) = p_{max} \left(\frac{V_{max}}{V(\theta)}\right)^{k_e} \tag{3.17}$$

$$T_e(\theta) = T_{max} \left(\frac{V_{max}}{V(\theta)}\right)^{k_e-1} \tag{3.18}$$

[1]Top Dead Center

where k_e is equal to the exponent of the firing cycle at the respective load before and after the TDC.
Equations 3.13, 3.14 describe the gradual transition, from the phase of the cycle where the pressure and temperature values are close to the corresponding values of the motored cycle, to a phase where the pressure and the temperature is greater than those of the motored cycle. This pressure and temperature difference between the firing cycle and the motored cycle is due to the combustion. The effect of the combustion becomes stronger as the fuel is progressively burnt and it is inserted in equations 3.13 - 3.14 through the term $\overline{PR}(\theta)$, which is an ascending function of the crank angle. Therefore, the term $1-\overline{PR}(\theta)$ signifies the descending effect of the motored cycle and the term $\overline{PR}(\theta)$ signifies the ascending effect of the combustion. A schematic representation of the combustion modeling process is presented in figure 3.2, where the interpolation approximation followed, is depicted.

3.2.4 Summary of the Model

According to the above presented methodology the model for the cylinder pressure and temperature is described in equations 3.19 and 3.20.

$$p(\theta) = \begin{cases} p_{ivc}\left(\frac{V_{ivc}}{V(\theta)}\right)^{k_c} & ,\theta = [IVC, SOC] \\ (1-\overline{PR}(\theta))p_c(\theta) + \overline{PR}(\theta)p_e(\theta) & ,\theta = [SOC, EOC] \\ p_D\left(\frac{V_D}{V(\theta)}\right)^{k_e} & ,\theta = [EOC, EVO] \end{cases} \tag{3.19}$$

$$T(\theta) = \begin{cases} T_{ivc}\left(\frac{V_{ivc}}{V(\theta)}\right)^{k_c-1} & ,\theta = [IVC, SOC] \\ (1-\overline{PR}(\theta))T_c(\theta) + \overline{PR}(\theta)T_e(\theta) & ,\theta = [SOC, EOC] \\ T_D\left(\frac{V_D}{V(\theta)}\right)^{k_e-1} & ,\theta = [EOC, EVO] \end{cases} \tag{3.20}$$

3.2.5 Calculation of the in Cylinder Volume

The volume the working fluid takes up in the cylinder is a function of the crank angle. It is determined by the position of the piston, which in turn is a function of the crank angle. The crank angle takes values between [0,720] degrees since the engine is a four stroke one. The equation used to describe the position of the piston as a function of crank angle is

$$s(\theta) = r\left(\frac{l+r}{r} - \sqrt{\frac{l^2}{r^2} - \sin^2(\theta)} - \cos(\theta)\right) \tag{3.21}$$

Using equation 3.21, equation 3.22 is derived

$$V(\theta) = V_{cl}\left(\frac{1}{\epsilon-1} + \frac{s(\theta)}{2\epsilon}\right) \tag{3.22}$$

where:

- V_{cl} is the clearance volume of the cylinder.

- ϵ is the compression ratio.
- r is the crank angle radius.
- l is the length of the connecting rod.
- θ is the running crank angle.

3.3 Combustion Parameters Analysis

In this section the process of defining various combustion parameters and a number of derivative traces which were implemented in Simulink is described. These parameters are required because they are inserted as inputs to the described in cylinder model.

3.3.1 Definition of the SOC and EOC Angles

In order to define θ_{SOC} and θ_{EOC}, the heat release analysis method is used, using in cylinder pressure experimental data. The data were acquired from experiments conducted in October of 2008 at the engine load of 25% and the measurements refer to cylinder 5. In this method, there is no clear distinction between the burned and the non-burned part of the air and fuel mixture, instead the mixture is regarded as homogeneous. This analysis is based on the first Thermodynamic law, calculating the heat absorbed by the working fluid, using only the cylinder volume and the pressure trace.
Since the analysis refers to the closed part of the cycle, there is no exchange of mass between the under examination open system and its environment. Therefore, the first Thermodynamic law can be written as in equation 3.23.

$$\frac{dU}{d\theta} = \frac{dQ}{d\theta} - \frac{dW}{d\theta} + \Sigma\frac{dH_{oi}}{d\theta} \tag{3.23}$$

where:

- $\frac{dU}{d\theta}$ is the change of the internal energy of the working fluid.
- $\frac{dQ}{d\theta}$ is the change of heat offered to the system.
- $\frac{dW}{d\theta}$ is the change of work produced by the working fluid.
- $\Sigma\frac{dH_{oi}}{d\theta}$ is the sum of the heat transferred between the system and its environment.

Equation 3.23 can be rewritten as in equation 3.24 for the combustion case

$$\frac{dQ_{hr}}{d\theta} = \frac{dU}{d\theta} + \frac{dW}{d\theta} + \frac{dQ_{ht}}{d\theta} \tag{3.24}$$

where

- $\frac{dQ_{hr}}{d\theta}$ is the whole amount of heat released by the combustion of the fuel.
- $\frac{dQ_{ht}}{d\theta}$ is the total amount of heat transferred through the walls of the cylinder.

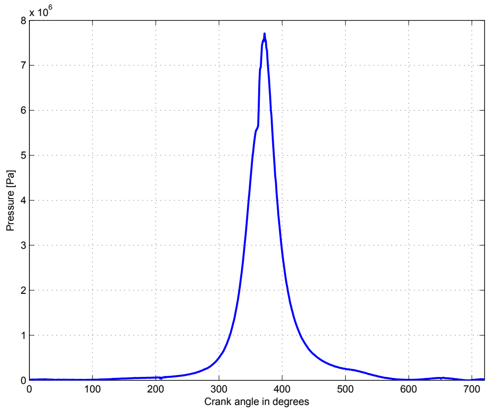

Figure 3.3: Experimental data of in cylinder pressure.

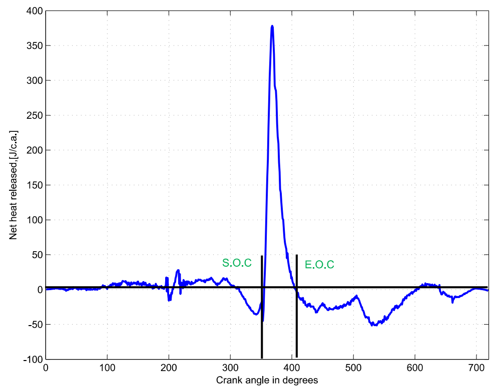

Figure 3.4: Net heat released diagram from experimental data.

- $\frac{dU}{d\theta}$, $\frac{dW}{d\theta}$ as defined above.

Equation 3.24 can be divided in two parts as in equation 3.25

$$\frac{dQ_{hr}}{d\theta} = \underbrace{\frac{dQ_n}{d\theta}}_{\frac{dU}{d\theta}+\frac{dW}{d\theta}} + \frac{dQ_{ht}}{d\theta} \tag{3.25}$$

where $\frac{dQ_n}{d\theta}$ symbolizes the net heat released by the fuel and is absorbed entirely by the working fluid in order to change its internal energy and the work it produces. The term $\frac{dQ_{ht}}{d\theta}$ is the heat lost through the walls of the cylinder.

The net heat released is then calculated according to 3.26 assuming that the working fluid is a perfect gas, with constant temperature throughout the system. This temperature defines a specific value for the parameter $\gamma = \frac{c_p}{c_v}$. Even though this assumption can be challengeable, since the temperature in the combustion strongly deviates, the work of Krieger and Borman [25] states that this hypothesis inserts a small error margin. In other words, from the start to the end of the combustion the properties of the working fluid change, but in favor of simplicity one can safely assume that γ remains constant. The net heat released is given by equation 3.26

$$\frac{dQ_n}{d\theta} = \frac{\gamma}{\gamma - 1} p \frac{dV}{d\theta} + \frac{1}{\gamma - 1} V \frac{dp}{d\theta} \tag{3.26}$$

In figure 3.3 the pressure data are presented and the net heat released per crank angle is presented in figure 3.4, for an experiment from MAN L16/24 at LME.

The pressure data were filtered with the help of Matlab. The Savitzky - Golay[2] filter was used. Figure 3.4 can give a great amount of information for the combustion. One can notice that at 320 degrees the curve reaches negative values for the first time, before it reaches zero again at 357 degrees. This is when the combustion commences. This range of angles between 320 and 357 signifies the combustion lag part of the cycle, when the fuel has been injected, but is in the process of absorbing heat from the already compressed air. The heat released stays positive but descends as soon as it reaches the

[2]This filter is efficient maintaining the upper and lower extrema of a function. One defines the order of the curve interpolating the data and the frame size.

maximum extrema 364 degrees, before the rate of the heat released becomes negative. The end of the combustion is signified by the point, at which the curve reaches zero again at 430 degrees. Thus, the angles $\theta_{SOC} = 357^o$ and $\theta_{EOC} = 430^o$ can be defined. Finally, one can relate the remarks made on figure 3.4 with the form of the pressure trace depicted in figure 3.3.

3.3.2 Determination of the Polytropic Exponents

The motored and the 25% load cycles were examined. Firstly, the log-log diagrams of pressure and volume were plotted and then specific points in the compression and expansion asymptotes were selected. These points define the polytropic exponents according to equation 3.27.

$$p_1 V_{cyl1}^{\gamma} = p_2 V_{cyl2}^{\gamma} \Rightarrow \frac{p_1}{p_2} = \left(\frac{V_{cyl1}}{V_{cyl2}}\right)^{\gamma} \rightarrow \gamma = \frac{\log p_1 - \log p_2}{\log V_{cyl1} - \log V_{cyl2}} \tag{3.27}$$

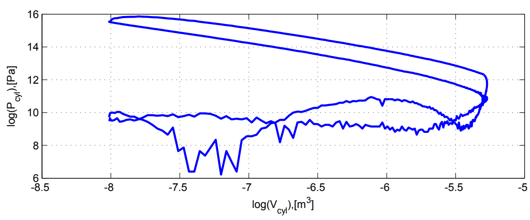

Figure 3.5: Logarithmic representation of pressure and volume traces at 25% load.

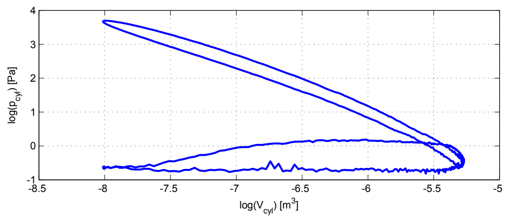

Figure 3.6: Logarithmic representation of pressure and volume traces for the motored cycle.

The calculation of the polytropic exponents and the points selected, are presented in table 3.1. The results of the tables 3.1 and 3.2 confirm the results of Ebrahimi [28], stating that as the heat offered to the working fluid augments, the polytropic exponents are expected to decrease. The exponents are those presented in table 3.2.

3.3.3 Pressure Ratio Analysis

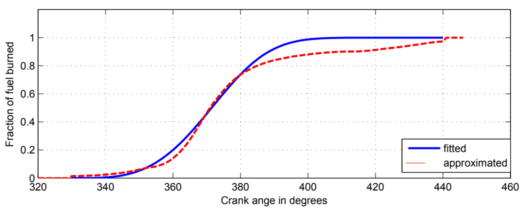

Figure 3.7: Fitted and approximated Wiebe functions using a single function approach.

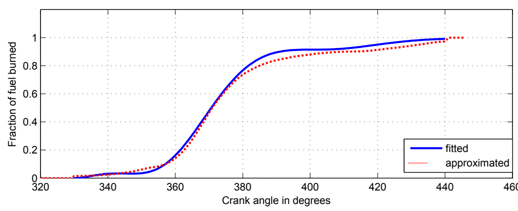

Figure 3.8: Fitted and approximated Wiebe functions using a triple function approach.

The S-type curve is depicted in figure 3.9. It ascends from 5% at 357 degrees. This can be attributed to the fact that the pressure trace of the loaded cycle is deviating from the motored cycle trace before the start of the combustion. This pressure difference in

Load Case	Part of Cycle	Coordinates	1st point	2nd point
Motored	Compression	X	6.268	7.201
Motored	Compression	Y	12.89	14.31
Motored	Expansion	X	6.268	7.662
Motored	Expansion	Y	12.89	14.78
25%	Compression	X	6.233	7.831
25%	Compression	Y	12.98	15.28
25%	Expansion	X	5.755	7.395
25%	Expansion	Y	13.35	15.59

Table 3.1: Points selected for the calculation of k_c and k_e

Load Case	Part of Cycle	Exponent
Motored	Compression	$k_c = 1.4285$
Motored	Expansion	$k_e = 1.4070$
25%	Compression	$k_c = 1.3950$
25%	Expansion	$k_e = 1.3658$

Table 3.2: Calculated polytropic exponents

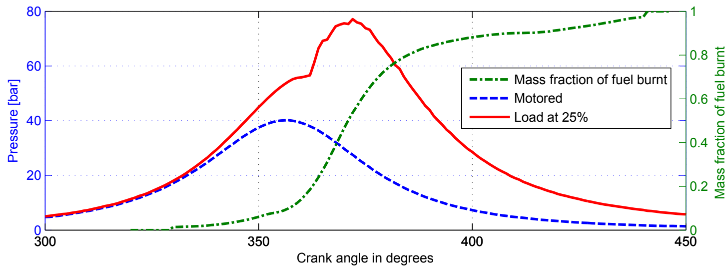

Figure 3.9: The loaded and motored cycles, with the S type curve of the mass fraction.

turn can be attributed to the fact that the working fluid in the loaded cycle is heated from the cylinder walls, thus augmenting the temperature and hence the pressure. This leads to the assumption that approximately 5% of the fuel is burnt instantly at the start of the combustion. At 364 degrees the pressure of the loaded cycle reaches its maximum. This event coincides with the angle where the S function has reached the value 0.5. This implies that, as soon as the loaded cycle has reached its maximum pressure, approximately 50% of the fuel injected has been burned. From that point on, until the end of the combustion at 430 degrees the fuel is burned at a much smaller pace, since the rest 50% of the fuel is burned, in the following 60 degrees which is a much larger range than the 7 degrees at which the fast burning phase of the combustion takes place.

Having acquired an approach of the mass fraction burned as a function of the crank angle, the duration of the combustion, θ_{SOC} and θ_{EOC} the parameters a and m of the mass fraction burned Wiebe function described in equation 3.5 are defined, adopting the least square error method.

Using the least square error fitting toolbox provided by Matlab, which is suitable for the approximation of non linear functions, the parameters a and m are defined. These parameters according to Stiesch in [30] define specific characteristics of the combustion. The constant m defines the form of the Wiebe function, which accounts for the heat release curve. The constant a describes the efficiency of the combustion. For the single Wiebe function the percentage of the fuel burnt at the end of the combustion can be written as in equation 3.28 and 3.29.

$$\eta_{conv} = \frac{Q_n}{Q_{hr}} = 1 - e^{-a} \tag{3.28}$$

or

$$a = -ln(1 - \eta_{conv}) \tag{3.29}$$

where η_{conv} is the conversion efficiency.
The first approach for a, m fitting 3.5 derives the following values

$$a = 6.5154$$

and

$$m = 2.5040$$

The square norm of the error achieved is 0.2044. The fitted and the experimental curves are presented in figure 3.7. Substituting α in 3.28 yields for the conversion efficiency $\eta_{conv} = 1$, which means that practically the combustion is perfect.

From figure 3.7 one can see that in the late parts of the combustion the experimental Wiebe function is not fitted adequately. Therefore, as suggested by Yeliana in [29] a three Wiebe-type approximation is adopted, with six parameters $a_1, m_1, a_2, m_2, a_3, m_3$ and three weighting factors ρ_1, ρ_2, ρ_3. The equation fitted is 3.30.

$$x(\theta) = \rho_1 \left[1 - e^{-a_1\left(\frac{\theta-\theta_{SOC}}{\Delta\theta}\right)^{m_1+1}}\right] + \rho_2 \left[1 - e^{-a_2\left(\frac{\theta-\theta_{SOC}}{\Delta\theta}\right)^{m_2+1}}\right] + \rho_3 \left[1 - e^{-a_3\left(\frac{\theta-\theta_{SOC}}{\Delta\theta}\right)^{m_3+1}}\right] \tag{3.30}$$

The results of the approach and the weights selected are presented in table 3.3.

Parameter	Value
ρ_1	3
ρ_2	-1
ρ_3	-1
a_1	5.9225
m_1	1.0330
a_2	10.9727
m_2	3.2266
a_3	48.0804
m_3	1.5486

Table 3.3: Results from least square error approximation of the three Wiebe function method.

The square norm of the least square error method achieved is 0.0166. The error is 12 times smaller using this approach. The fitting achieved using this method is presented in figure 3.8.

3.3.4 Estimation of Air Flow during the Intake

The flow of air during the intake phase of the cycle, into the cylinder, from the intake manifold is calculated in order to define the air to fuel ratio of the cycle, which is essential to the combustion. The main parameters in this case is the pressure upstream and downstream of the intake valve. The difference of these two parameters is what forces the fluid to move from the intake manifold into the cylinder. The process is non-linear, however one can expect that the greater the mean effective area of the orifice and the difference between the upstream and downstream pressure, the greater the amount of air induced in the cylinder. This is quite important as in general, the amount of air induced is expected to be greater since there is additional air injected in the intake manifold, which leads to an increased manifold pressure, which in turn causes an augmentation of the upstream and downstream pressure difference.
The pressure in the cylinder, is slightly smaller than the pressure in the intake manifold. This is confirmed by the actual measurements of the engine. During the intake process the relative pressure trace is slightly negative, causing a suction which drives the air into the cylinder. However a model to predict this trace is not developed, since the accuracy that it would add would not compensate for the complexity of such a process. Therefore, it is assumed that the downstream pressure is constantly, slightly smaller than that in the manifold. Hence, the pressure difference is considered equal to the intake manifold's pressure minus 0.17 bar which is the average pressure difference. In figure 3.10 one can see the in cylinder pressure in comparison with the mean value of the intake manifold pressure. Equation 3.31 is used in order to calculate the intake flow. The following assumptions are made in order to use a simple formulation, assuming that the air induced is compressible.

- The orifice is considered isothermal. No losses occur in the accelerating part until the narrowest point. The potential energy stored in the flow is converted entirely into kinetic energy causing no increase in the entropy of the flow.
- The flow after the narrowest point is considered fully turbulent. This assumption means that the pressure in the narrowest point in the valve is no different than the downstream pressure.
- The upstream and downstream temperatures are the same, or in other words the kinetic energy that the working fluid may have gained inside the orifice is dissipated into thermal energy.

$$\dot{m}(t) = cd \cdot A(t) \cdot \frac{p_{up}(t)}{\sqrt{R \cdot T_{up}}} \cdot \Psi\left(\frac{p_{up}}{p_d}\right) \tag{3.31}$$

where

- $cd \cdot A(t)$ is the effective area of the valve, with the pressure discharge coefficient cd accounting for friction losses. The effective area of the valve is already calculated from PhD students of LME/NTUA.
- p_{up} and p_d are the pressure traces upstream and downstream the valve. Here are considered as the intake manifold and cylinder pressure traces respectively.
- R is the specific air constant.

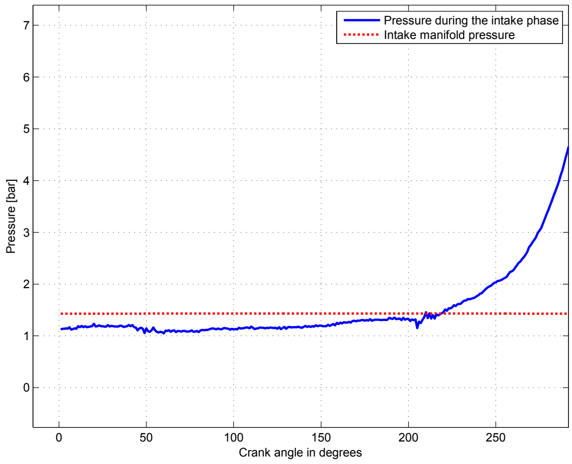

Figure 3.10: Comparison of in-cylinder pressure and intake manifold pressure during the intake phase.

- T_{up} is the temperature in the intake manifold.

The flow function Ψ is defined as in equation 3.32.

$$\Psi\left(\frac{p_{up}}{p_d}\right) = \begin{cases} \sqrt{\kappa\left(\frac{2}{\kappa+1}^{\frac{\kappa+1}{\kappa+1}}\right)} & , p_d < p_{cr} \\ \left[\frac{p_d}{p_{up}} \cdot \sqrt{\frac{2\kappa}{\kappa-1}\left[1-\frac{p_d}{p_{up}}^{\frac{\kappa-1}{\kappa}}\right]}\right] & , p_d < p_{cr} \end{cases} \tag{3.32}$$

where

- k=1.4, with the air considered as an ideal gas.
- p_{cr} defined as the critical pressure, at which the flow reaches sonic conditions. In other words, the difference in pressure becomes so great that the air is induced fast in the narrowest point in the valve, therefore its velocity reaches values close to 1 Mach. It is defined as in equation 3.33

$$p_{cr} = \left[\frac{2}{\kappa+1}^{\frac{\kappa}{\kappa-1}}\right] \cdot p_d \tag{3.33}$$

3.3.5 Properties of Gas-Air Mixture

In order to derive the properties of the gas air mixture, the approximation proposed by Kyrtatos [7] is used. The internal energy and the enthalpy of the mixture are calculated as a function of the temperature, the pressure and the air to fuel ratio. The equations used are based on curves, fitted to experimental results. The mixture is considered homogeneous.

$$u(T) = k_1(T) - k_2(T)\Phi, \ [kJ/kg] \tag{3.34}$$

where the constants k_1, k_2 and Φ are described in equations 3.35, 3.36 ,3.37.

$$k_1 = 0.692T + 39.17 \cdot 10^{-6}T^2 + 52.9 \cdot 10^{-9}T^3 - 228.62 \cdot 10^{-13}T^4 + 277.58 \cdot 10^{-17}T^5 \tag{3.35}$$

$$k_2 = 3049.39 - 5.7 \cdot 10^{-2}T - 9.5 \cdot 10^{-5}T^2 + 21.53 \cdot 10^{-9}T^3 - 200.26 \cdot 10^{-14}T^4 \quad (3.36)$$

$$\Phi = \frac{A_r/F_r}{A_{st}/F_{st}} \quad (3.37)$$

The constant of air R is described in equation 3.38.

$$R = 0.287 + 0.02\Phi,\ [kJ/kgK] \quad (3.38)$$

The enthalpy of the mixture is given in equation 3.39.

$$h = u + RT,\ [kJ/kg] \quad (3.39)$$

The thermal capacities c_p, c_v are derived according to equations 3.40 and 3.41.

$$c_p = dh/dT,\ [kJ/kgK] \quad (3.40)$$

$$c_v = du/dT, [kJ/kgK] \quad (3.41)$$

3.3.6 The Mean Indicated Effective Pressure

In figure 3.1 one can see two loops. The area contained in the loop defined by BCDEF, corresponds to the closed cycle (the part where the valves are closed) while the one defined by GAB corresponds to the open cycle (the part where at least one of the valves is open). Defining as the indicated positive work W_i^+ the area contained in the closed cycle and as the indicated negative work W_i^- the area contained in the open cycle, the trace $W_i = W_i^+ - W_i^-$ is defined as the indicated work. W_i is calculated as in equation 3.42.

$$W_i = \oint pdV \quad (3.42)$$

The indicated work is an important trace of the engine's cycle, however it is not a liable measure to compare the performance of different engines, since Wi is calculated as function of the cylinder volume, which differs from one engine to another. Therefore, a more objective measure of the performance of each cylinder is implemented by dividing W_i by the displacement volume V_d. This gives a trace with pressure units which is defined as in equation 3.43 .

$$IMEP = \frac{W_i}{V_d} \quad (3.43)$$

The trace IMEP is the indicated mean effective pressure. It is an indication of the mean value of the pressure in the cylinder.
Similarly to W_i one can define the trace W_r which corresponds to the mechanical losses of the engine. One can define a representative measure of the mechanical losses with pressure units by diving W_r by the displaced volume. This trace defined as FMEP, is the friction mean effective pressure. According to Theotokatos [22] the friction mean effective pressure for the MAN L16/24 can be calculated by equation 3.44.

$$FMEP = 0.138 + 0.001303 \cdot N_{eng} + 0.029 \cdot IMEP \quad (3.44)$$

where Neng in RPM and IMEP in bar. Equation 3.44 calculates FMEP in bar.
The difference between IMEP and FMEP defines a new trace BMEP which is an objective indication of the break work produced by the piston divided by the displacement

volume. Through BMEP one can define the torque T produced by the engine per cycle on the crankshaft with the use of equation 3.45.

$$T = \frac{N_{cyl} V_d BMEP}{2\pi n_c},\ [Nm] \tag{3.45}$$

where

- n_c is the number of revolutions per cycle, which in the case of a 4 stroke engine is 2.
- N_{cyl} is the number of cylinder of the engine, which is 5.

Finally, based on the indicated mean output torque per cycle and given the engine's rotational speed the power P delivered by the engine can be calculated according to equation 3.46.

$$P = \frac{2\pi T N_{eng}}{60},\ [W] \tag{3.46}$$

with N_{eng} in RPM.

Chapter 4

Simulation and Model Validation

In this chapter the implementation of engine modeling equations is described. In particular, the discrete, crank angle based events during the combustion were implemented. The modeling elements were the analogue valve for air injection, the cylinder volume, the pressure, the temperature, the intake of air, the air to fuel ratio, the net heat release, the torque, the power produced and the specific fuel consumption.

4.1 Model Calibration

Suitable initial values are required for the convergence of the model following its start in simulation. The aim of the calibration is to set initial conditions for the intake manifold's temperature and pressure, the exhaust manifold's temperature and pressure, the temperature and pressure for the fresh air inserted in the cycle and for the exhaust gas as well. The initial conditions of the engine running at 25% percent of the rated engine load are presented in table 4.1. This is a process that one is supposed to follow for each run at different load, as all the above engine parameters are affected.

4.2 Modeling Elements

The model is structured in such a way that the impact, on the rest of the engine, of the constantly changing properties of the working fluid in the engine cylinders is taken into account. Traces that affect the behavior of the engine such as the torque output and the exhaust flow of the cylinders are calculated and updated in a cycle to cycle basis. The main assumption is that the cylinders of the engine produce the same fraction of

Initial Condition	Value
Ambient Pressure	0.95 bar
Ambient Temperature	297 K
Intake Manifold Pressure	1.34 bar
Intake Manifold Temperature	307 K
Exhaust Manifold Pressure	1.20 bar
Exhaust Manifold Temperature	680 K
Turbocharger Shaft Speed	26200 RPM

Table 4.1: Initial Values of the model

the total torque per cycle. The torque produced as an input to the engine's shaft, is calculated using the brake effective pressure and is multiplied at the end of each cycle with the number of cylinders. The diagram of the model can be seen in figure 4.1.

4.2.1 The Air Injection Valve Block

The valve installed for the air injection is modeled as a needle valve as far the orifice is concerned, while the actuator is modeled as a second order linear actuator. The cross section of the valve can be seen in figure 1.4. The equation describing the flow through the valve is equation 3.31, which is used to calculate the flow inside the engine cylinders through the intake valve as well. The parameters of equation 3.31 are presented below.

- The pressure upstream is the pressure of the air provided by the air bottle. The air bottle stores air pressurized at 30 bar, with the pressure of the air reaching the valve regulated at 6 bar. This selection is based firstly on the upper limit the actuator poses for the pressure difference it can withstand, which is 10 bar. Taking in mind that the downstream pressure is approximately 1.3 bar, an approximate 5 bar pressure difference is created. Secondly, the additional amount of air inserted in the cycle is selected to be at most half the amount of air the compressor provides running steady at 25% load. The reason for this is the surge avoidance, which among others is one of the objectives of the thesis.

- The downstream pressure is selected as the pressure inside the intake manifold, with a 2% augmentation to account for possible pressure losses.

- $k = 1.4$ with the air considered as a perfect gas.

- $R = 287J/kgK$

- $T_{up} = 300K$ as the temperature of the air in the air cell.

- A(h) is the instantaneous orifice passage area as a function of the required displacement of the valve h. It is calculated as in equation 4.1. This approximation of the orifice area is suggested by Matlab and is available in [32].

$$A(h) = \begin{cases} 0 & , h = 0 \\ \pi \cdot [d_s - h\sin(\frac{a}{2})\cos(\frac{a}{2})]h\sin(\frac{a}{2}) & , 0 < h <= hmax \end{cases} \tag{4.1}$$

where

- h_{max} is the maximum stroke of the valve which is 1.5 cm according to the manufacturer.

- d_s is the orifice diameter which is 3.8 cm.

- a is the angle that the far ends of the valve form. Since according to the manufacturer's scheme the valve is flat at its far end, the angle is selected as 90 degrees.

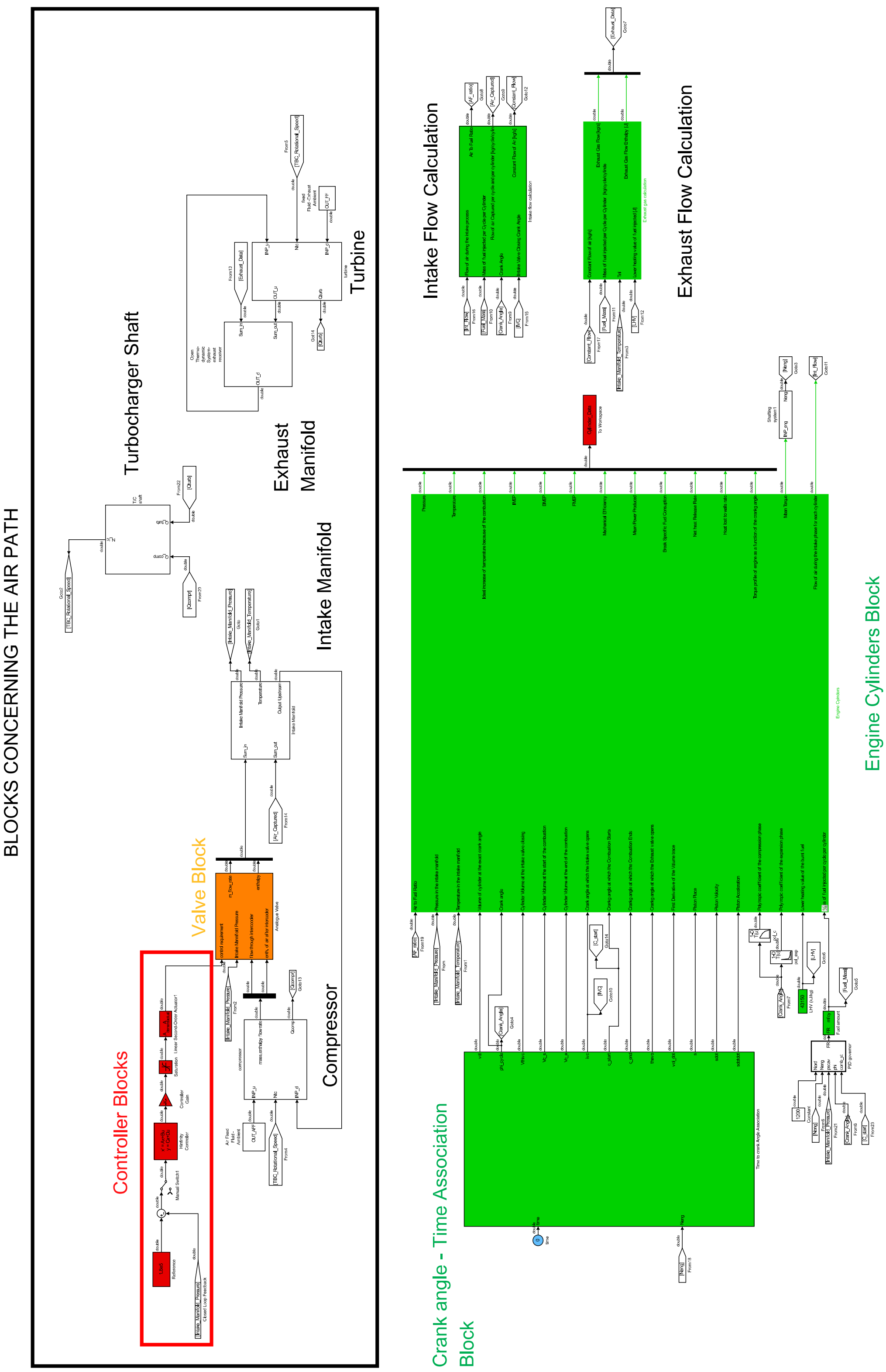

Figure 4.1: The developed engine model.

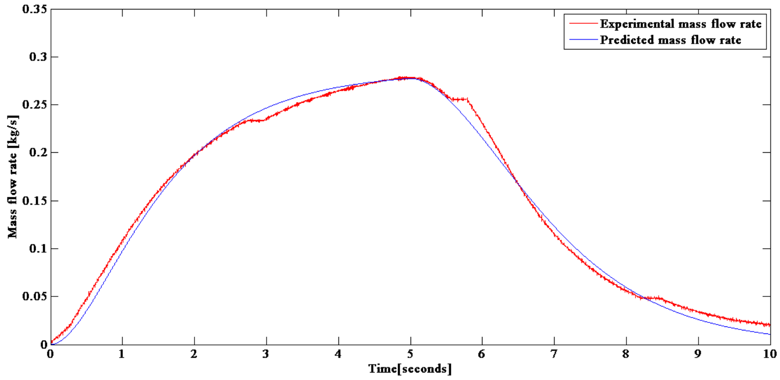

Figure 4.2: Experimental and modeled mass flow.

The actuator's natural frequency and dumping ratio as selected in such a way that the actual behavior of the actuator is modeled. During experiments on the valve a 100% opening of the valve was required and once it reached its peak the valve was required to close. The results of the experiment gave guidance on defining the rate the valve opens and closes and verified the theoretical results regarding the mass flow. According to the experimental data a critical dumping ratio was suitable ($\zeta = 1$) and the natural frequency selected was $\omega_n = 1.05\ rad/s$. The experimental and the simulated mass flow through the valve, with the valve opening at 100% percent is depicted in figure 4.2 The mass flow from the valve is considered as adiabatically mixed with the flow from the compressor. Therefore the properties of the flow towards the intake manifold are described as in the set of equations 4.2.

$$\begin{aligned} \dot{m}_{total} &= \dot{m}_{air\ injected} + \dot{m}_{compressor} \\ H_{total} &= h_{air\ injected}\dot{m}_{air\ injected} + h_{compressor}\dot{m}_{compressor} \end{aligned} \tag{4.2}$$

The Simulink representation of the above is depicted in figure 4.3.

4.2.2 Time to Crank Angle Association block

In this block the running time and the rotational engine speed are used as inputs in order to calculate the total radians that the engine has covered. The current crank angle of the engine is calculated by decreasing the covered angles by the number of the previous cycle times 4π. This way the running time is associated uniquely to a crank angle and a cycle that this angle occurs. The only assumption made is that the piston starts from TDC the intake process. This is considered as the start of each cycle and therefore the engine crank angle is zero at this point. The equations described in 3.21 and 3.22 for the place of the piston and the in cylinder volume respectively were also implemented in this block. Apart from the in cylinder volume and the place of the piston the first derivative of the volume was calculated and the velocity and the acceleration of the piston as well. From this block information about specific events of the cycle are derived. Characteristic events of the cycle are considered the start and the end of the combustion, the volume at these angles and the start and the end of the intake and exhaust process. The block is presented in figure 4.4.

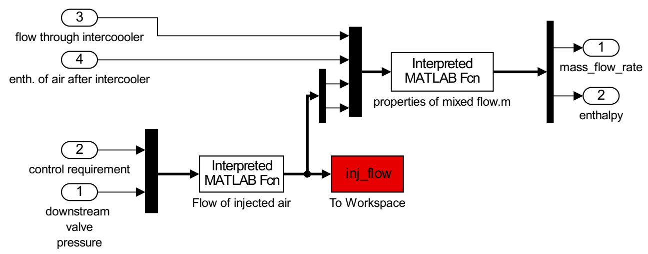

Figure 4.3: Simulink representation of the adiabatic mix of the flows from the valve and the compressor.

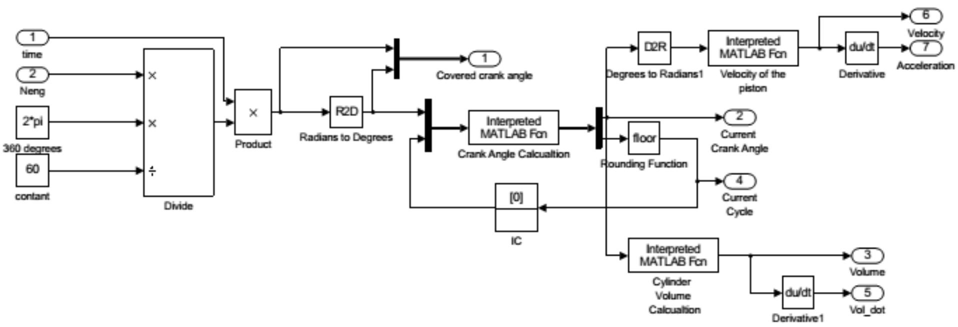

Figure 4.4: The block associating time with the crank angle.

4.2.3 The Cylinders Block

The cylinders block implements the theory described in chapter 3 in order to produce the pressure and the temperature calculations. These calculations provide the required information about the torque output of the cylinders and the efficiency of the engine on a cycle to cycle basis. The development of such a model gives a more accurate approximation of the engine's behavior in real time operation, but not an entirely liable one, because the firing order of the cylinders is not included. The model predicts the in cylinder pressure from which the engine parameters of IMEP, FMEP, BMEP and mechanical efficiency are derived. At the end of each cycle, the torque output of the engine is updated. The torque trace is calculated through the BMEP trace and the volume of displacement of each piston. Based on the torque output and the engine's

rotational speed the power per cycle produced is also calculated. With the help of the power per cycle trace and the input of the mass fuel injected per cycle and per cylinder, calculated as a function of the position of the governor, the brake specific fuel consumption is derived.
The governor block has been altered in order to update the rack position only during a crank angle margin of 20 degrees before the start of the combustion. The difference between the ordered rotational speed of the engine and the actual rotational speed of the engine is given as a feedback to the PID controller only during this margin. Otherwise, the controller would give a command with no immediate effect on the Torque and hence the engine's rotational speed.
The net heat release rate and the net heat release sum per cycle is approximated according to the process followed in subsection 3.3.1. Finally, based on the observation of the measured in cylinder pressure data of the approximately constant pressure difference between the intake manifold and the cylinder (as stated in subsection 3.3.4), the air induced in the cylinders as a function of the intake valve opening is calculated. The cylinder block is presented in figure 4.5.

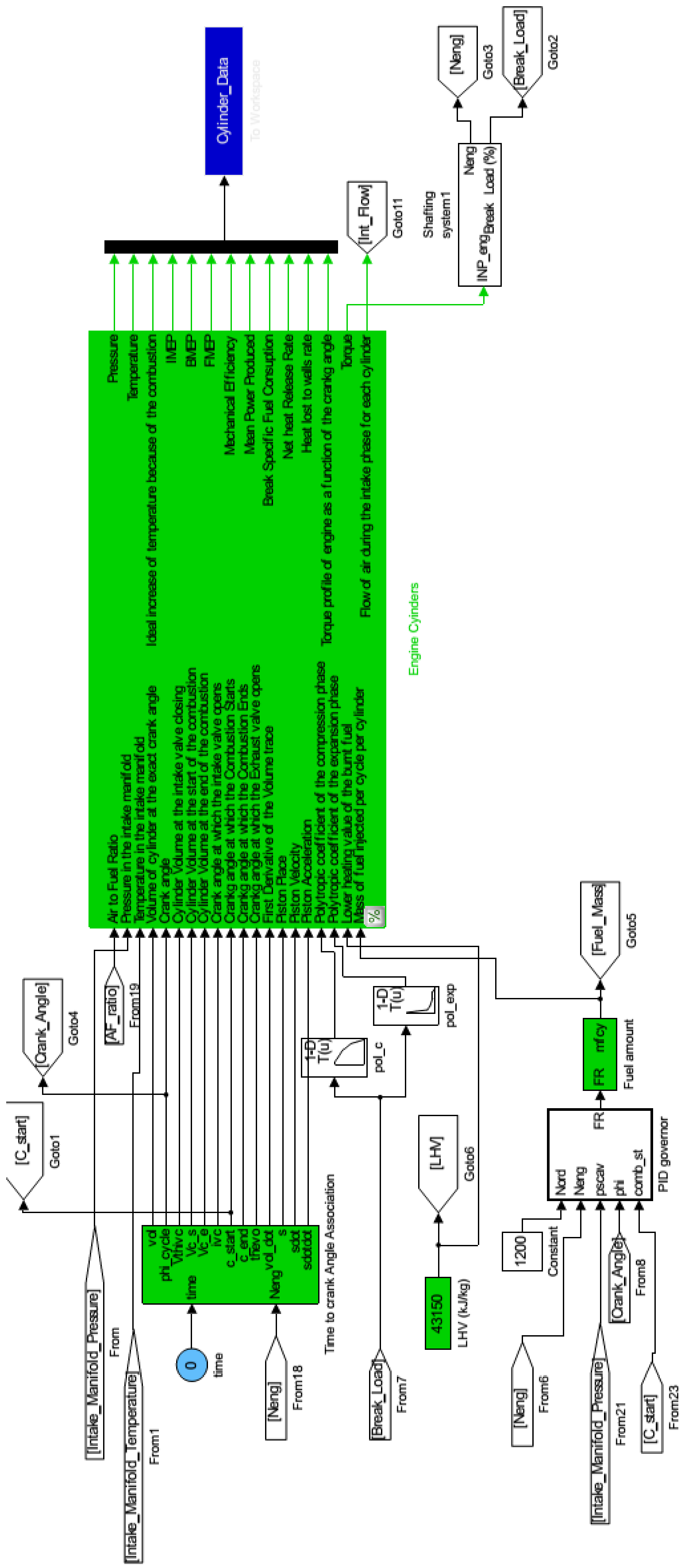

Figure 4.5: The cylinder block.

4.2.4 Intake Flow Block

This block receives as an input during the intake phase the flow of air that is inserted in each cylinder. This flow is integrated in order to calculate the amount of air inserted in each cylinder per cycle. Multiplying the amount of air inserted in each cylinder per cycle with the number of the cylinders and the number of the engine's cycles per second, the flow of air per second towards the cylinders is derived. These calculations take place during the intake phase. At the end of the intake phase, the air to fuel ratio of the cycle is calculated by dividing the amount of air captured in the cylinder to the fuel injected per cycle in each cylinder. The block is depicted in figure 4.6.

4.2.5 Exhaust Flow block

The exhaust flow block updates the flow and the enthalpy of the exhaust gases towards the turbine at the end of each exhaust gas blow out phase. The block receives as an input the constant flow of air calculated by the intake flow block, the temperature of the exhaust manifold, the lower heating value of the fuel and the amount of fuel injected per cycle and cylinder. The enthalpy of the exhaust gases is a sum of the enthalpy of the fuel and the air inducted in the cycle at the intake phase. The specific enthalpy of the air is calculated as a function of the temperature in the exhaust manifold. The total enthalpy provided by the fuel is defined by multiplying the lower heating vale with the total fuel injected every second. It was chosen not to implement the equations of compressible fluids in order to calculate the exhaust gas flow per crank angle, as it was done for the intake process, so as not to burden the Simulink model additionally. This selection is justified based on the assumption that there is no accumulation of air anywhere in the the engine and therefore the same amount of air inserting the cylinders is blown out.

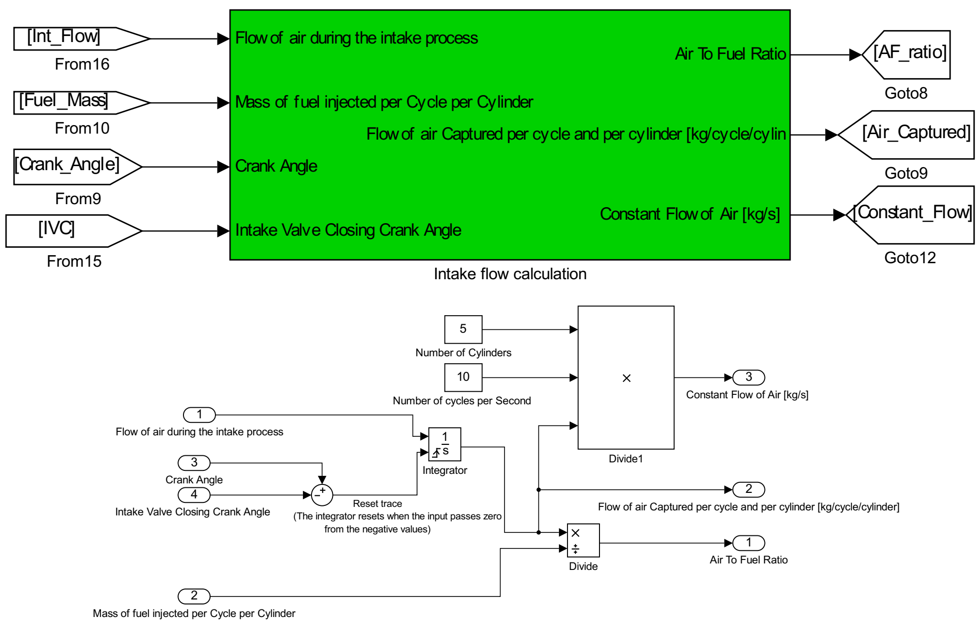

Figure 4.6: The block calculating the air to fuel ratio.

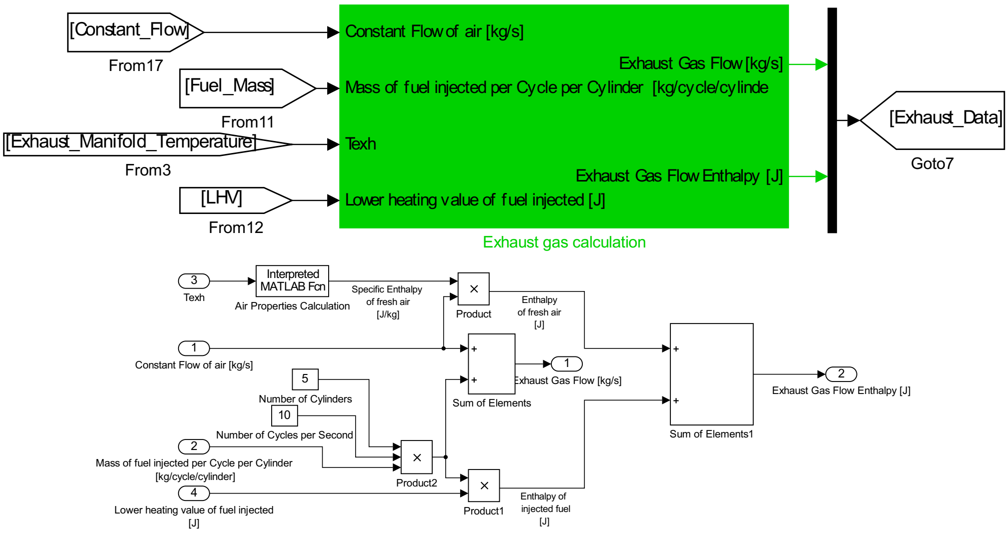

Figure 4.7: The block calculating the exhaust flow.

4.3 Mean Value Modeling Elements

The above mentioned functions were completed with the work of [22] and [23], for the entities of compressor turbine and manifolds. In that work the engine model was of mean value type, with all calculations carried out in the time domain.

4.3.1 The Compressor

The compressor receives as an input the thermal characteristics of the air, downstream and upstream the compressor. That is the intake manifold and the ambient environment respectively. The compressor rotating speed is inserted as an input. The block loads the compressor map which has been digitized for this thesis for this specific compressor ie ABB TPS48, shown in figure 4.8. In the compressor block, the downstream-upstream pressure ratio and the rotational speed of the turbocharger shaft are used as the data, from which the compressor derives the efficiency and the volumetric flow of the compressor. The downstream pressure is the intake manifold's pressure, with a 2% augmentation, to account for the pressure losses of the flow. The compressor block updates the mass flow and the enthalpy of the flow towards the intake manifold. The difference between the upstream and downstream enthalpy of the flow indicates the power required for the compressor to maintain its rotational speed. Dividing the power with the rotational speed, one gets the torque the compressor absorbs from the turbocharger shaft.

4.3.2 The Manifolds

The intake and the exhaust manifolds receive as inputs the enthalpy and the flow rates that enter and exit the system. The main parameters of the calculations are the temperature and the estimated volume of each manifold. Based on the initial conditions given to the blocks and the change of flow rates in and out of the manifolds one gets

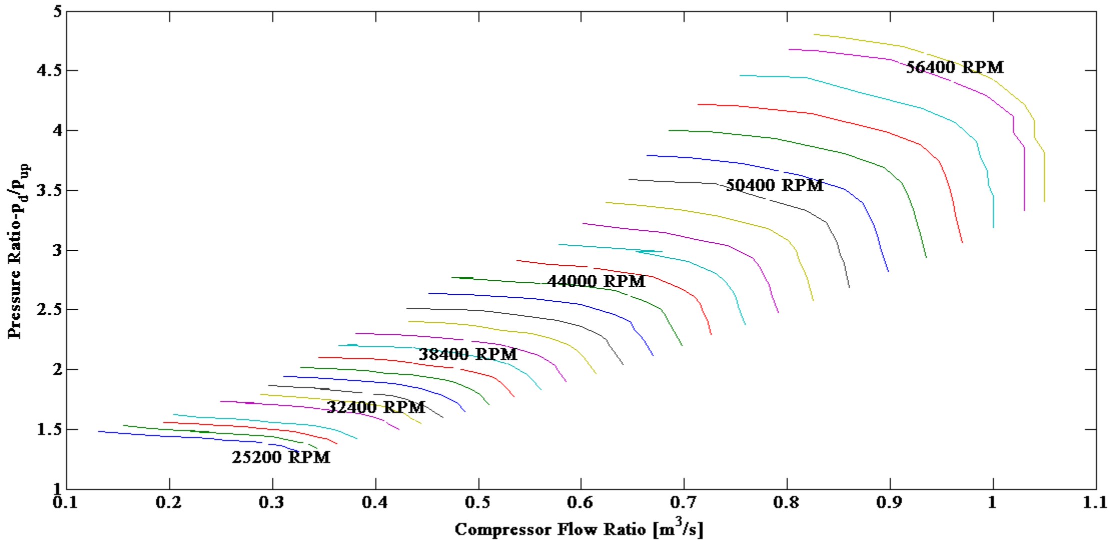

Figure 4.8: The compressor map with the rotational speed as parameter.

the instant mass flows and the temperature inside the manifolds. The pressure trace is derived from a simple application of the basic law of gases.

4.3.3 The Turbine

The turbine block loads the map which relates the effective geometrical areas of the turbine and the efficiency of the turbine with the pressure ratio downstream and upstream and receives as inputs the geometric area of the turbine, the pressure and temperature traces downstream-upstream the turbine and the mass flow rate from the exhaust manifold. The map does not take into account the rotational speed, but rather perceives the turbine as an orifice with constant cross sections. The block calculates the static temperature and pressure at the outlet of the turbine with the help of the the efficiency indication of the map, in order to derive the total downstream enthalpy. The difference between the total enthalpies downstream and upstream indicates the power absorbed from the gas by the turbine and offered to the turbocharger shaft. Using for the first calculation an initial assumption for the shaft rotational speed and then using the change of the rotational speed from the balance of the compressor and turbine torques, the torque which drives the shaft is calculated.

4.4 Model Verification

In this section the simulation results are compared to measured ones. The measurements are taken from runs of the engine at 25% of the rated engine load.

4.4.1 Pressure

The pressure produced by the simulation is compared with the the measured pressure trace in figure 4.9. The p-V diagram of both simulated and experimental traces is presented in figure 4.11. The relative error can be seen in figure 4.10. The relative error during the closed cycle, which is the main issue of concern, is smaller that 5%.

This value of the relative error appears mainly at the beginning of the compression and at the end of the expansion. This can be justified by the fact that at the start of the compression and the end of the expansion, as can be seen in figure 3.4, the slopes of the logarithmic p v diagram appear to differ from the slopes of the rest of the process. This deviation from the isentropic behavior can be attributed to heterogeneousness of the working fluid in the cylinder after the closing of the intake valve and at the start of the blow out process. Nonetheless the deviation from the simulated pressure trace is still limited. The error at the combustion start reaches a local maximum. This can be attributed to the methodology followed. According to Matekunas [14] and [15] the pressure ratio curve and the heat release curve reach the 50% fuel mass fraction burnt point with approximately 2 degrees difference. Therefore, a higher error occurs locally, because at this point a sharp pressure augmentation takes place.

4.4.2 Temperature

Results from simulation for in cylinder temperature are presented in figure 4.12. For the in cylinder temperature there were no measurements available from MAN L16/24 for validation. The temperature of the working fluid inserted in the cylinder has the same temperature as the temperature in the intake manifold at the start of each engine cycle. The heat absorbed at this part of the cycle because of the already heated cylinder walls is neglected. It gradually increases as the compression occurs and augments sharply at the crank angle where the combustion starts. During the expansion the temperature descends. Until the end of the expansion the temperature is calculated with thermodynamic equations. After the exhaust valve opening the temperature descends until it reaches again the temperature of the intake manifold. The temperature trace is defined assuming that from the point where the exhaust valve opens, it descends linearly with the crank angle to the intake manifold temperature.

4.4.3 Heat Release Rate

The heat release rate curve between the measured and the simulated cycle is depicted in figure 4.13. The sum of the net heat released is depicted in figure 4.14. The latter is calculated, by integrating the simulated net heat release rate. Its form is similar to the mass fraction burnt function, as approximated in subsection 3.3.3 and depicted in figure 3.8.

4.4.4 Air induced in the cylinder

The flow of air towards one cylinder and the total amount of air trapped in the intake process are depicted in figure 4.15. The latter is calculated, by integrating the former.

4.4.5 Traces Calculated on a Cycle Basis

The traces calculated on a cycle basis are considered the IMEP, the FMEP, the BMEP, the mechanical efficiency, the torque and the mean brake power of each cylinder. The results of the IMEP, the Power and the torque produced are presented in the following figures, in which the calculation of each trace during a 10 seconds operation (100 engine cycles) is depicted. For the shake of comparison the mean value of each measurement, according to the experimental data, is plotted as well.

In the following figures the depicted traces do not appear to be constant but rather deviating between limits close to the average measured corresponding traces. In figure 4.16, the torque appears to deviate between 1005 Nm and 985 Nm, staying constantly close to the average measured torque, which is equal to 994.8 Nm.

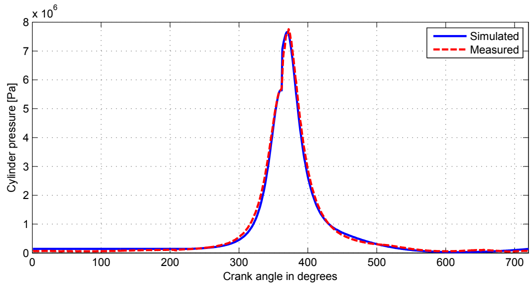

Figure 4.9: The simulated and measured pressure traces.

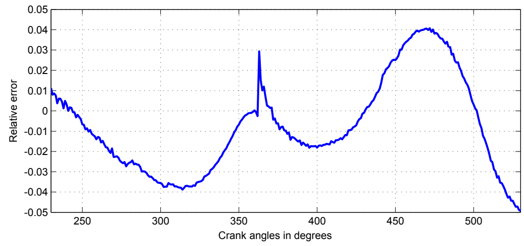

Figure 4.10: The relative error between the pressure traces in the closed cycle of the engine.

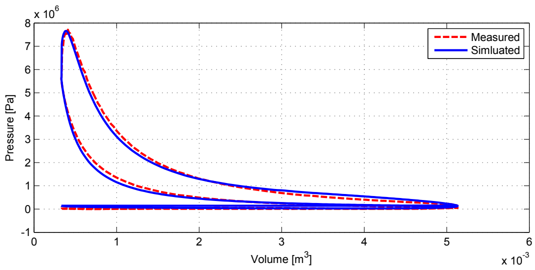

Figure 4.11: Simulated and measured p-V diagram.

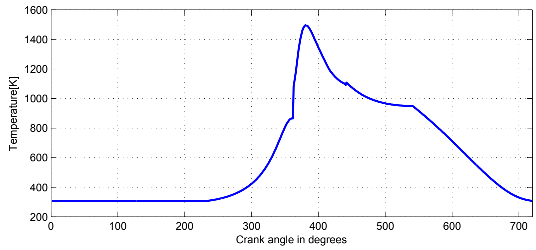

Figure 4.12: The simulated temperature trace.

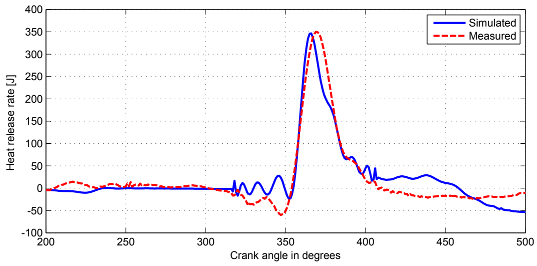

Figure 4.13: Simulated and measured heat release rate.

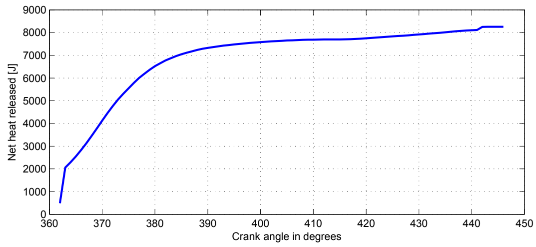

Figure 4.14: The net sum of the heat released by the fuel.

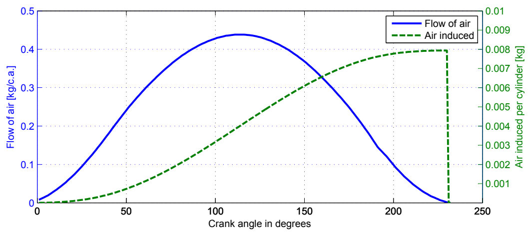

Figure 4.15: The flow of air into the cylinder and the total amount of air captured per cycle.

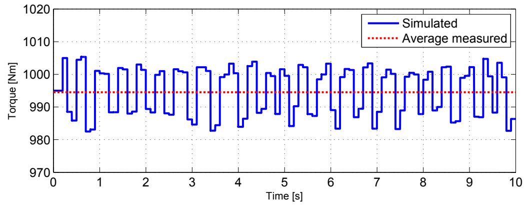

Figure 4.16: The calculated mean torque per cycle and the mean measured torque.

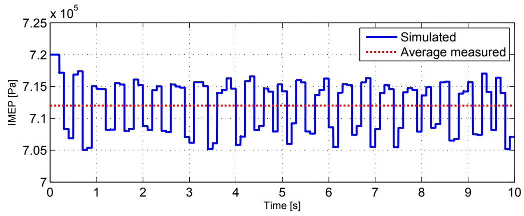

Figure 4.17: The calculated IMEP and the mean measured IMEP.

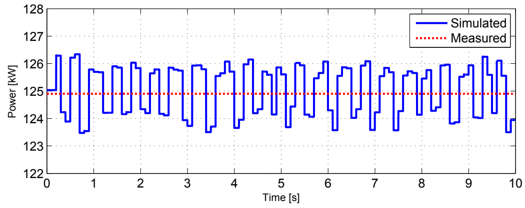

Figure 4.18: The calculated mean power per cycle and the mean measured power.

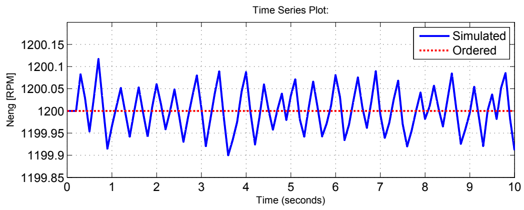

Figure 4.19: The calculated rotational speed of the engine and the ordered engine speed.

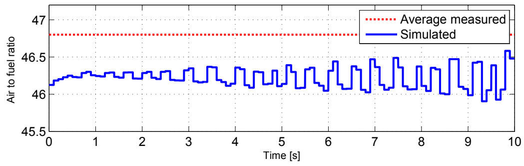

Figure 4.20: The air to fuel ratio calculated on a cycle basis and the average air to fuel ratio measured.

Chapter 5

Controller Design and Implementation

In this chapter the process of the robust controller development is described. The controller was designed based on the linearized model acquired with numerical methods from the non-linear model. The linear model has a transfer function form with the output being the intake pressure and the input being the valve position. With the linear model available, the robust controller was designed. Details from the selection of the controller parameters and their evaluation are also presented. Finally, the controller was tested in simulation with both the linear and the non-linear models.

5.1 The Linear Model

In order to acquire a linear model from a complicated non-linear model, one can either perform an analytical linearization through calculations of the derivatives of the equations of the system (Jacobian matrices), or a numerical one through the processing of perturbations in a computational environment.
In this thesis, the numerical method was chosen, because firstly three engine maps intervened in the linearization path (the compressor and turbine maps and the rack position to fuel injected map) and secondly because of the complexity between the model interconnections.
In the Matlab environment Simulink provides the Linear Analysis Toolbox, which gives the capability to derive a linear model from a complex non-linear process representation. The procedure started by defining a set of operating instances at which the model would run in equilibrium. Then the input and output signals in the model were defined and for these variables the linear model will provide a relation. At each instant the toolbox would force a set of perturbation signals in the input based on the output response a transfer function would be calculated. Since the linearization was performed at a specific operating point, the derived function is appropriate only for this particular point. The frequency response of the model derived through the linearization process is depicted in the Bode diagrams of figure 5.1. The continuous transfer function of the selected system is described in equation 5.1, whereas the discrete transfer function (sampling time 0.001 seconds, zero order hold) is described in equation 5.2.

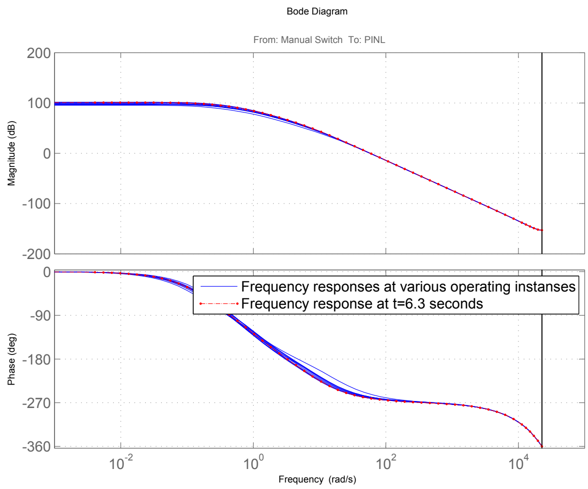

Figure 5.1: The frequency response of the model trimmed at various operating instances.

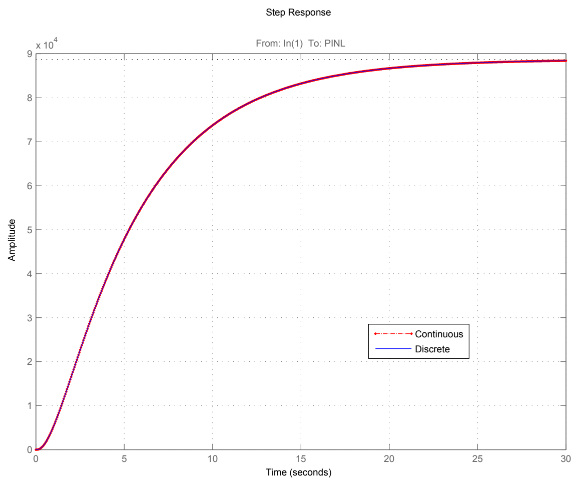

Figure 5.2: The step input response of the continuous and discrete transfer functions.

$$pinl_{continuous}(s) = -2.11e-06\frac{(s)(s+251.1)(s+9.851)(s+1.502)(s+0.904)}{(s+262)(s+11.44)(s+9.063)(s+1.39)(s+0.99)^2} \tag{5.1}$$

$$pinl_{discrete}(z) = 8.779e-08\frac{(z+3.729)(z-1)(z-1)(z-0.9986)(z-0.9657)(z+0.2677)}{(z-0.9643)(z-0.9984)(z-0.9987)(z-1)^3} \tag{5.2}$$

The step response of both the continuous and the discrete realization of the model is depicted in figure 5.2. It can be seen that the two transfer functions have identical responses.

5.2 Controller Design

Based on the acquired continuous transfer function a robust controller was designed. The design objectives are summarized as follows:

- The converged value is desired to be tracked steadily with no steady state oscillations around the reference value.
- The output (pressure in intake manifold) should follow the reference input.
- The intake pressure signal should converge with no overshoot.
- The controller shall generate signals ranging from 0 to 1, without violating the maximum allowed limit.

The control requirements in robust control are achieved through the specifications of the weighting functions. Three weighting functions were chosen in order to implement the above mentioned requirements. The most important weighting function is the performance weight, which bounds and forms the shape of the sensitivity function (S). Secondly, the control input was bounded to secure that the supplied control values are smaller than 1. Finally, care was taken to bound the complementary performance function so as to limit the effects from the noise in the measurements and to secure that T is greater than 1 in small frequencies. The steps followed to design the controller are described below.

Scaling of the system

In this application the plant was normalized with its infinity norm. This norm defines the scaling gain. The scaling gain is

$$g_{scale} = 8.8680e + 04$$

Thus, the controller is designed for a non dimensional plant. The error signal inserted as an input to the controller is normalized with the same scaling gain. The normalized system is the system upon which the augmentation takes place, through the inclusion of the weighting functions.

Order reduction of the system

The order of the transfer function of the linearized system is now reduced. In this way the lower order model will provide a controller with lower order, a beneficial feature for implementation. The transfer function of the reduced model is described in equation 5.3. The Bode diagram of both the reduced and the original model is depicted in figure 5.3. For frequencies lower that 10 rad/s the reduced model retains the characteristics of the original model.

$$pinl_{reduced} = 0.0021358 \frac{[s - (5.2431 + 8.4032i)][s - (5.2431 - 8.4032i)]}{(s + 0.2017)(s + 1.039)} \tag{5.3}$$

Evaluation of the transfer function of the linearised reduced system

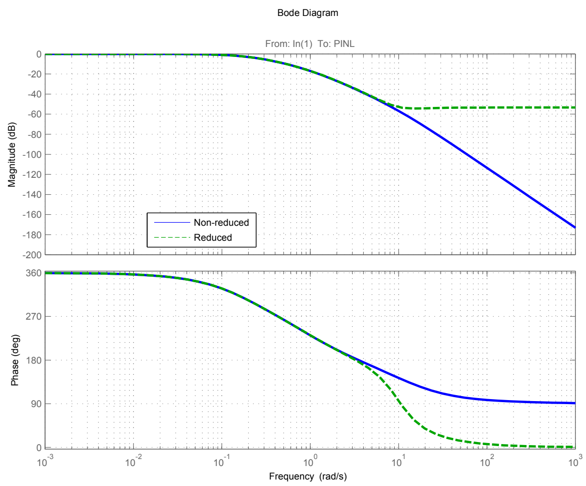

Figure 5.3: The Bode diagram of the reduced and the non reduced model.

The transfer function 5.3 contains two conjugate RHP zeros, which are unstable. These RHP zeros pose certain limitations to control: The main cause of concern is the bandwidth and the control gain limitation posed by the RHP zeros. Firstly, over a certain controller gain the closed loop poles (the poles of the complementary sensitivity function T) tend to reach the values of the open loop zeros (the zeros of the transfer function L). This is concluded from equation 5.4. As the controller gain takes higher values the closed loop poles of the system are moving close to the open loop zeros. A system with poles in the RHP is unstable, therefore care should be taken to avoid great control gains. Thus, the feedback control gain is upper limited.

$$T(s) = \frac{L(s)}{1 + L(s)} = \frac{K(s)G(s)}{1 + K(s)G(s)} \tag{5.4}$$

To examine the bandwidth limitation of the RHP open loop zeros on the control design, the theorem described in [2] by Zames stating that if the system has no RHP poles the bounded sensitivity function $|W_P S|$ has as a lower limit the value of the weight W_P at the area of frequencies near the real part of the conjugate zeros. This limitation is posed in order to secure control stability. Therefore,

$$||W_P S|| \geq |W_P(z)| \tag{5.5}$$

Since there is this lower limitation of the bounded sensitivity function and the objective is to secure that

$$||W_P S||_\infty \ < \ 1 \tag{5.6}$$

it is at least required that

$$|W_P(z) < 1| \tag{5.7}$$

Adopting the form of the weighting function described in equation 2.42 the requirement in 5.7 yields that

$$|W_P(z)| \Rightarrow \ |\frac{z/M_P + \omega_B}{z + \omega_B A}| < 1 \Rightarrow \ \omega_B < -\frac{x}{M_P} + \sqrt{x^2 + y^2(1 - \frac{1}{M_P^2})} \tag{5.8}$$

The real and the imaginary parts of the conjugate pair of zeros are symbolized as x and y respectively. It is thus concluded that, according to how strict the performance requirements are (summarized as the value selected for M_P) the bandwidth is upper limited. The limit is lower for tight control (small M_P values) and greater for loose control (greater M_P values). Therefore, the weighting specifications M_P and ω_B are not selected independently, but rather the latter is calculated as a function of the former.

Weight selection

The weighting functions specifications are selected next. The performance weighting function is described by equation 2.42 and the closed loop weighting function by equation 2.44. The selected specifications are outlined in table 5.1.

Specification/Weight	W_P	W_U	W_T
peak M [-]	1.052	-	1.035
bandwidth ω_B [rad/s]	0.8725	-	0.8725
order n [-]	2	1	2
gain [-]	1	$10^{1.25}$	1

Table 5.1: The selected specifications for the weighting functions

- M_P and M_T are selected to be small, in order to achieve the tracking of the trace adequately, in steady state conditions. This selection yields a low bandwidth upper limit, to satisfy the stability criterion.
- ω_{BP} and ω_{BT} are both selected to be equal to the upper limit of the performance function bandwidth. It is the greatest bandwidth achievable, taking in mind that M_P and M_T are selected close to 1, to achieve acceptable reference tracking.
- The order of the weight W_P is selected 2, to compensate for the low upper limit of the bandwidth. Thus, S stays below 0.707 dB for a greater range of frequencies. This secures that the error signal is not amplified over these frequencies. The order of the weight W_T is selected 2, so as to achieve noise rejection in high frequencies.
- The gain of W_u is selected as $10^{1.25}$ a value for which the maximum expected control requirement (close to 2 bar) was achieved and the control input did not produce a signal greater than 1.

The Bode diagrams of the frequency response of the L, S, T and KS transfer functions are depicted in figures 5.4 and 5.5.
The continuous transfer function of the controller is described in equation 5.9 and the corresponding discrete transfer function (sampling time 0.001 seconds, zero order hold method), is described in equation 5.10.

$$Khinf_{continuous} = 1.3993 \frac{s^2 + 0.2918s + 0.02166}{(s + 0.02593)(s + 0.02968)} \tag{5.9}$$

$$Khinf_{discrete} = 1.3993 \frac{z^2 - 1.88z + 0.9577}{(z - 0.95)^2} \tag{5.10}$$

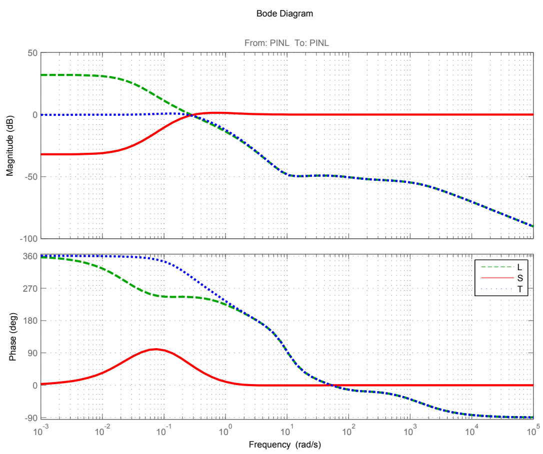

Figure 5.4: The Bode diagram of the L, S, T transfer functions of the system.

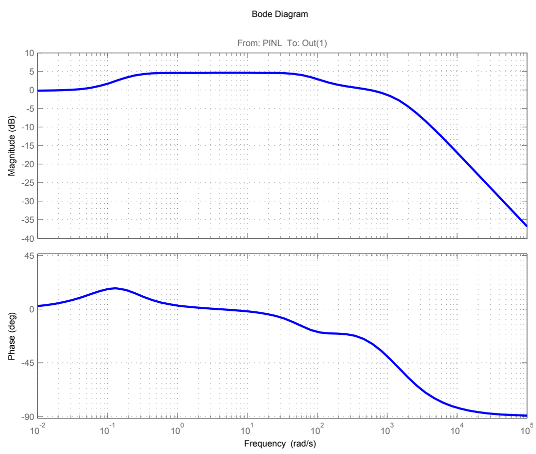

Figure 5.5: The Bode diagram of KS of the system.

The closed loop transfer function T is described in equation 5.11. T is stable and the RHP open loop zeros have not moved to the place of the poles of the closed loop function. The poles of T lie on the LHP and therefore T is considered stable. Hence, closed loop instability which is a matter of concern under the presence of RHP zeros in the transfer function of the system is avoided.

$$T(s) = 0.0037187\frac{(s+0.1175)(s^2-10.57s+95.76)}{(s+1.039)(s^2+0.3735s+0.04131)} \tag{5.11}$$

5.3 Linear Model Simulation

In order to evaluate the controller performance, simulation with the linear model is performed. The model has a conventional feedback structure and is depicted in figure 5.6. The offset point for the initial intake manifold pressure is 1.35 bar. In figure 5.7 the step response to a step reference of 1.65 bar is depicted. The output response has an overshoot of 0.025 bar and then it converges to a steady state value with a steady state error of 0.01 bar. This is expected due to the RHP zeros of the system. In figure 5.8 the required valve displacement is depicted. The controller requires the valve to deviate 55% of its original position, and before the output reaches the reference value for the first time, the control command is reduced to a 35 % steady displacement. In the simulation, a white noise [1] signal was added in the feedback loop, to simulate possible noisy measurements.

5.4 Non-linear Simulation

In this section, the integration of the controller in the non linear system is described. The simulation concerned a 10 s engine operation, which corresponds to 100 engine cycles. It is considered that the engine runs in steady state conditions, at the start of the simulation. The air injection starts at the beginning of the simulation. The intake

[1] A White noise is a signal defined with statistically uncorrelated values in time, with a constant spectral density. The mean value is zero and the variance is finite.

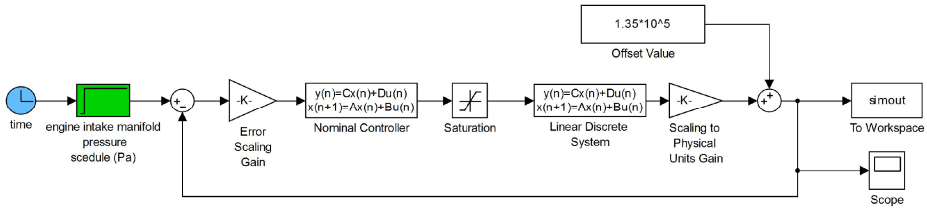

Figure 5.6: The closed loop system with the linear model

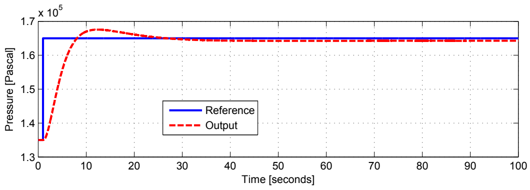

Figure 5.7: The step reference and the step response of the closed loop linear system.

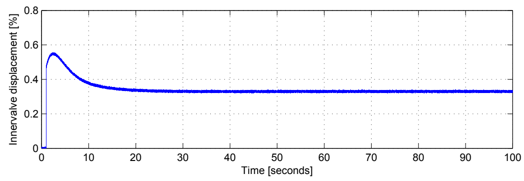

Figure 5.8: The control output of the controller in the linear simulation.

manifold pressure reference is 1.65 bar, at a load equal to 25 % of the maximum load. The effect of air injection on various engine parameters is examined in the corresponding figures.

5.4.1 The Intake Manifold Pressure

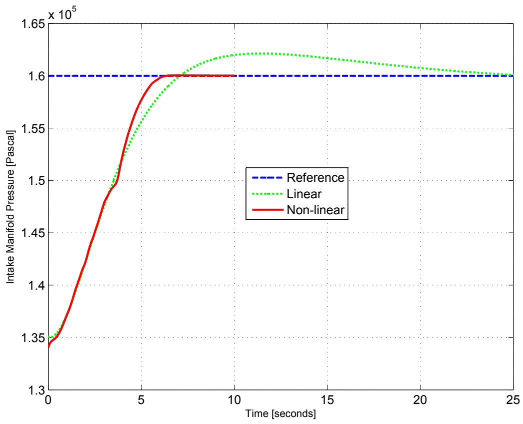

Figure 5.9: Comparison of the intake manifold pressure in the linear and the non linear model.

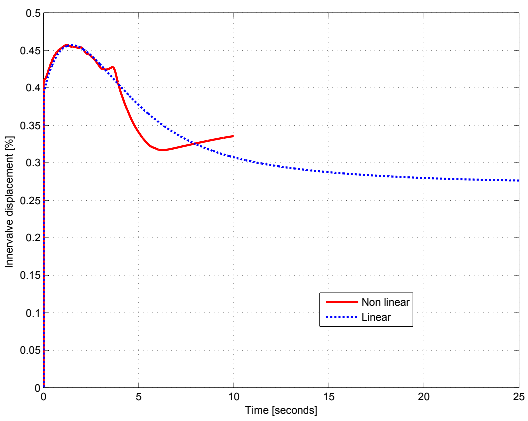

Figure 5.10: Comparison of the control command of the robust controller designed, in the linear and the non linear model.

In figure 5.9 the intake manifold pressure in the linear and the non-linear model are compared. The first remark is that the linear trace, during the initial transient period from the start of the simulation until the 4th s, follows adequately the non-linear trace. After the 4th s, the two traces appear to differ. This is attributed to the

fact that the system model is reduced, therefore dynamics in higher frequencies were neglected. Moreover, in the non-linear model the valve actuator is explicitly included, adding slower dynamics in the system, causing the overshooting avoidance. In the linear model it is included in the general transfer function of the system.
The non linear model converges slowly and with no overshoot to the reference value at the 6th s. After the 6th second the reference is tracked with no steady state error, until the end of the simulation.
In figure 5.10 the control command in the linear and the non linear model are compared. As already noted, the two control signals are similar until the 4th s.

5.4.2 Injected Air Flow

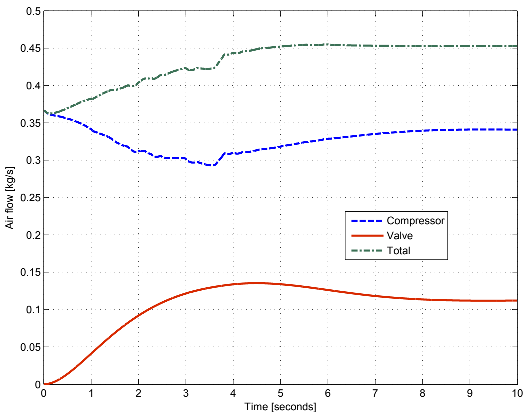

Figure 5.11: The flows of air during the air injection process from the valve and the compressor.

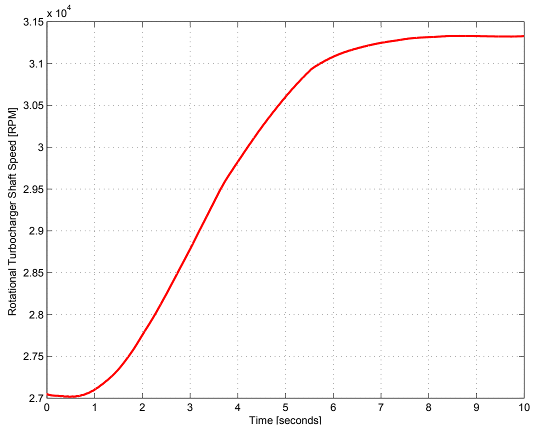

Figure 5.12: The rotational speed of the turbocharger shaft.

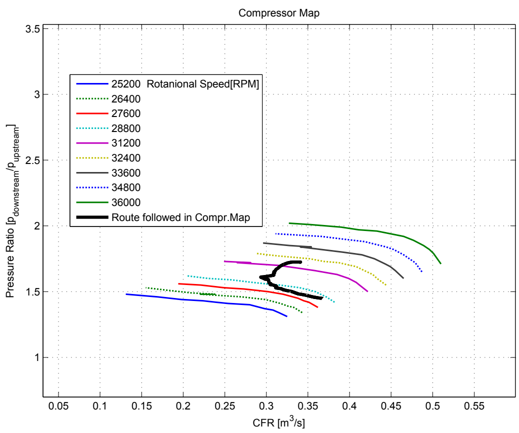

Figure 5.13: The route followed on the compressor map during the air injection procedure.

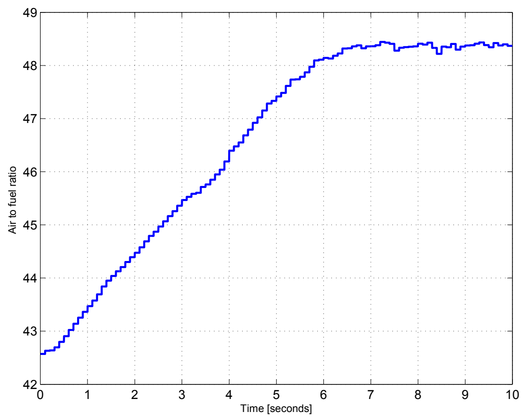

Figure 5.14: The air to fuel ratio during the air injection process.

In figure 5.11 the flow rate of air, during the air injection process, from the valve and from the compressor are depicted. The compressor flow rate decreases, as additional air is injected downstream the compressor at the start of the process. The trajectory of the pressure ratio and the compressor provided flow rate on the compressor steady state map during the air injection process is depicted in figure 5.13. The reason of the flow decrease from the compressor is that as the air induced in the cylinders is constant due to the constant engine speed, the additional amount of air can be provided externally. Figure 5.14 shows the respective air to fuel ratio. In figure 5.12 the rotational speed of the turbocharger shaft during the air injection process, is depicted.

5.4.3 Fuel Injection

In figure 5.15 the rack position and the mass fuel injected per engine cycle and per cylinder are depicted. The feedback to the speed controller is the error between the required rotational speed (1200 RPM) and the actual rotational speed of the engine. The governor based on this error regulates the rack position in order to keep the engine's speed close to the reference value. As can be seen in this figure the rack position indicates a decrease in the fuel injected as the additional air injected causes the torque produced by each cylinder to augment.

In figure 5.18 the curve representing the kilograms of fuel consumed, for the production of one kW is descending each cycle since the start of the air injection process. From this figure, it can be concluded that the air injection process, as a means of augmenting the intake pressure, decreases the cost of the production of each kW. Nevertheless, the production of compressed air is a matter of concern. The compressor filling the air cells consume diesel oil, or fraction of the exhaust gases. Therefore, it is possible that the overall cost of producing compressed air overwhelms the benefits of the air injection.

The rotational speed of the engine is depicted in figure 5.16, whereas the torque produced is depicted in figure 5.17. The ratio between the fuel consumed and the power produced per cycle is depicted in figure 5.18.

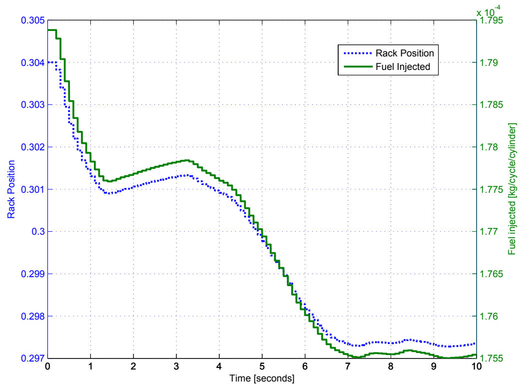

Figure 5.15: The rack position and the injected fuel mass.

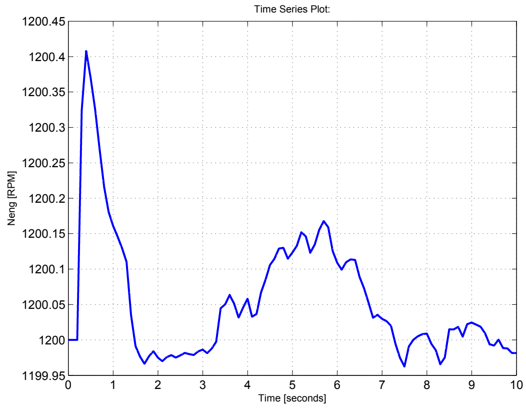

Figure 5.16: The rotational speed of the engine during the air injection process.

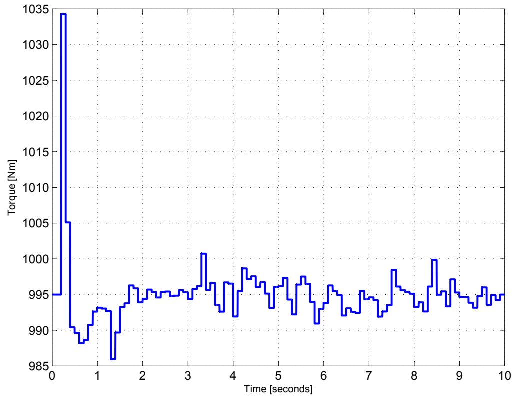

Figure 5.17: The torque produced by the engine during the air injection process.

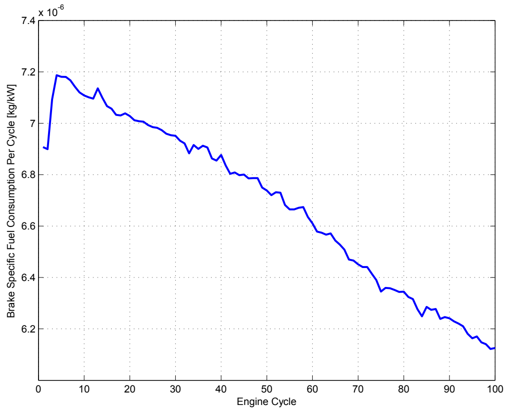

Figure 5.18: The brake specific fuel consumption per cycle.

5.4.4 In Cylinder Traces

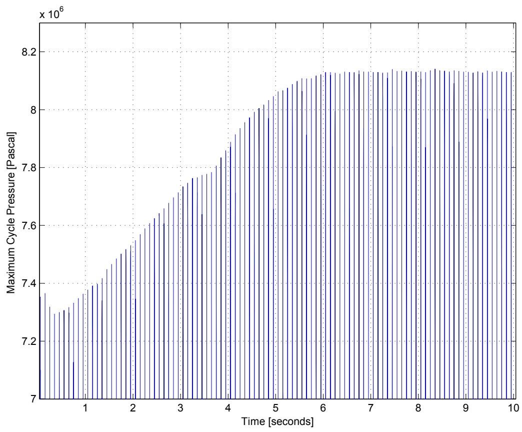

Figure 5.19: The maximum cylinder pressure per cycle.

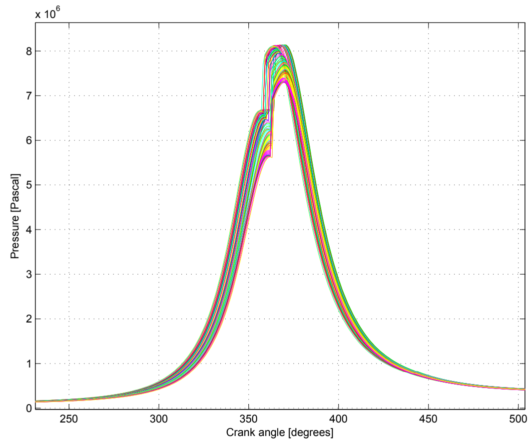

Figure 5.20: The in cylinder pressure per cycle.

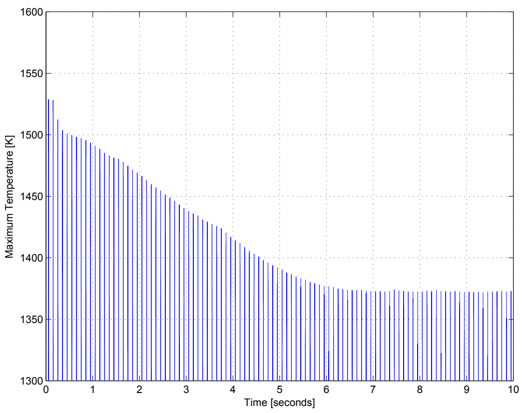

Figure 5.21: The maximum in cylinder temperature per cycle.

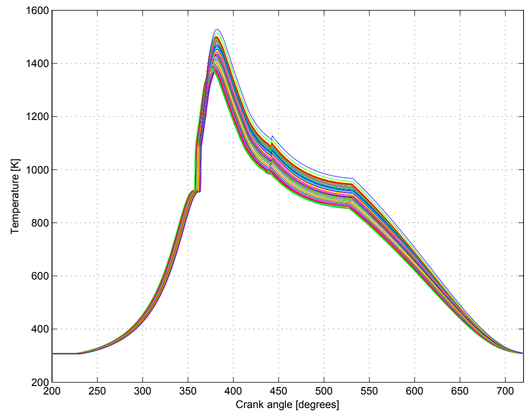

Figure 5.22: The in cylinder temperature per cycle.

The in cylinder pressure trace and the in cylinder temperature, for all engine cycles during the simulation of 10 s are depicted in figures 5.20 and 5.22 respectively, whereas the maximum pressure and temperature of each cycle are depicted in figures 5.19 and 5.21 respectively. The pressure trace is affected by the air injection process in more than one ways. The compression phase offsets from a higher pressure due to the augmented intake pressure. Therefore, the combustion phase commences from a constantly higher pressure as well.

Nevertheless, apart from the augmented intake pressure, as more fresh air flows in the cylinder, the maximum ideal temperature increase (defined as dT_{comb} in equation 3.10) decreases, during the control process. The reason for this, is that the heat released from the combustion, is used to heat up a greater amount of air. Hence, the maximum temperature of the cycle is also affected towards lower values. This remark is stated by Black in [17] as well. According to Black, when there is surplus of air, the temperature of the mixture is decreased, because the additional products of the combustion process (H_2O, N_2, O_2) absorb a fraction of the heat released by the combustion. Finally, the

fuel injected per cycle is gradually decreasing as depicted in figure 5.15. Similarly, this affects towards lower values the maximum temperature as well.
The overall augmention of pressure in the compression phase of the cycle, according to the model developed, overwhelms the two other contradicting effects of the air injection procedure. Thus, greater maximum pressure is achieved.

5.5 Controller Implementation in the Experimental Facility

The controller already integrated in the non linear, Simulink, crank angle based model of the MAN L16/24 experimental engine, is then used as a means of achieving closed loop control of the intake manifold pressure. The tests were carried out, using a USB data acquisition card and a Simulink interface, depicted in figure 5.23. Through the interface, the intake pressure signal was acquired, and the control command was produced.
From the Simulink interface the data acquired were the control command and the intake manifold pressure. However, in order to examine the effects of the closed loop air injection, additional data concerning the engine were required. This set of data was acquired using the AVL data acquisition card, which is typically used by the Laboratory, for data acquisition purposes concerning the MAN L16/24 experimental engine. The measurements under consideration were the in cylinder pressure trace from cylinder 1, the torque produced by the engine, the injected mass flow, the compressor provided flow, the exhaust gas temperature, the rotational speed of the engine and the turbocharger.

Signal Conversion

The measured pressure signal was acquired as an electrical potential difference and the produced control command was converted to an electrical potential difference as well. As far as the intake pressure signal is concerned, 1 Volt measured corresponded to 10^5 Pa. In equation 5.12, the transfer function relating the required percentage of the valve maximum opening and the corresponding potential difference is described.

$$V[Volt] = \frac{25 + Op[\%]}{12.5} \tag{5.12}$$

Signal Filter

The measured intake manifold pressure contained a great amount of noise in the measurement, therefore, a low-pass[2] filter was integrated, in order to achieve a more reliable estimation. The Bode diagram of the transfer function of the filter is depicted in figure 5.24. The specifications of the filter are described in table 5.2. The design method of the filter was the elliptic method. Elliptic filters offer steep roll off characteristics, without the necessity of increasing the order of the filter. Therefore, the order of the filter is selected 1. The frequency over which, the effect on the measurement of the

[2]A low-pass filter decreases the amplitude and therefore the effect of sinusoidal forms of high frequencies. The noise in measurements typically consists of such high frequencies sinusoidal waveforms.

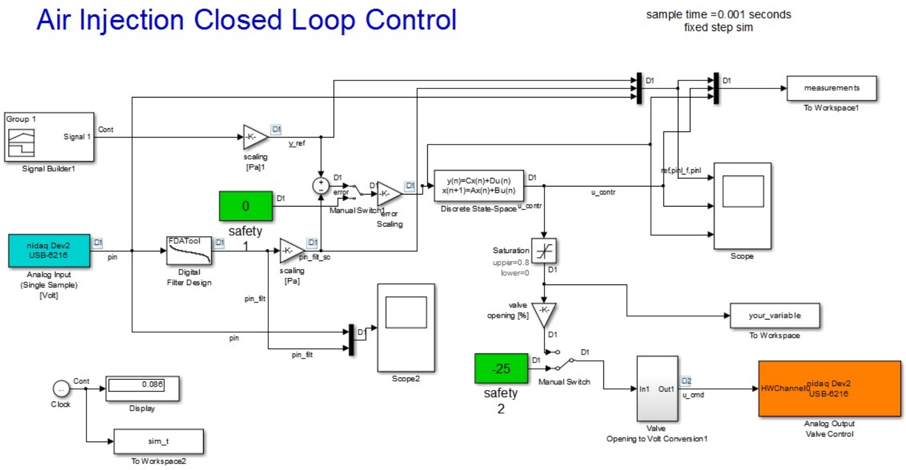

Figure 5.23: The Simulink interface.

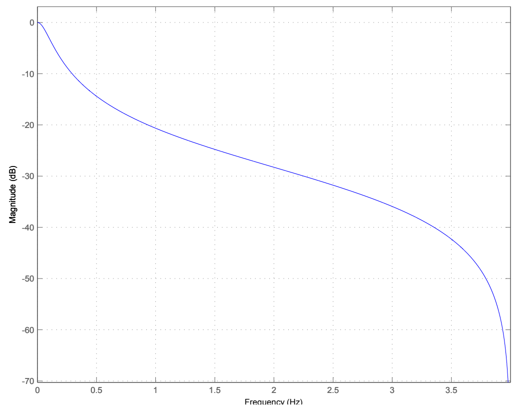

Figure 5.24: The Bode diagram of the low pass filter.

Response Type	Lowpass
Design Method	Elliptic
Order	1
Maximum Frequency Passing	0.05

Table 5.2: The design specifications of the low pass filter.

high frequency wavelengths is decreased, is 0.05 Hz.

Chapter 6

Experimental Results

In this chapter, the results from the air injection experiments carried out at LME using the robust controller are presented. The experiments are divided according to the reference setpoint. The main set of experiments were carried out using a single step type reference. The results which are presented concern both the control performance and the effect of air injection on various parameters in the engine (e.g. turbocharger rotational speed, compressor mass flow, in cylinder pressure). Apart from this set, the control results of experiments using a double step, a triple step and a ramp as setpoint reference are presented.

6.1 Experimental Schedule

In table 6.1 the schedule of the experiments carried out, using an impulse type reference is described, for single step input reference. For the load of 25%, linear models are derived through linearization, as described in previous chapters.

Experiment	Duration [s]	Load [%]	Offset [bar]	Setpoint [bar]
1	10.00	20	1.30	1.60
2	10.00	20	1.30	1.75
3	10.00	20	1.30	1.90
4	10.00	25	1.34	1.64
5	10.00	25	1.34	1.79
6	10.00	25	1.34	1.94
7	10.00	30	1.42	1.72
8	11.25	30	1.42	1.87
9	11.25	30	1.42	2.00

Table 6.1: The schedule of the experiments, for single step input.

6.1.1 Experiments at 25 % Engine Load (nominal)

The results from the experiments 4, 5 and 6 are examined first. The load of 25% is considered as the nominal operating point, as for this operating point, the linear engine model was used for the controller design. In order to validate the results of the developed model, the experimental results of the experiments are compared with the simulation results.

Experiment 4: Results

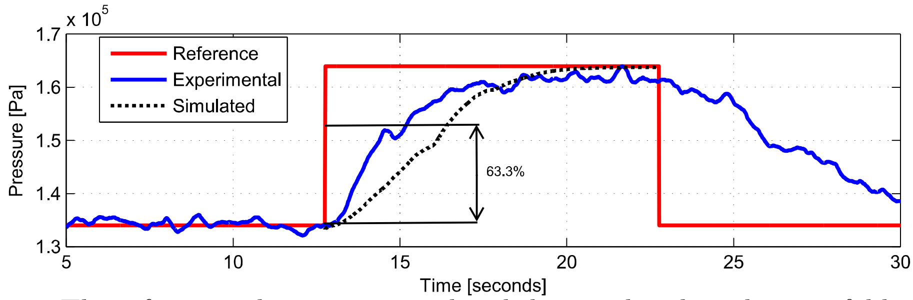

Figure 6.1: The reference, the experimental and the simulated intake manifold pressure.

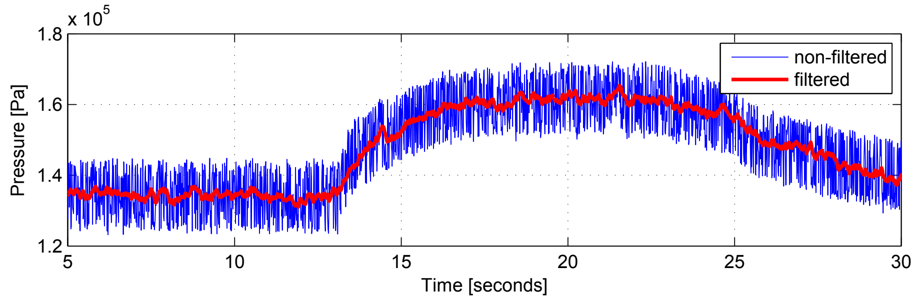

Figure 6.2: The filtered and the non filtered measurement.

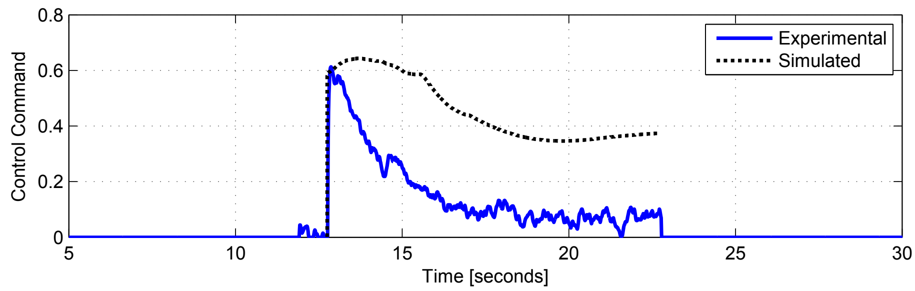

Figure 6.3: The control command produced by the controller.

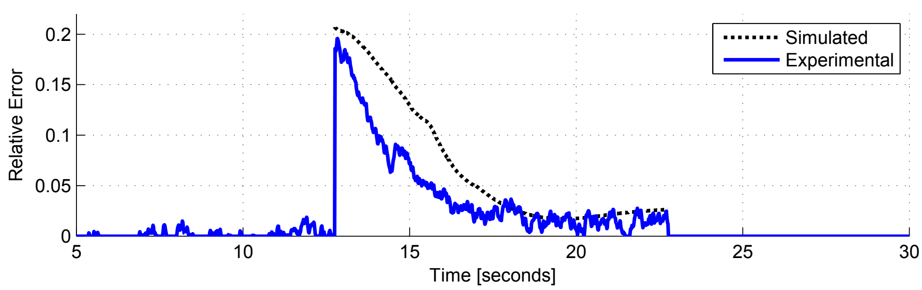

Figure 6.4: The relative error achieved.

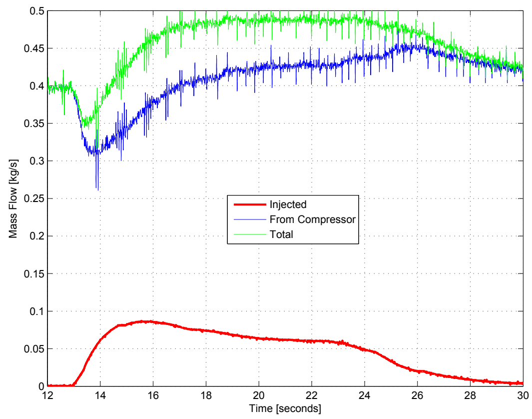

Figure 6.5: The experimental injected and compressor provided mass flows.

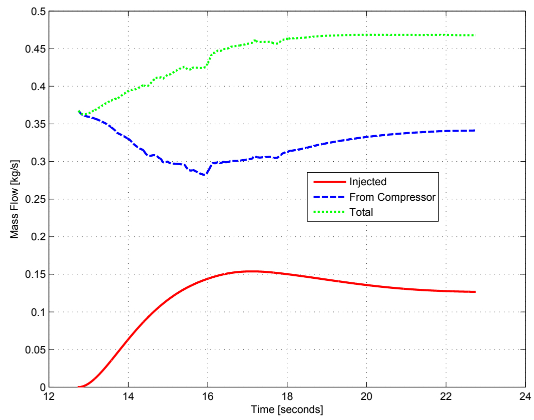

Figure 6.6: The simulated injected and compressor provided mass flows.

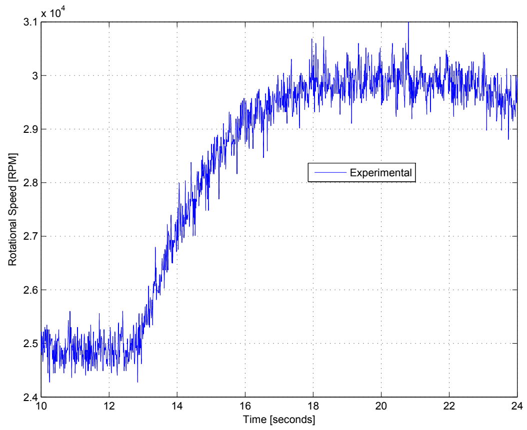

Figure 6.7: The experimental compressor rotational speed.

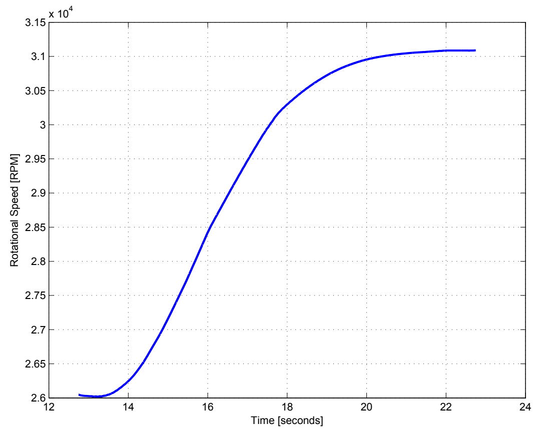

Figure 6.8: The simulated compressor rotational speed.

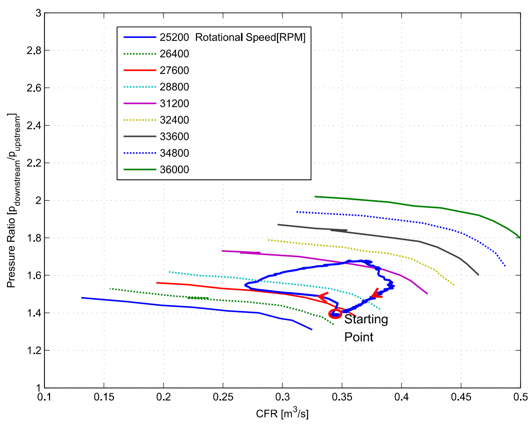

Figure 6.9: The experimental trajectory of the compressor air flow rate and the pressure ratio.

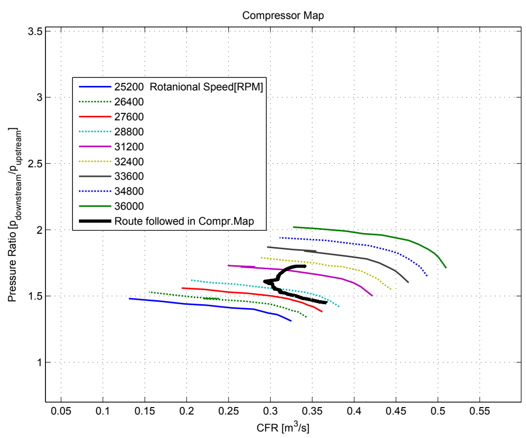

Figure 6.10: The simulated trajectory of the compressor air flow rate and the pressure ratio.

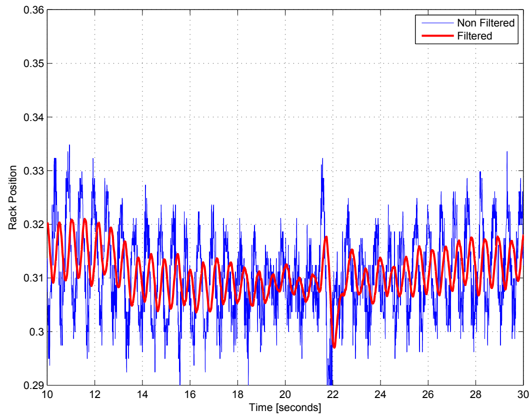

Figure 6.11: The experimental rack position.

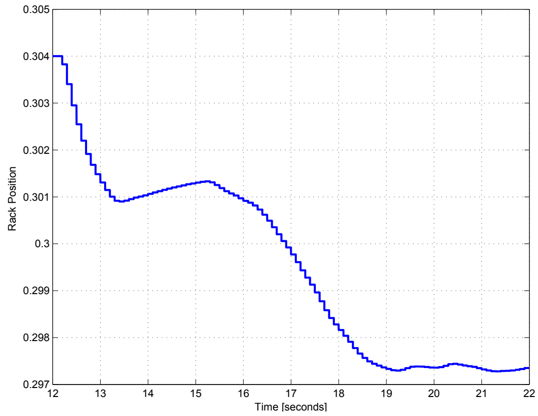

Figure 6.12: The simulated rack position.

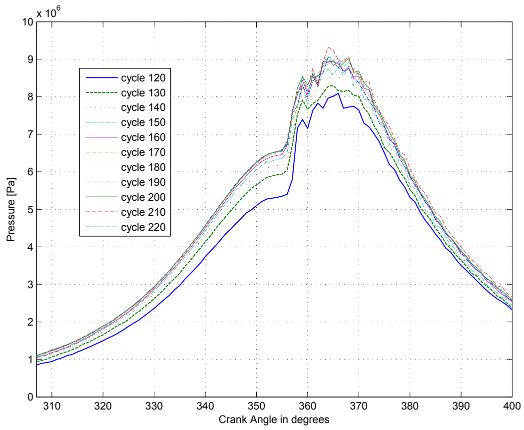

Figure 6.13: The experimental in cylinder pressure trace.

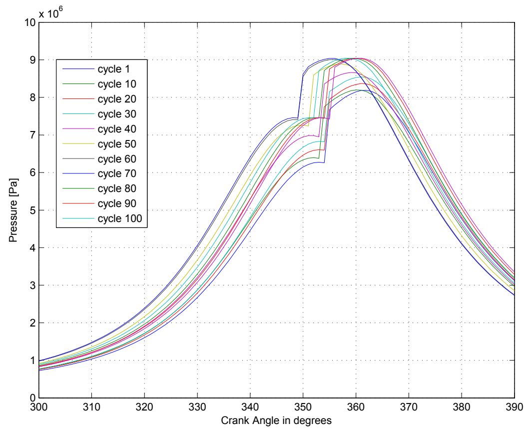

Figure 6.14: The simulated in cylinder pressure trace.

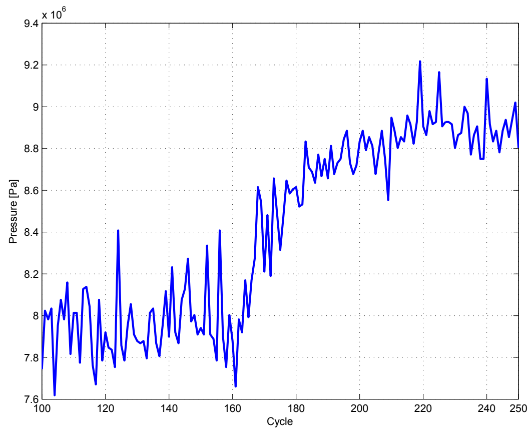

Figure 6.15: The experimental maximum in cylinder pressure trace per cycle.

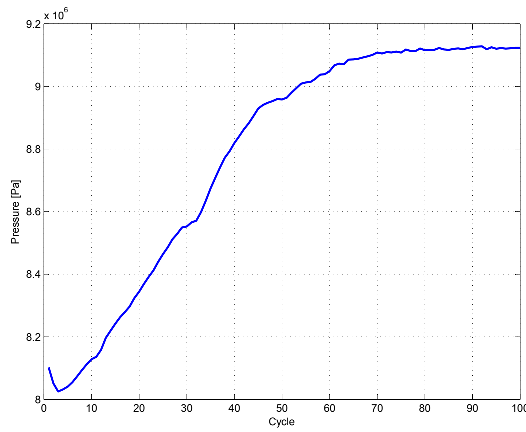

Figure 6.16: The simulated maximum in cylinder pressure trace per cycle.

Experiment 4 : Comparison between experimental and simulation results

In figure 6.1 the reference and the actual intake manifold pressure are shown, and in figure 6.2 the filtered and the measured pressure traces are depicted. The control command during the control process is depicted in figure 6.3, while the error achieved is depicted in figure 6.4.
In figure 6.1, the experimental and the simulated pressure traces are compared and the time constants [1] of both curves are marked. The experimental time constant is 1.75 seconds and the simulated time constant is 2.47 seconds. Reversing these constants, it is derived that the actual bandwidth is 0.5414 rad/s, whereas the simulated is 0.4049 rad/s. Examining the Bode diagram 5.4, the crossover frequency is 0.4049 rad/s as well. Hence, as confirmed by the results, the actual bandwidth, differs from the predicted one by 8 %. The deviations between the experimental and the simulated results have as a common cause the inaccuracies in the modeling of the dynamics of the system. To this difference contribute assumptions and simplifications (ie linearization, model reduction of linearized plant, various elements like compressor map etc.) that typically take place.
In figure 6.3, the commands of the controller produced in the experiment and in the non linear simulation, are compared. Even though both controllers produce initially the same control command, the one in the simulation decreases at a slower rate, because the non linear model's reaction to air injection is slower than the one of the actual system, therefore it does not converge to the setpoint as fast as the experimental trace.
In figures 6.5 and 6.6 the experimental and simulated injected and the compressor provided mass air flows are depicted. In figures 6.7 and 6.8 the experimental and simulated compressor rotating speed are described. Finally, the experimental and simulated trajectory of the air flow and the upstream-downstream compressor pressure ratio are depicted in figures 6.5 6.6. The simulated results appear to follow the experimental results.
In figures 6.5 6.6 the maximum experimental injected flow reaches the value 0.09 kg/s whereas in the simulated the value is 0.15 kg/s. Moreover the maximum is reached at second 15.2 in the experiment, whereas the simulated reaches the maximum at second 16.3.
In figure 6.7 the rotational speed of the turbocharger reaches a lower maximum rotational speed than the one in the simulation, depicted in figure 6.8. This is expected since in the simulation the additional air induced in the engine is greater, therefore the torque on the turbocharger shaft is greater as well. This offset reaches the value of 1000 RPM.
In figure 6.9 the trajectory of the flow provided by the compressor and the pressure ratio, reaches nearest to surge instability at the point of the lowest compressor provided flow rate. This point is approximately the same in the simulation, therefore it can be stated that the model is capable of indicating whether the compressor flow rate is close to reaching instabilities, even though the compressor map refers to normal operating situations, whereas this case contains transient features (rack deviation, rotational speed of the turbocharger deviations etc.).
In figures 6.11 and 6.12 the rack position during the air injection process is indicated.

[1] The time constant of a signal is the time between the commence of the process and the instant the 63.3 % of the reference signal is reached.

High frequency oscillations of due to noise are seen in the measured rack signal. In simulation the rack position drops, indicating that the air injection process, aiming to augment the in cylinder pressure, acts beneficially in terms of fuel consumption. A similar drop is also shown in the experimental results.
In figures 6.13 6.14 the in cylinder pressure cycles are plotted. This set of experimental data was acquired from cylinder 1. In figures 6.15 6.16 the maximum pressure per cycle is depicted. The model gives an accurate estimation of the maximum pressure during the air injection process, since the transition of the pressure trace towards greater traces is efficiently predicted.

Experiment 5: Results

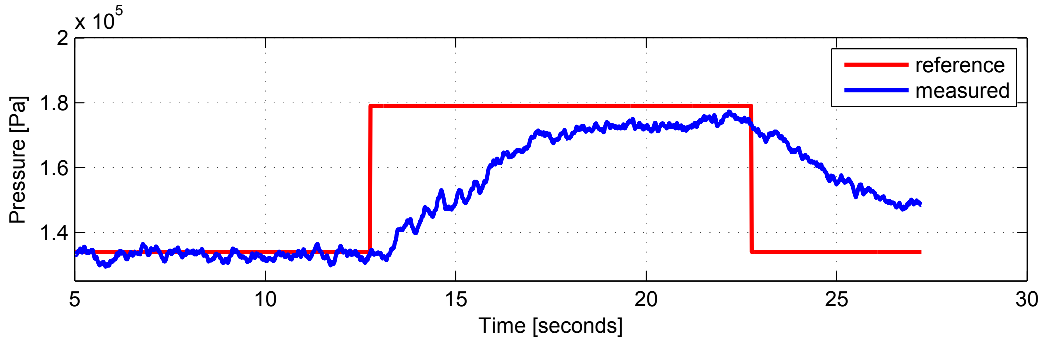

Figure 6.17: The reference and the experimental intake manifold pressure.

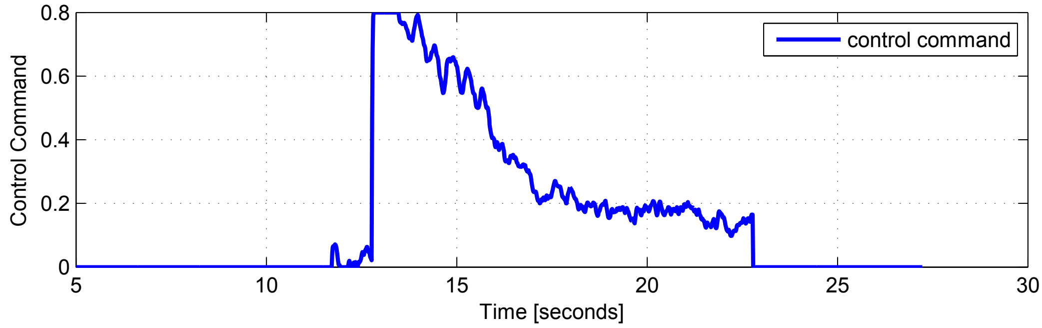

Figure 6.18: The control command during the air injection process.

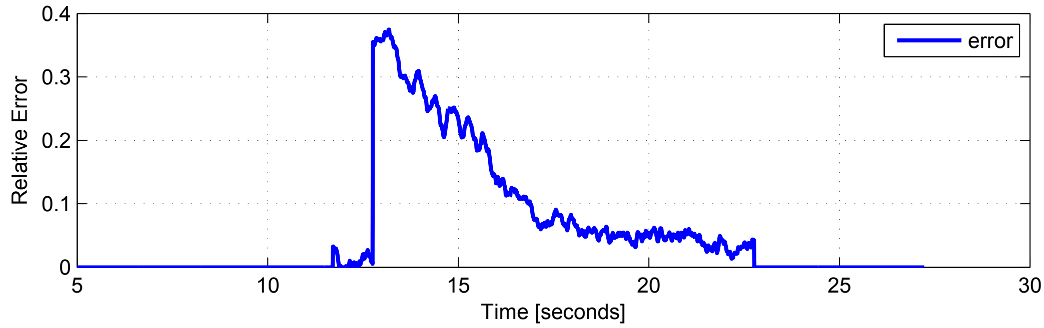

Figure 6.19: The relative error achieved.

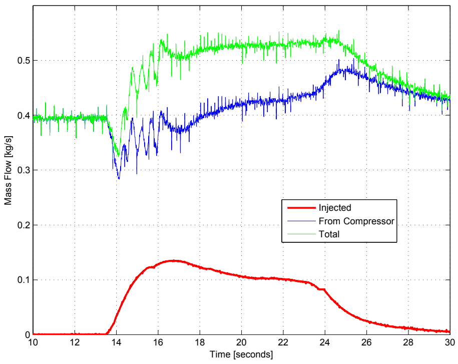

Figure 6.20: The injected and compressor provided mass flows.

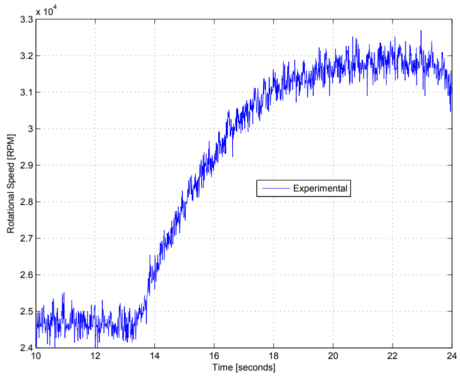

Figure 6.21: The rotational speed of the turbocharger shaft.

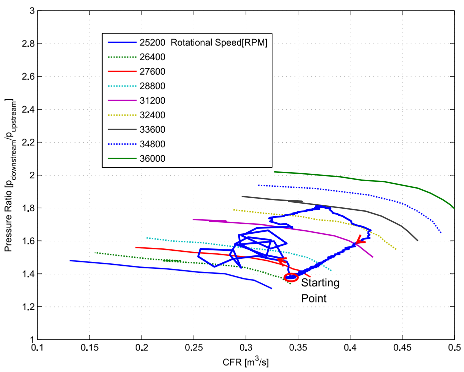

Figure 6.22: The trajectory of the compressor air flow rate and the pressure ratio.

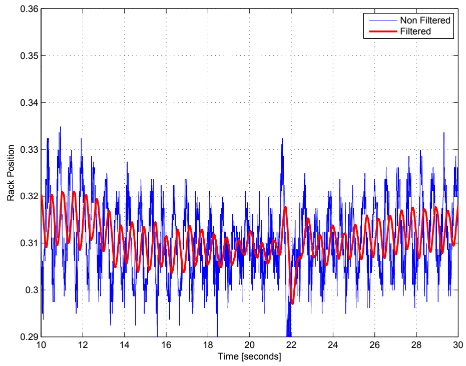

Figure 6.23: The rack position during the air injection process.

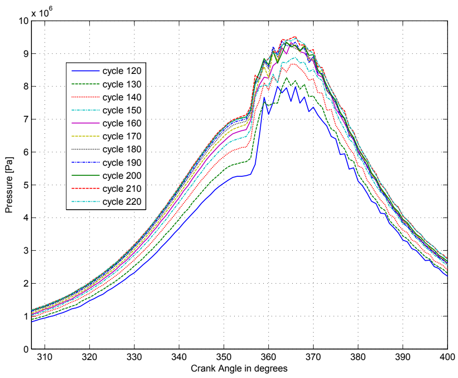

Figure 6.24: The in cylinder pressure.

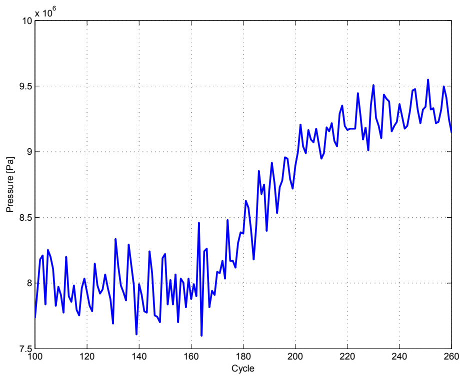

Figure 6.25: The maximum in cylinder pressure.

Experiment 6: Results

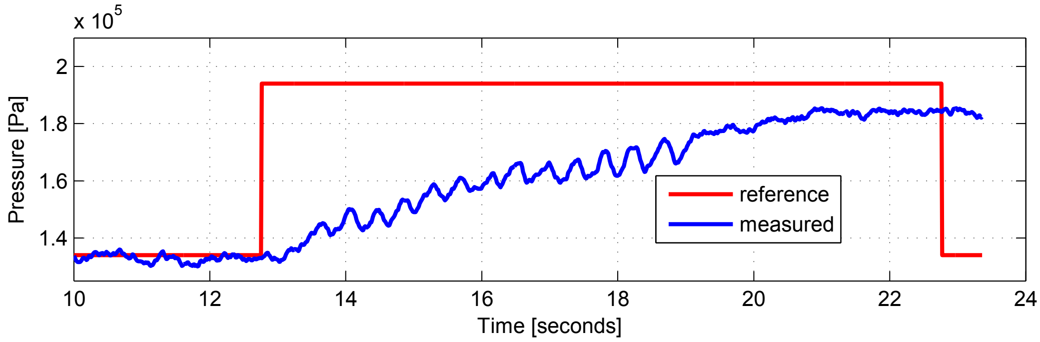

Figure 6.26: The reference and the experimental intake manifold pressure.

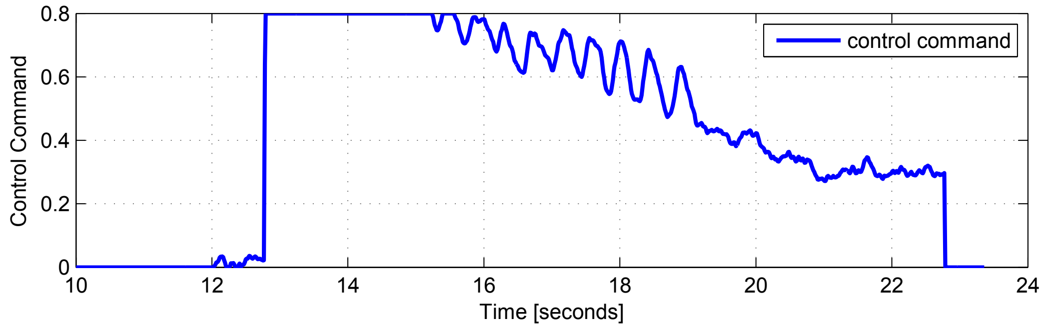

Figure 6.27: The control command during the air injection process.

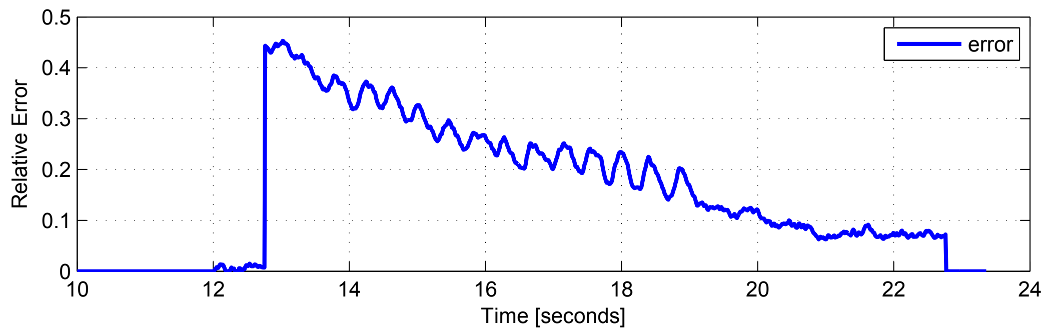

Figure 6.28: The relative error achieved.

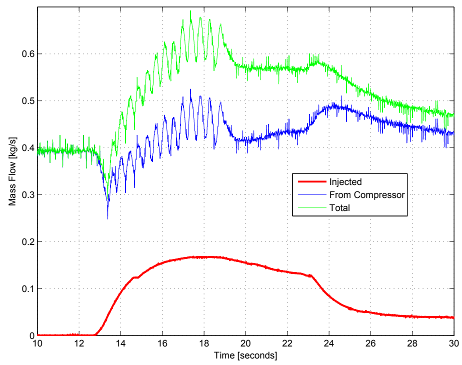

Figure 6.29: The injected and compressor provided mass flows.

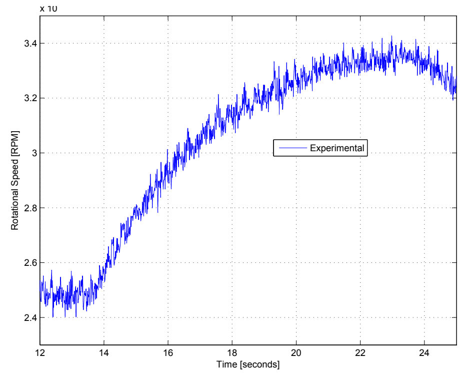

Figure 6.30: The rotational speed of the turbocharger shaft.

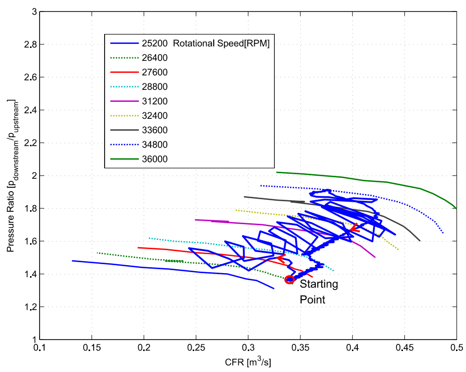

Figure 6.31: The trajectory of the compressor air flow rate and the pressure ratio.

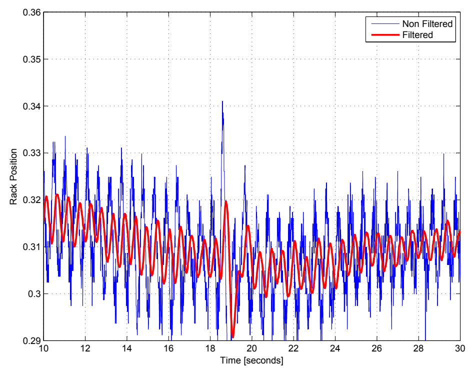

Figure 6.32: The rack position during the air injection process.

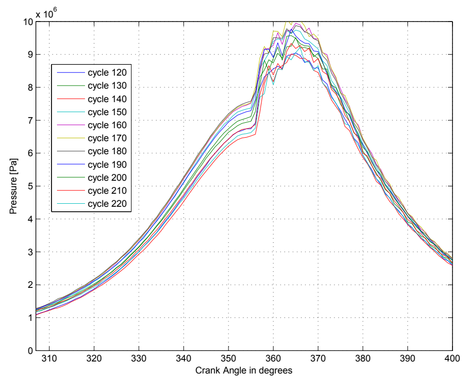

Figure 6.33: The in cylinder pressure.

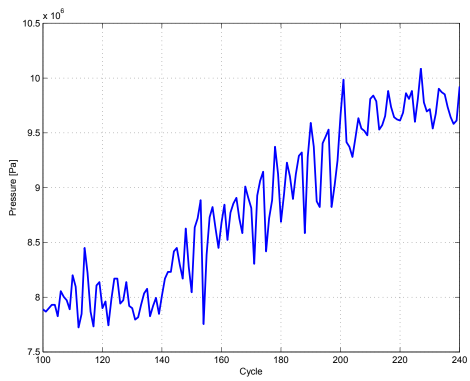

Figure 6.34: The maximum in cylinder pressure.

6.1.2 Experiments at 20 % Load

Experiments were carried out at a load lower than the nominal engine load (25%) of the design. The aim in this set of experiments was to reach to a conclusion, on whether the controller is capable of delivering efficient control results in cases other than the considered one during the design. The initial intake manifold pressure was measured 1.30 bar.

Experiment 1: Results

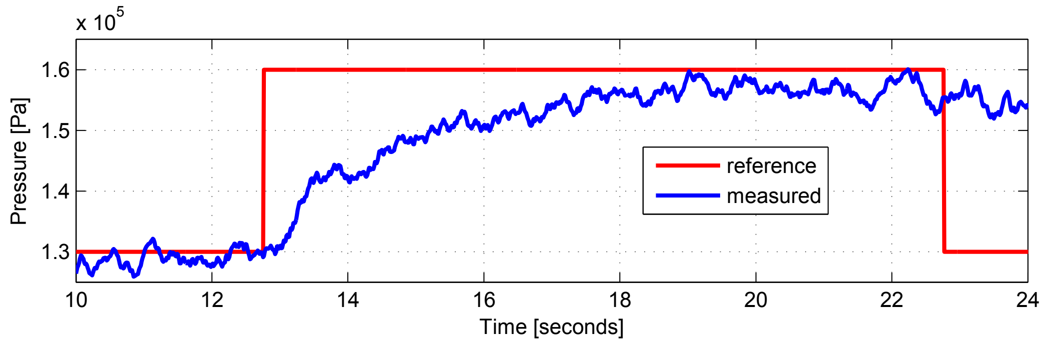

Figure 6.35: The reference and the experimental intake manifold pressure.

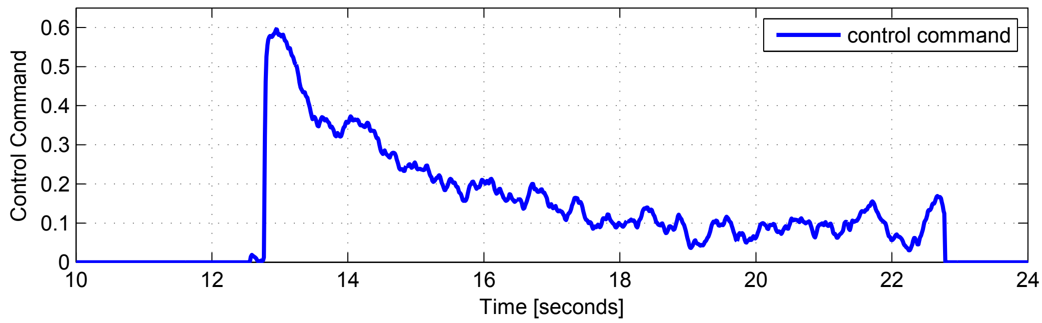

Figure 6.36: The control command during the air injection process.

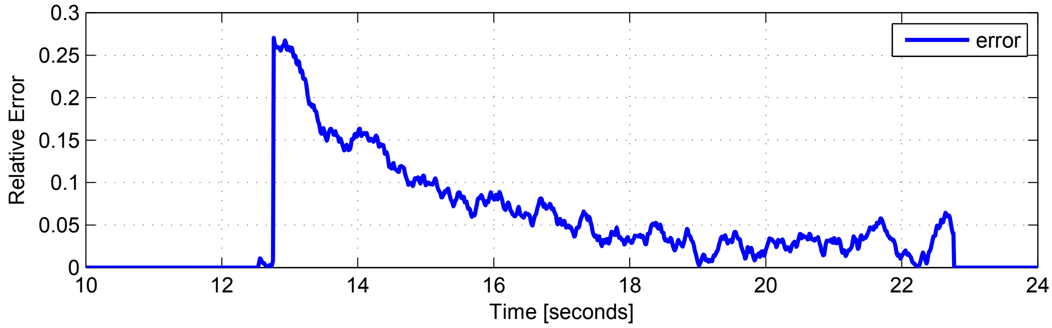

Figure 6.37: The relative error achieved.

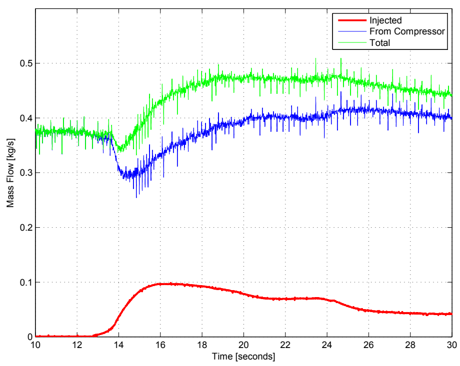

Figure 6.38: The injected and compressor provided mass flows.

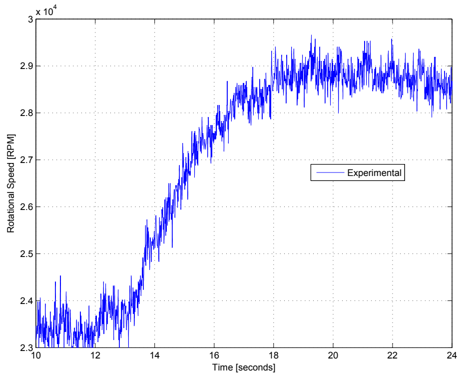

Figure 6.39: The rotational speed of the turbocharger shaft.

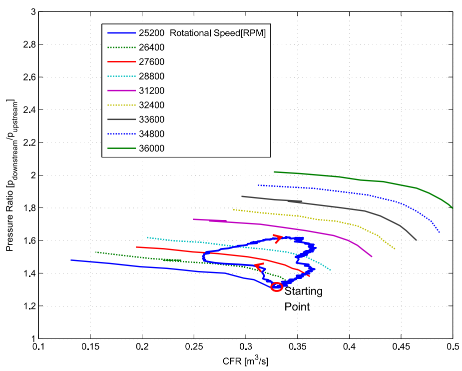

Figure 6.40: The trajectory of the compressor air flow rate and the pressure ratio.

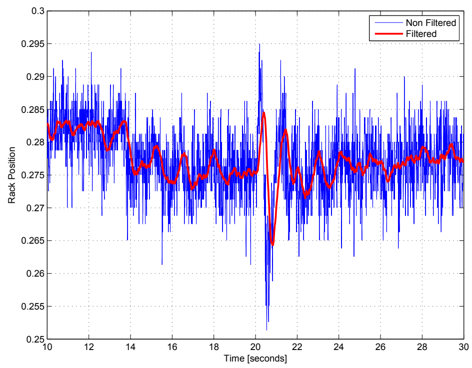

Figure 6.41: The rack position during the air injection process.

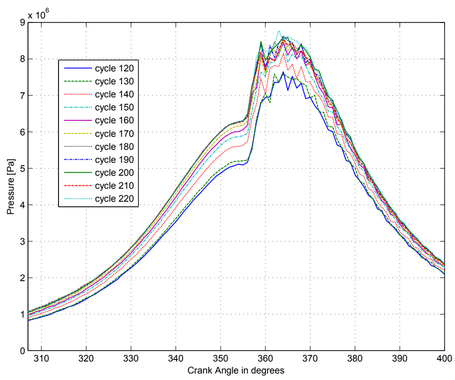

Figure 6.42: The in cylinder pressure.

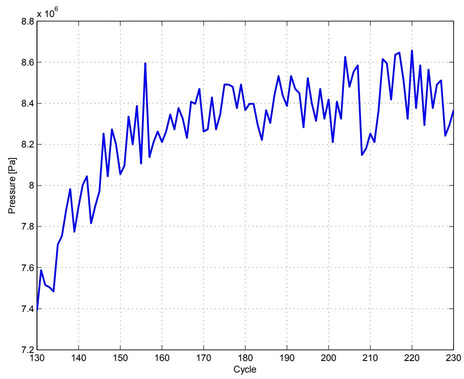

Figure 6.43: The maximum in cylinder pressure.

Experiment 2: Results

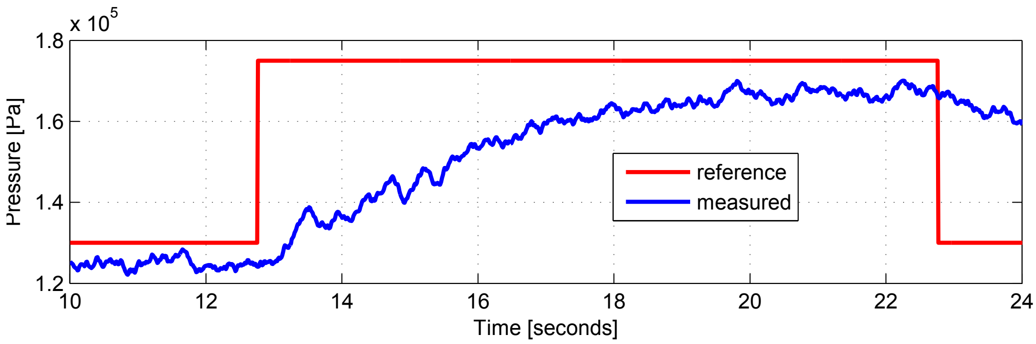

Figure 6.44: The reference and the experimental intake manifold pressure.

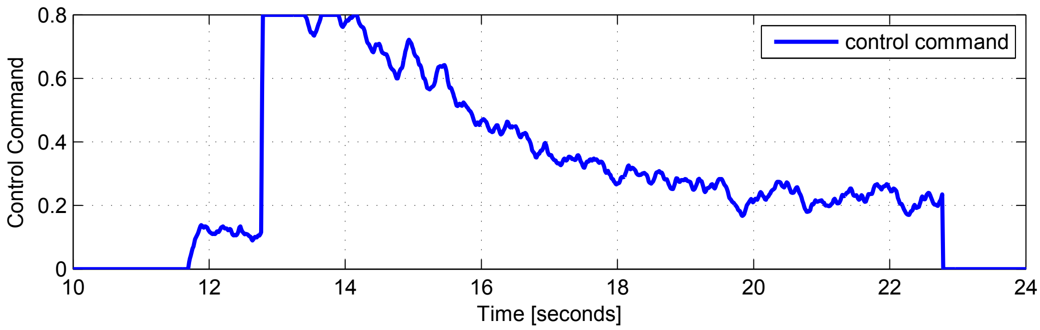

Figure 6.45: The control command during the air injection process.

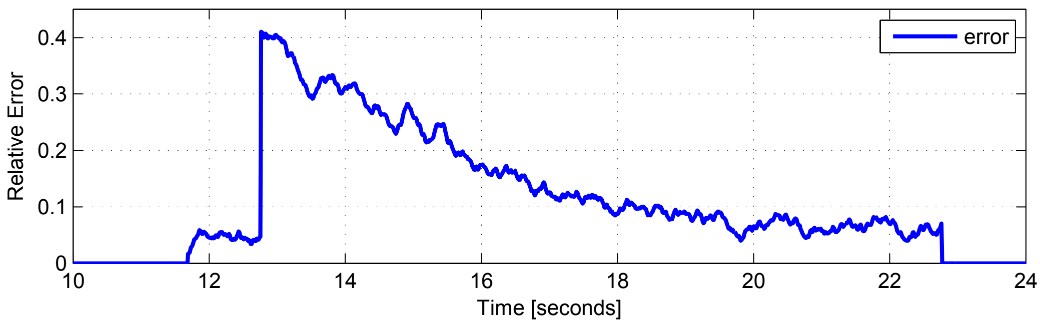

Figure 6.46: The relative error achieved.

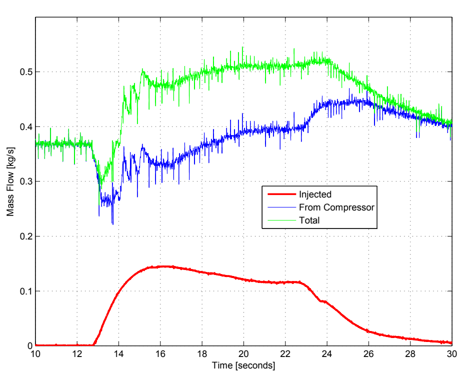

Figure 6.47: The injected and compressor provided mass flows.

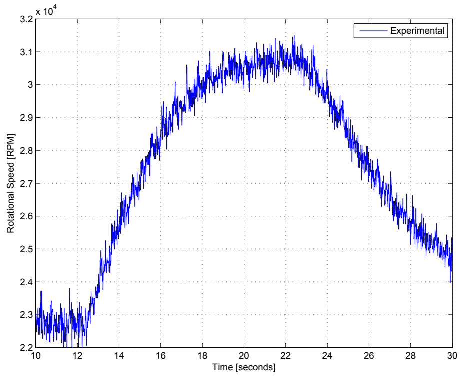

Figure 6.48: The rotational speed of the turbocharger shaft.

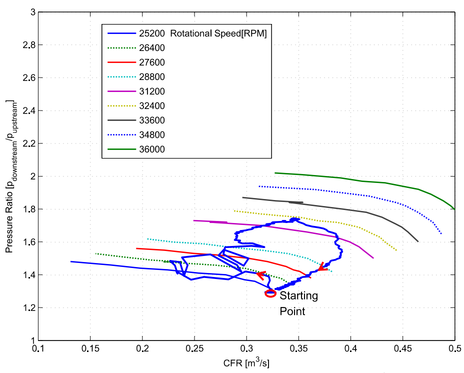

Figure 6.49: The trajectory of the compressor air flow rate and the pressure ratio.

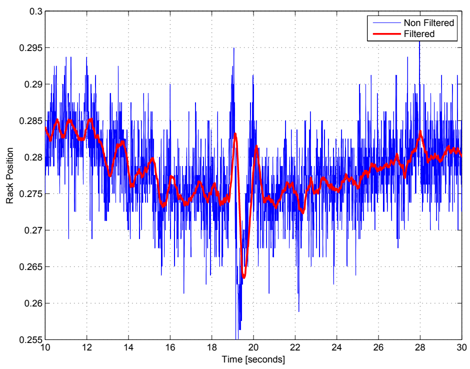

Figure 6.50: The rack position during the air injection process.

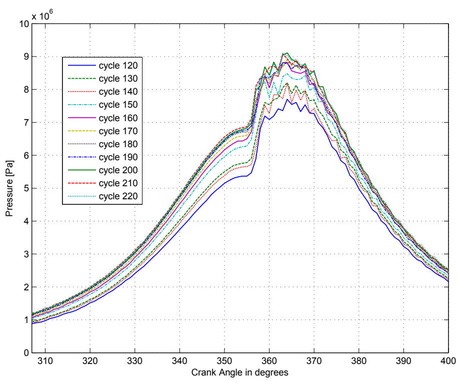

Figure 6.51: The in cylinder pressure.

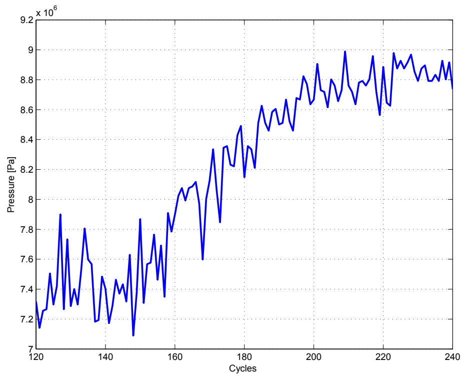

Figure 6.52: The maximum in cylinder pressure.

Experiment 3: Results

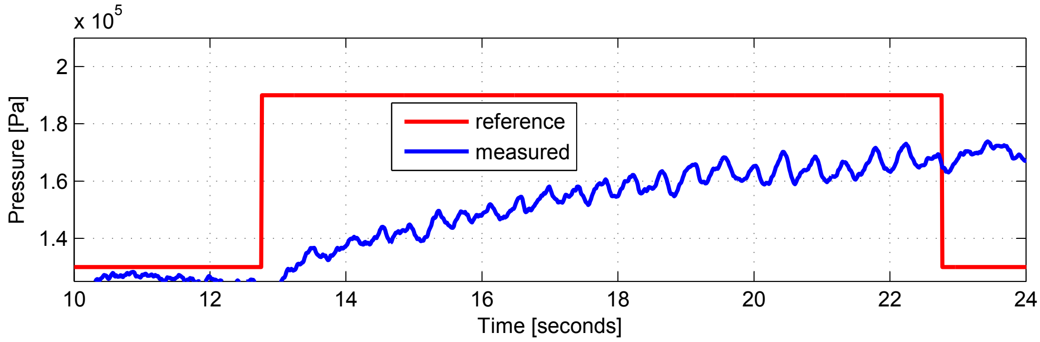

Figure 6.53: The reference and the experimental intake manifold pressure.

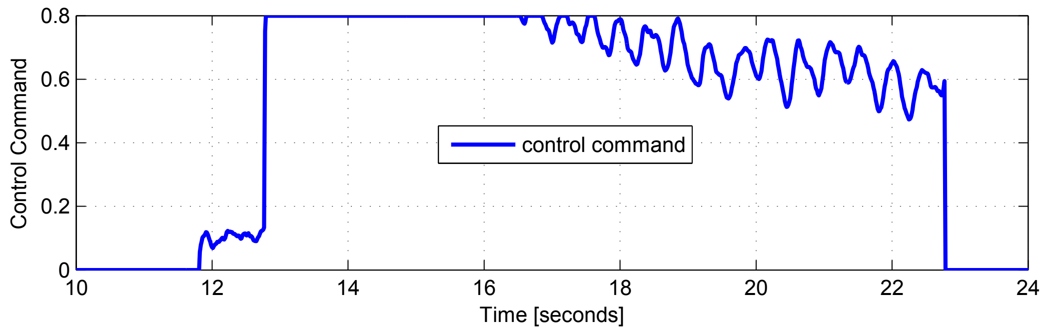

Figure 6.54: The control command during the air injection process.

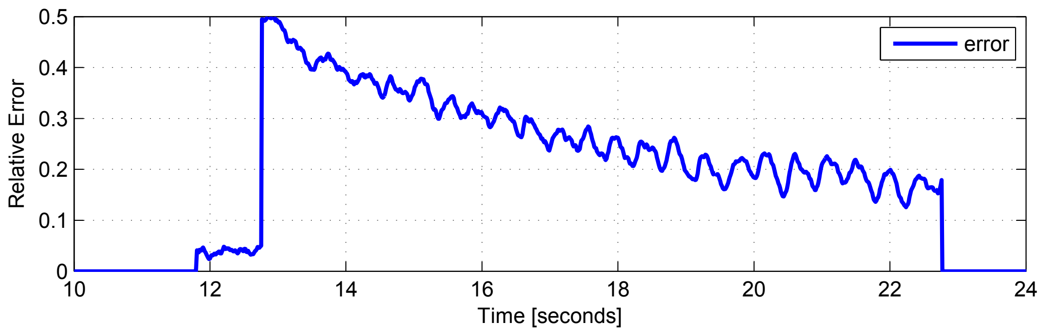

Figure 6.55: The relative error achieved.

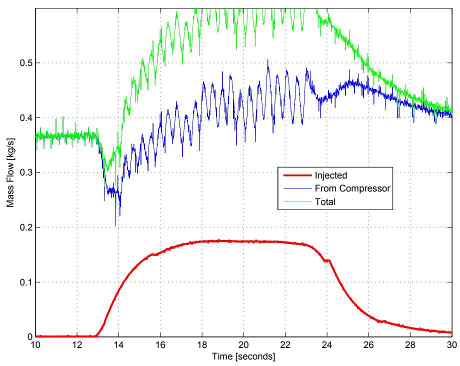

Figure 6.56: The injected and compressor provided mass flows.

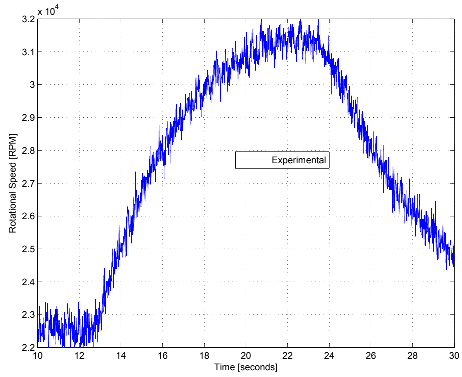

Figure 6.57: The rotational speed of the turbocharger shaft.

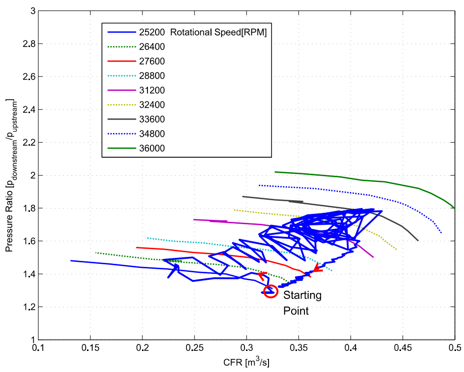

Figure 6.58: The trajectory of the compressor air flow rate and the pressure ratio.

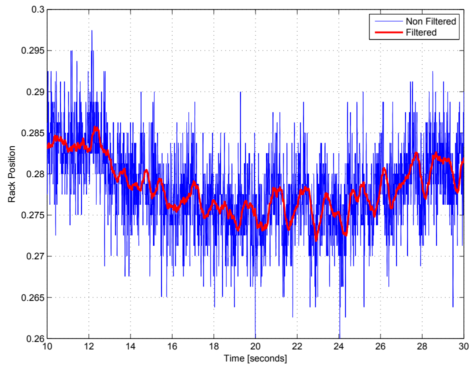

Figure 6.59: The rack position during the air injection process.

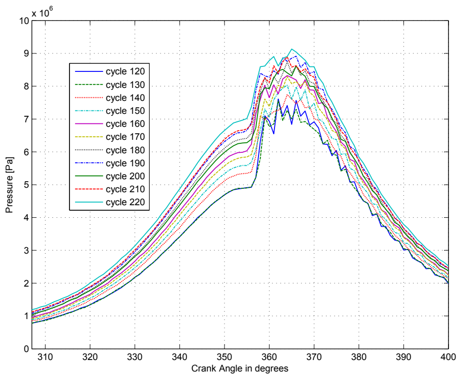

Figure 6.60: The in cylinder pressure.

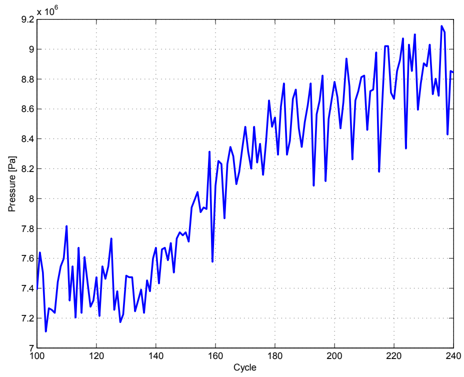

Figure 6.61: The maximum in cylinder pressure.

6.1.3 Experiments at 30 % Load

Experiments were carried out at a load greater than the nominal load of the design. The aim in this set of experiments was to reach a conclusion, on whether the controller is capable of delivering efficient control results in cases other than the considered one during the design. In particular in this case a higher operating point (30%) than the nominal point (25%) is examined. This case of experiments is regarded rather easier for control implementation, because the operating point on the compressor map is away from the region over which instabilities occur.

Experiment 7: Results

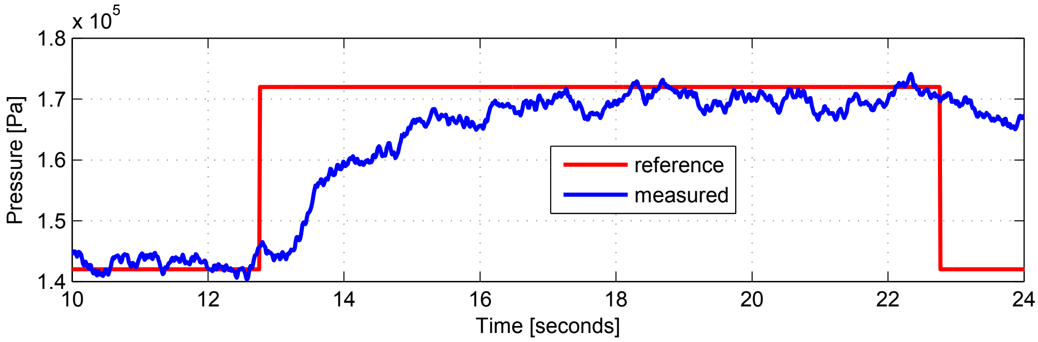

Figure 6.62: The reference and the experimental intake manifold pressure.

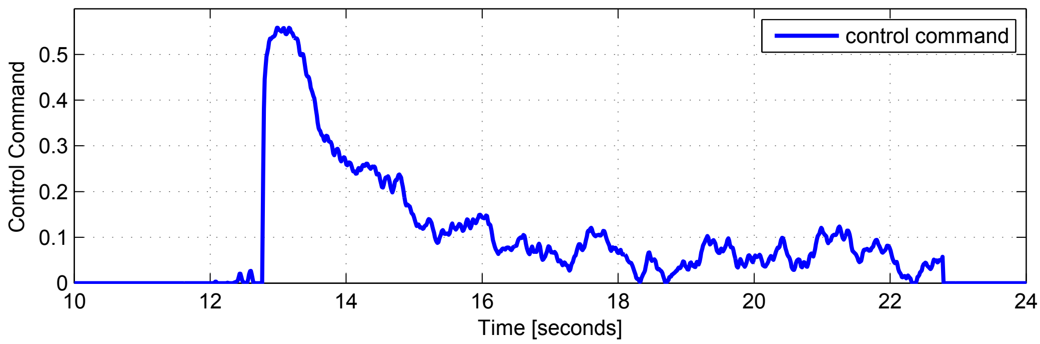

Figure 6.63: The control command during the air injection process.

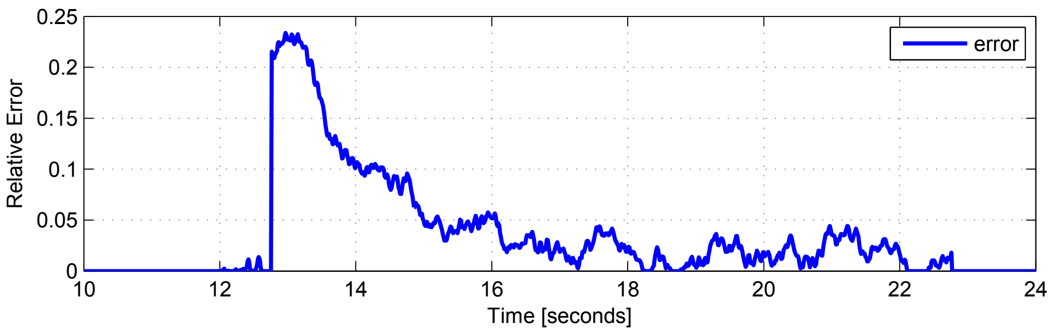

Figure 6.64: The relative error achieved.

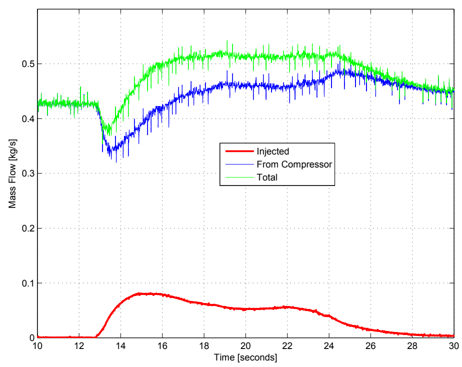

Figure 6.65: The injected and compressor provided mass flows.

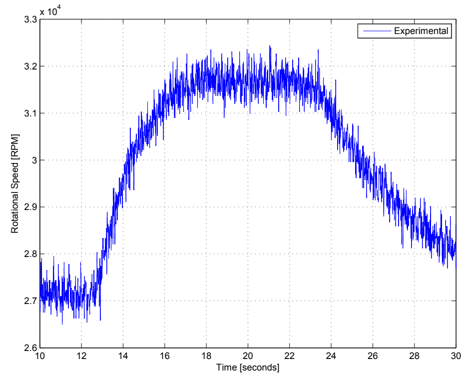

Figure 6.66: The rotational speed of the turbocharger shaft.

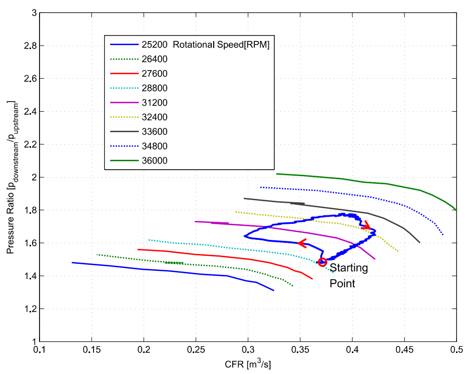

Figure 6.67: The trajectory of the compressor air flow rate and the pressure ratio.

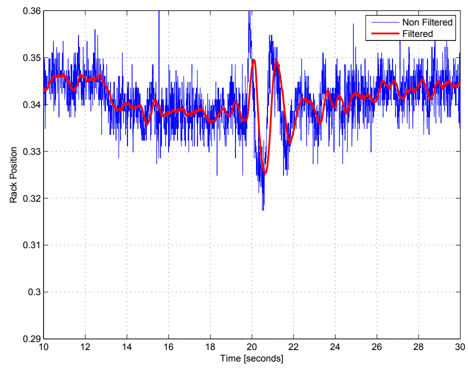

Figure 6.68: The rack position during the air injection process.

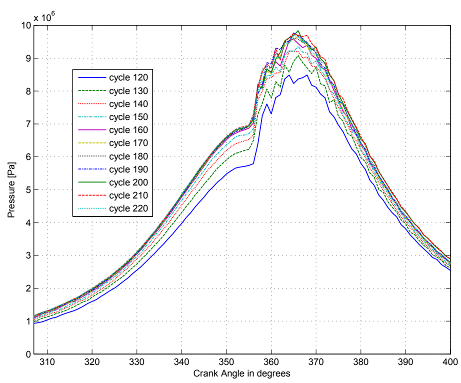

Figure 6.69: The in cylinder pressure.

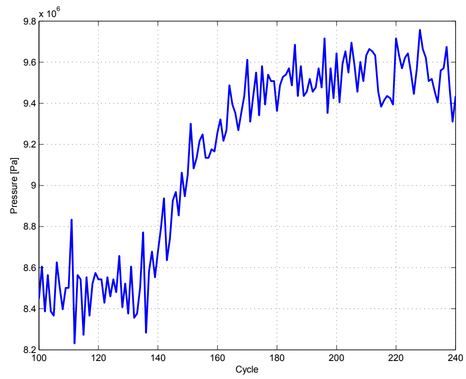

Figure 6.70: The maximum in cylinder pressure.

Experiment 8: Results

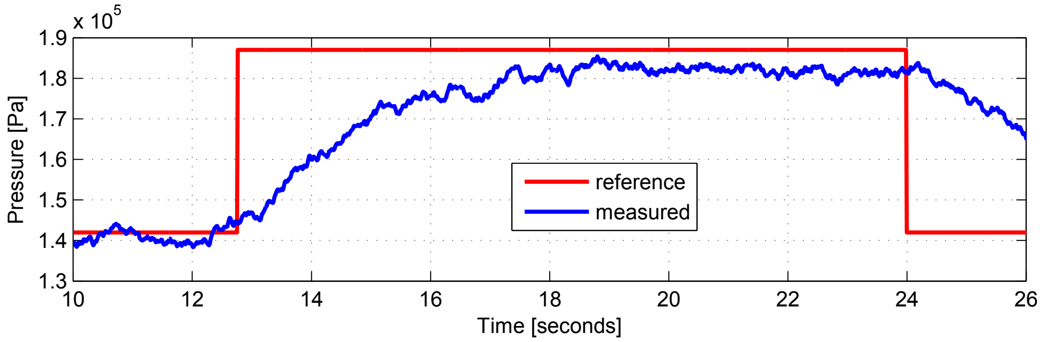

Figure 6.71: The reference and the experimental intake manifold pressure.

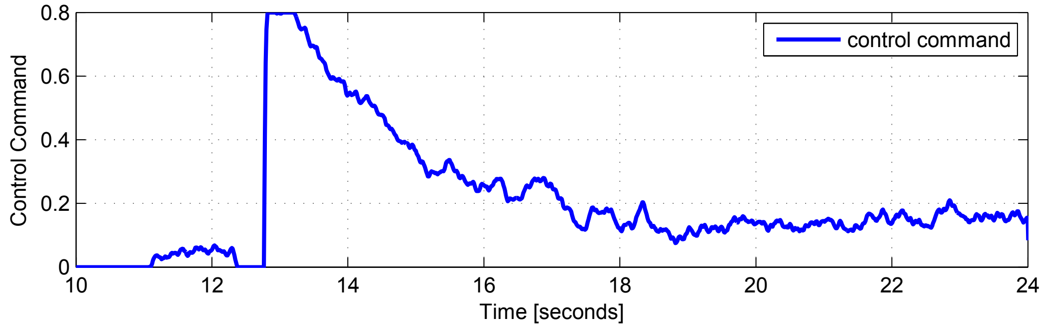

Figure 6.72: The control command during the air injection process.

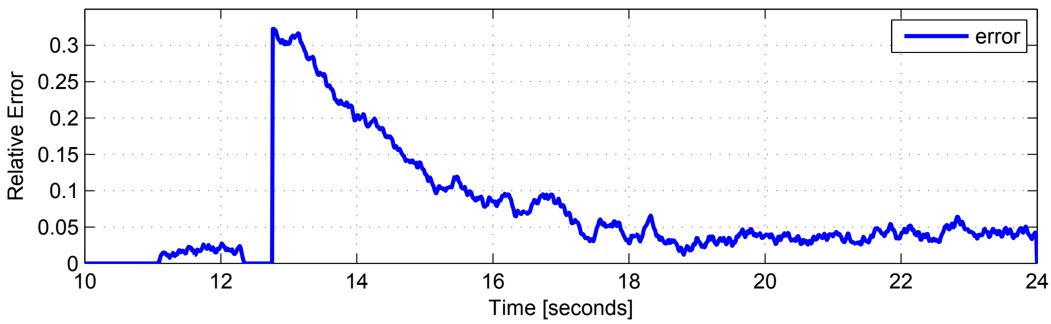

Figure 6.73: The relative error achieved.

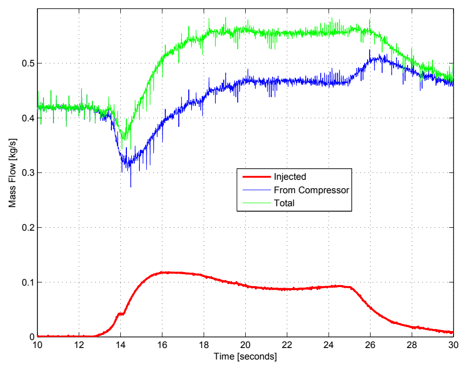

Figure 6.74: The injected and compressor provided mass flows.

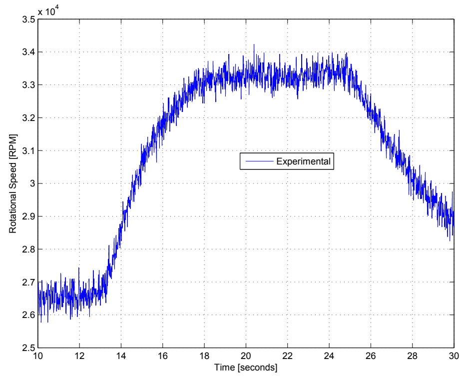

Figure 6.75: The rotational speed of the turbocharger shaft.

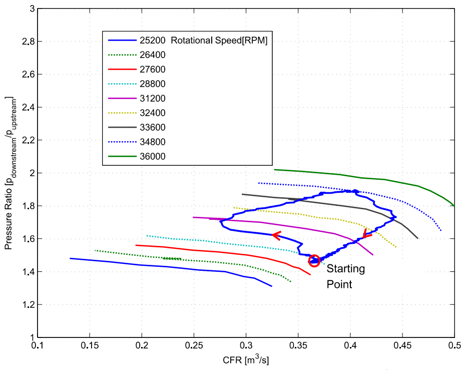

Figure 6.76: The trajectory of the compressor air flow rate and the pressure ratio.

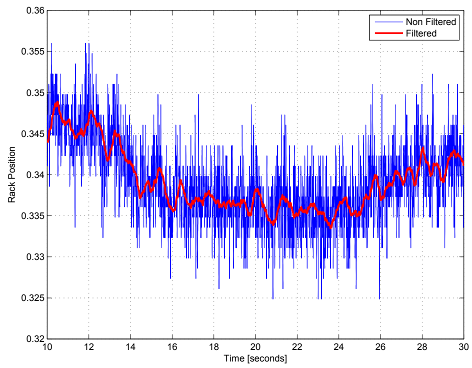

Figure 6.77: The rack position during the air injection process.

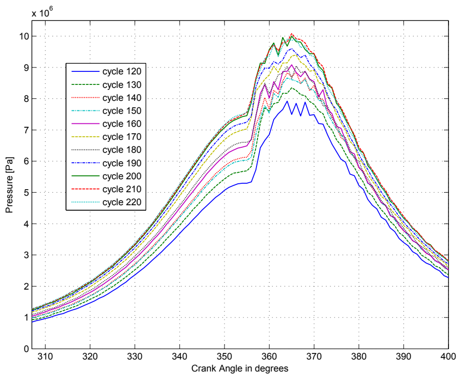

Figure 6.78: The in cylinder pressure.

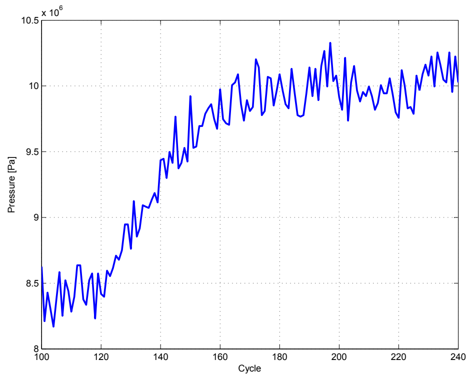

Figure 6.79: The maximum in cylinder pressure.

Experiment 9: Results

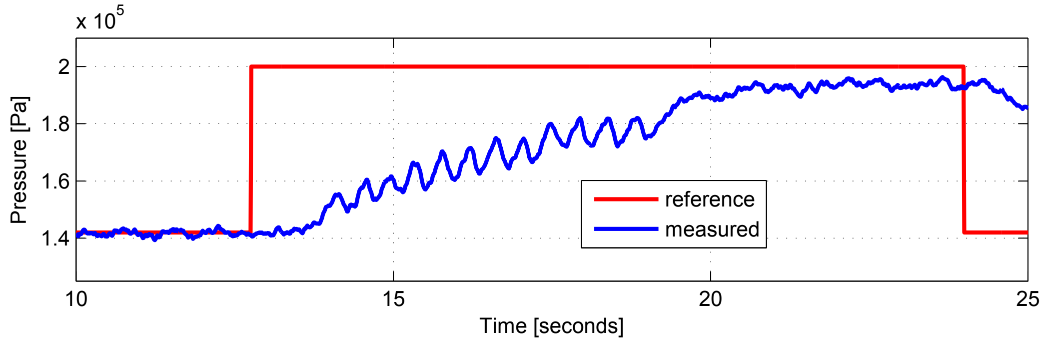

Figure 6.80: The reference and the experimental intake manifold pressure.

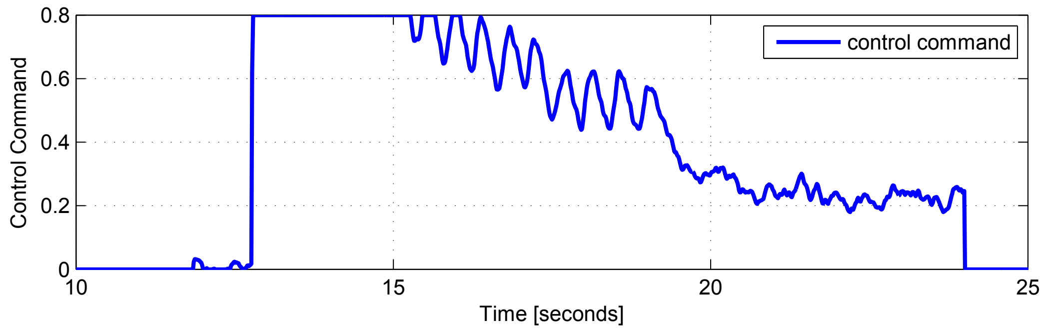

Figure 6.81: The control command during the air injection process.

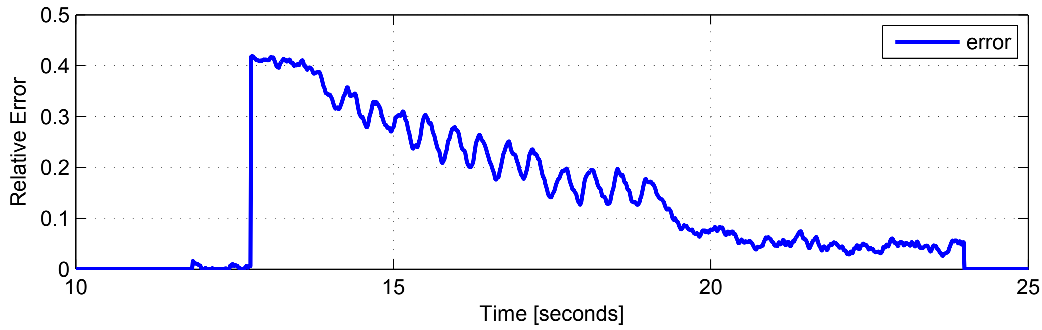

Figure 6.82: The relative error achieved.

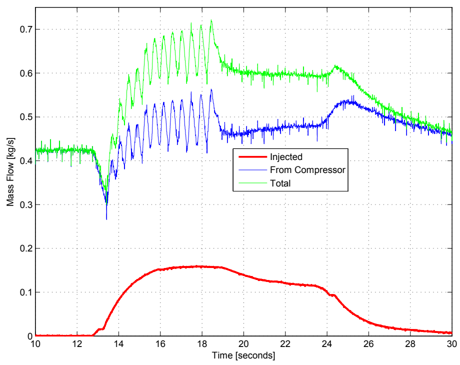

Figure 6.83: The injected and compressor provided mass flows.

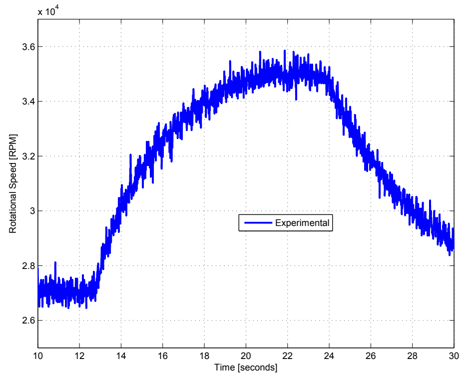

Figure 6.84: The rotational speed of the turbocharger shaft.

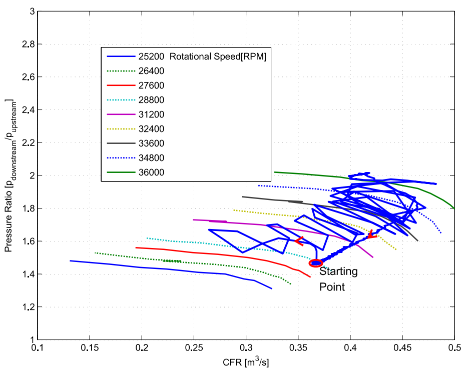

Figure 6.85: The trajectory of the compressor air flow rate and the pressure ratio.

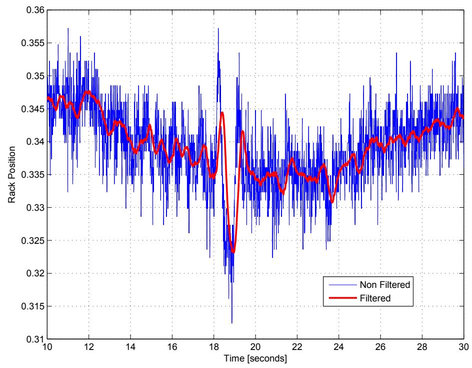

Figure 6.86: The rack position during the air injection process.

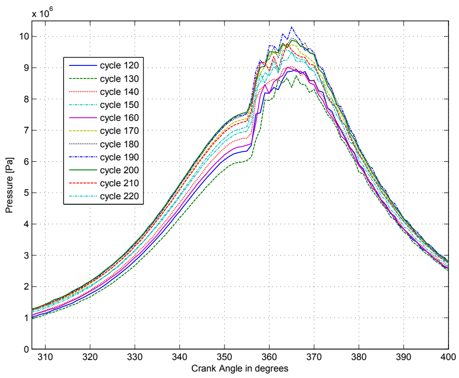

Figure 6.87: The in cylinder pressure.

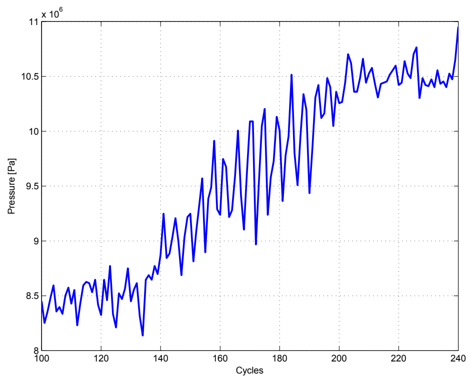

Figure 6.88: The maximum in cylinder pressure.

6.1.4 Remarks

Experiment 4

In this experiment the reference trace was tracked accurately as shown in figure 6.1, since the final steady state error achieved was lower than 3 % as depicted in figure 6.4. The control command according to figure 6.3 was under the safety limit of 80 % was not surpassed, as a result of the design requirement that prevents the controller to overreact to small initial errors in the order of 20 %, as in this case.
The air injection under closed loop appeared to affect drastically the turbocharger. In figure 6.7 the rotational speed of the turbocharger shaft increased and reached steady state at its final value once the pressure in the intake manifold was traced. During the transient of the controlled variable, the air provided by the compressor decreased, because a fraction of the air induced in the cylinders was provided by the air injection process. Therefore, the compressor reaches to areas closer to the surge line, according to figure 6.9.
Once the controlled variable converged, the in cylinder maximum pressure remained over 89 bar, thus creating crank angle - in cylinder pressure profiles that correspond to greater loads in normal engine operation. This confirms that by augmenting the intake manifold pressure, the in cylinder pressure augments as well, as the motored pressure of the cycle is enhanced. The effect of the air injection on the motored pressure overwhelms, as predicted by the simulation, both the decrease in the maximum temperature of the cycle due to air injection and the fact that the fuel injected is decreased as the rack position in figure 6.11 indicates. To underline that, the maximum pressure increases reaching a steady average, once the controlled signal has converged. This indicates that the intake manifold pressure and the maximum pressure are closely related. Thus, affecting the former, the latter is accordingly affected. The above statement is based upon the comparison of the controlled variable and the maximum in cylinder pressure trace.

Experiment 5

In figure 6.17 the controlled variable converges, however with a steady state error of 5 %, as shown in figure 6.19. The control command shortly overpasses the safety limit of 80%. Had the upper limit been set to the maximum valve deviation, the pressure signal would be tracked even more accurately.
At the start of the control process, an instability is noticed in the compressor flow, as the flow heads towards the surge margin line. However, the instability is surpassed after 2 seconds, since the controller guides the compressor to greater pressure ratios, increasing the rotational speed of the turbocharger, as shown in figure 6.21. As can be noted in figure 6.22, these instabilities in the flow take place at an area of the map considered stable.
The rack position reaches, according to the indicating red line in figure 6.23, slightly lower values, which means that the fuel consumption has decreased more than in experiment 4.
The maximum pressure curve, depicted in figure 6.25, from cycle 220 until 240 when the control process ends is stabilized around an average maximum pressure of 93 bar.

Experiment 6

Here the reference value is increased more. In this case the controller encountered at the start of the procedure an initial error of 45%. The steady state error at the end of the control procedure is 7%. The control command produced exceeded the safety limit as shown in figure 6.27. As before, better tracking behavior could be expected if the command was not limited. However, safety could not allow for aggressive actuator operation.
In the experiment, at the start of the air injection process at second 12.7, until second 19.0 the compressor provided mass flow goes through stalling. The compressor pressure ratio due to the air injection augments. The rotational speed of the compressor increases due to the increase in the total air reaching the turbo. Hence, the compressor pressure ratio and the intake manifold pressure tend to augment as well. However, a fraction of the air induced in the cylinders is provided by the air injection. Therefore, the compressor provided flow is not fully induced in the cylinders and as such the already pressurized air at the outlet of the compressor prevents the incoming compressor flow. The compressor provided flow decreases until the already pressurized compressor flow is induced in the cylinders. Then, at this point the air the compressor induced in the engine does not realize a downstream area of greater pressure anymore, and since the rotational speed of the compressor has increased, the air is even more pressurized from the compressor, which tends to induce a greater amount of air. This pattern of oscillations is reiterated until the air injected is decreased, once the controlled signal is close to convergence. At the end of the control procedure the rotational speed of the compressor has increased enough to augment the compressor pressure ratio, hence the compressor provided flow, under the presence of additional air injection is greater than the one at the start of the process.
In figure 6.31, the trajectory of the compressor provided flow and the pressure ratio completes a repeating pattern of elliptic curves, as the above described pattern of oscillations occurs. Even though the compressor map during transient is not valid, the instabilities do not occur near the left far end of the map's isospeed curves, along which the surge line lies. In areas of the map which are considered stable, instabilities take place. However, once the injected flow reduces, the instabilities cease to exist because a greater fraction of the compressor provided flow is induced in the engine's cylinders. The maximum in cylinder pressure reaches for a short period of cycles between cycle 220 and cycle 240, a steady state of 97 bar. The air injection duration proved to be short, as the controlled signal did not manage to remain at the steady state for more than 2.4 seconds.

Experiment 1

In this experiment the engine load was 20% below the nominal load (25%). However, testing the controller on loads different than the nominal reveals its effectiveness margin. In this experiment the control signal converged 5 seconds after the air injection commenced. The relative error achieved was acceptable since it is lower that 5 %. The control command was bounded and as the error decreases, so does the control command.
In this case, as shown in figure 6.39, the rotational speed of the turbocharger converges to a constant value of 29000 RPM from second 18 until the end of the control process,

accordingly to the controlled variable.
As depicted in figure 6.40 the air injection leads to lower flow from the compressor but at the same time to greater pressure ratios, due to the enhanced rotational speed of the turbocharger. Hence, the trajectory of the compressor provided mass flow and the pressure ratio appear to move closer to the limits of the map, yet in stable areas. Nevertheless, instabilities are avoided, because in this case the flowjet is small in comparison to the compressor provided flow.
In accordance to the controlled variable, the maximum in cylinder pressure per cycle converges to a constant average value of 85 bar. The in cylinder pressure traces, as depicted in figure 6.42, are affected greatly during the compression part of the cycle. As shown, in each pair of successive engine cycles, the greatest deviations are marked at a crank angle region between the crank angle signifying the commence of the combustion and the crank angle at which the maximum pressure occurs.

Experiment 2

In this experiment the controlled signal converged, as depicted in figure 6.44, achieving however a higher relative error than the one in the previous case. The relative error after 19 s is in the area of 6%. The control signal surpassed the safety limiter for a short period of time.
In the experiment, after one second from the commence of the process, instabilities in the compressor provided flow occurred. In this load, the normal operating point of the compressor is closer to the surge limit, in relation to the nominal load of 25%. Hence, the compressor provided flow is more easily lead to stalling, by injecting air.
In the control process the compressor flow instability is regarded as a disturbance which the controller is supposed to reject. In this case, between seconds 14 and 16, such a disturbance occurs and the controller achieves rejection, augmenting the control command value from 59 % to 70 %.

Experiment 3

In this experiment, the controlled variable did not track the reference command satisfactorily. The intake manifold pressure reference augmentation of 0.45 bar was a great percentage of the initial pressure which was close to 1.28 bar. The compressor provided flow was not sustainable since the pressure in the intake manifold was greater than the pressure downstream of the compressor. Due to these great and constant fluctuations of the compressor provided flow, the controlled signal oscillated, and did not manage to track the reference. The amplitude of these oscillations was 0.2 bar. As such, the imposed disturbances on the controlled signal affected greatly the control process and the controller did not achieve their rejection.

Experiment 7

The engine load was 30%, which is greater than the nominal engine load (25%). At this load, the initial operation point on the compressor map is not close to the surge margin line, therefore additional air can be injected without decreasing the compressor provided flow to a point which would lead to instabilities.

The controlled variable converged, achieving a relative error less than 5 %. The control command was initially at 55 % and converged to an average control command below 10 %.
In figure 6.67 the trajectory of the air flow of the compressor and the pressure ratio is led closer to the surge margin line, without causing instabilities in the compressor flow. In figure 6.66 the rotational turbocharger shaft speed is depicted. The signal of the rotational speed converges to a steady average value and so does the maximum in cylinder pressure.
In this experiment the rack position decreases noticeably. In comparison with the other two corresponding experiments at the nominal load and at 20% load the rack position decreased in a greater extent and remained on this steady position, once the controlled signal converged.

Experiment 8

In this experiment the control signal converged, achieving a 5 % steady state error. The control command only for a limited period of time, of half a second, surpassed the safety limit.
In this case, the control process led the trajectory depicted in figure 6.76, closer to the surge margin line than case 7, without causing any instabilities to the flow.

Experiment 9

Experiment 9 was successful as well since the controlled signal converged, achieving a steady state error of 5%. However, in this case it should be noted that the air injection led the compressor to stalling. This led to instabilities of the compressor flow, which acted as disturbances on the controlled signal. The controller managed to reject the disturbances, better than any of the previous experiments, in which instabilities occurred.
It should be underlined that the occurrence of instabilities in this experiment signifies an upper limit of amount of injected air, over which the compressor flow cannot be sustained anymore without stalling.

6.1.5 Summary of Results

The control target in the outset of this thesis was to design a robust controller for the air injection system in a marine diesel engine. In table 6.2 an indication of the values of specific signals measured at the end of the control process is described. In the last two columns it is stated, whether the control process caused an instability to the system and which was the steady state relative error. The latter column can be considered as a means of evaluating the efficiency of the control process.
Table 6.3 provides an indication of the same signals with the engine under normal operation, without the effect of the air injection system.

No. Exp.	Load[%]	Rack	TC Speed [RPM]	Max. P_{cyl} [bar]	Instability	Rel. Error
1	20	0.275	2.90E4	85	×	4%
2	20	0.274	3.10E4	88	✓	7%
3	20	0.275	3.20E4	87	✓	20%
4	25	0.310	3.00E4	89	×	2%
5	25	0.310	3.15E4	94	✓	5 %
6	25	0.310	3.35E4	96	✓	7%
7	30	0.339	3.20E4	92	×	3 %
8	30	0.335	3.37E4	100	✓	5%
9	30	0.334	3.35E4	105	✓	4%

Table 6.2: Summary of the control effects on the engine.

Load [%]	Rack	SPTC [RPM]	Max. P_{cyl} [bar]
20	0.284	2.25E4	74
25	0.315	2.50E4	79
30	0.346	2.70E4	85

Table 6.3: Basic characteristic on various loads, under normal operation.

From the presented results a general conclusion on the margin of effectiveness of the designed robust controller can be reached. In the experiments carried out at the nominal load, the performance of the controller was efficient especially for the experiments 4 and 5. The instabilities which occurred during experiment 6 affected the performance of the controller, hence the achieved error was larger than the one achieved in the other experiments at the same load.
The controller functioned effectively at all three experiments carried out at 30% of the maximum load. The error in each case stayed below 5%. In experiment 9, the disturbance imposed on the system was the greater from all the other cases but still it was rejected and the controlled variable was led to convergence.
The controller did not operate satisfactorily in the case of experiment 3. Increasing the intake manifold pressure at loads lower than the nominal did not prove to be efficient. The compressor was led towards instability, since the operation point is already close to a region close to the surge margin line. Therefore, the robust controller is required to be redesigned for this operating point, using a corresponding model.
Based on the above in can be stated that the modeling methodology which provides

the linear model for the robust control design at the nominal point at 25% engine load proved successful. Experiments for 20% and 30% engine load proved the effective robustness of the H_∞ paradigm.

6.2 Double Step Type Reference at 25 % Load

Results

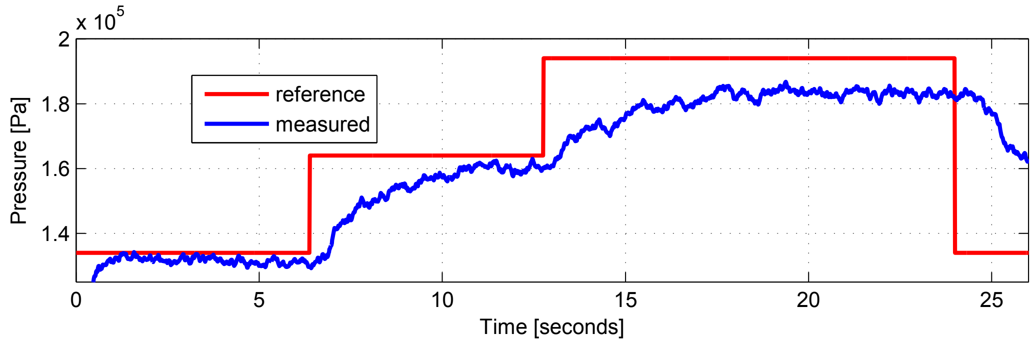

Figure 6.89: The reference and the experimental intake manifold pressure.

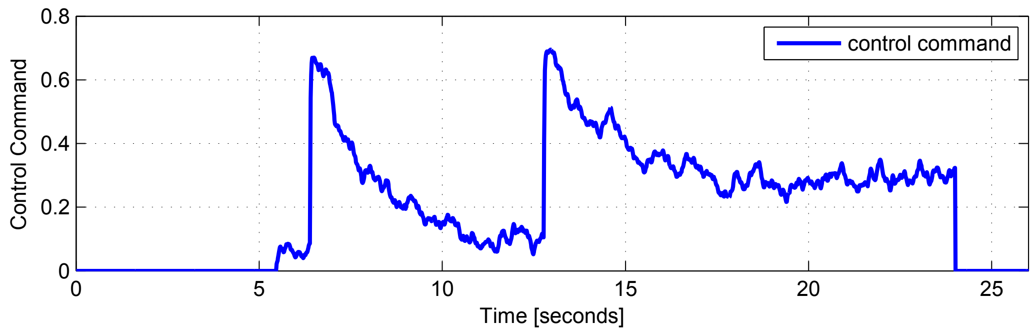

Figure 6.90: The control command during the air injection process.

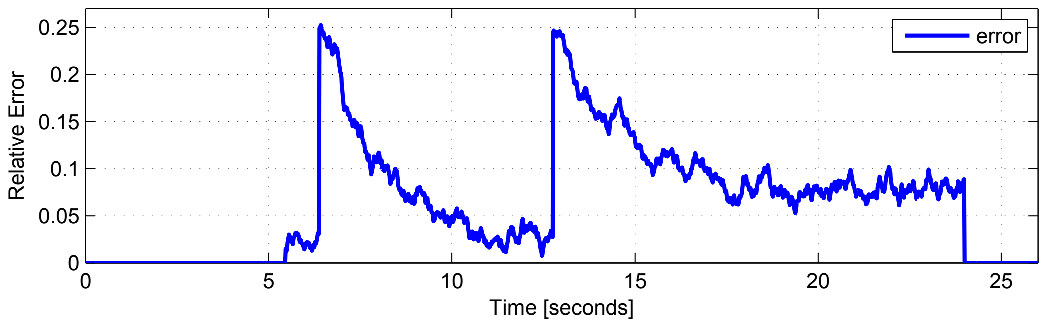

Figure 6.91: The relative error achieved.

6.3 Triple Step Type Reference at 25 % Load

Results

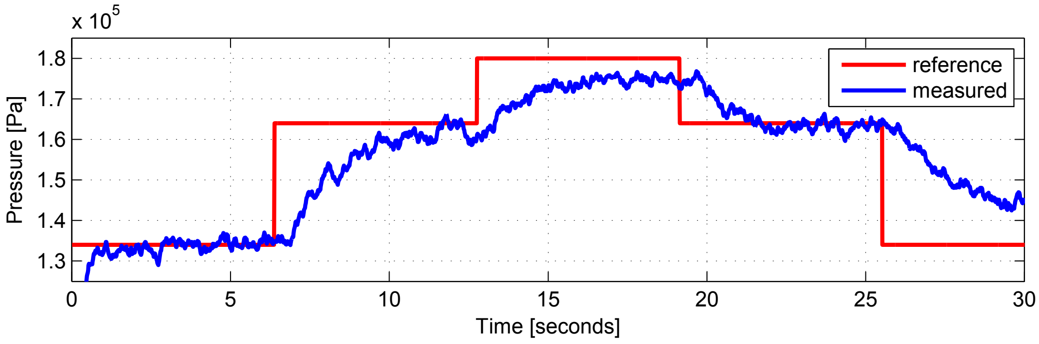

Figure 6.92: The reference and the experimental intake manifold pressure.

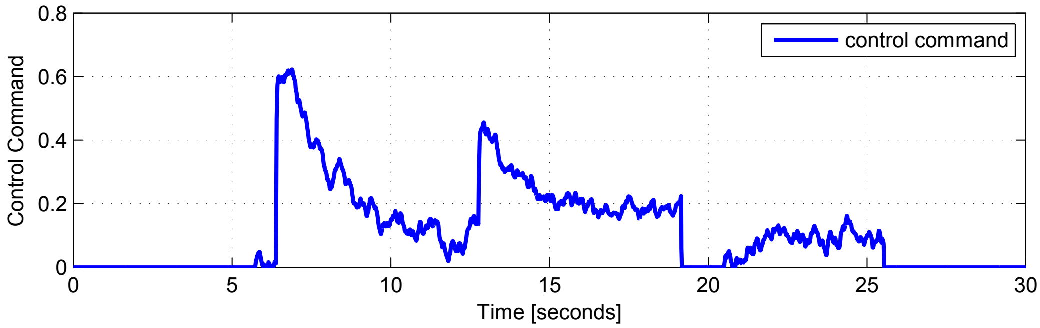

Figure 6.93: The control command during the air injection process.

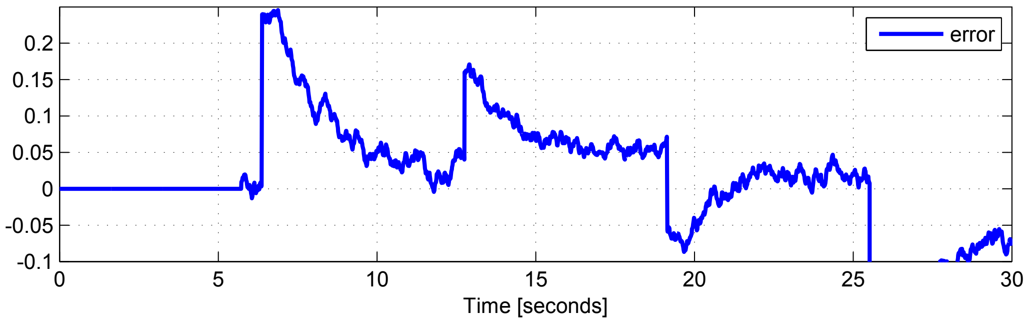

Figure 6.94: The relative error achieved.

6.4 Ramp Type Reference at 25 % Load

Results

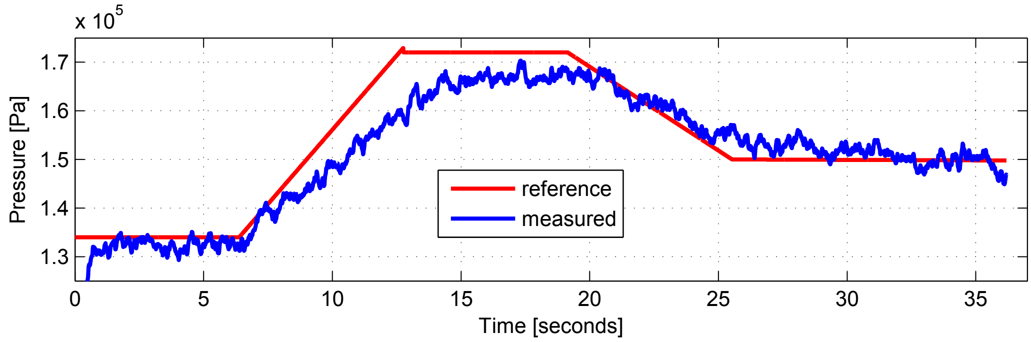

Figure 6.95: The reference and the experimental intake manifold pressure.

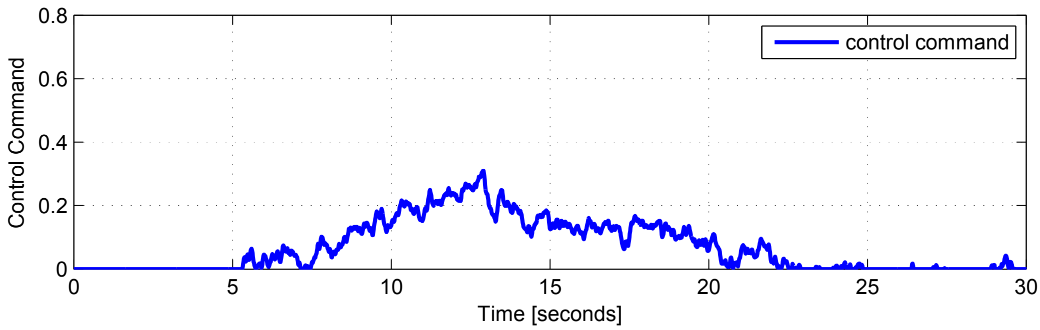

Figure 6.96: The control command during the air injection process.

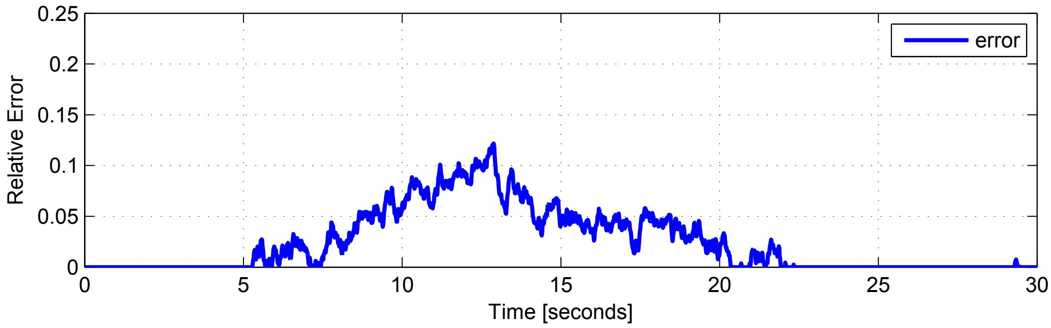

Figure 6.97: The relative error achieved.

6.5 Conclusions

After completing the presentation of the experimental results and having made remarks on them, a summary of the conclusions is made in this section.

- The controller was successfully designed in the control design environment and was then implemented, without the need to modify its characteristics.
- Its performance was pre-evaluated in the developed model of the engine and the results were similar to the experimental ones.
- The control performance was efficient at the nominal load (25 %) and at the 30% load.
- The experiments carried out at the load below the nominal were not as successful because the compressor was led to instability.
- The experiments carried out at the load over the nominal were successful because the total enthalpy of the exhaust gases reaching the turbine was greater, therefore the rotational speed hence the pressure ratio was greater.
- It can be derived by the experiments that the rotational speed of the turbocharger is a stabilizing factor for the compressor provided flow. The greater the rotational speed is, the greater the pressure ratio is as well, hence it is easier for the turbocharger to follow the augmentation of the intake manifold pressure, which is a downstream measurement for the compressor.
- The intake manifold pressure can affect greatly the rotational speed of the turbocharger and the in cylinder maximum pressure. In fact, the two latter signals appeared to follow the dynamic form of the controlled signal in time. Moreover, their transition to their final values was described by the exact time constant of the intake manifold pressure signal.

6.6 Future Work

- In this thesis one of the objectives was to design a method of avoiding compressor flow instabilities and such an algorithm was developed in simulation, adopting the leakage method of manipulating the control signal. This method was not experimentally tested. The compressor map was a way of predicting possible uncertainties. A model predictive controller (MPC) could be used in order to pre-evaluate the control reference in time, so as to lead the engine towards the desired intake manifold pressure, without leading the compressor flow through instabilities.
- An assumption was made to model the engine in a crank angle basis, was that the torque produced was calculated based on the break indicated effective pressure of each cylinder. The firing order could be implemented in the model and the torque forced on the crankshaft could be calculated on a crank angle basis.
- While selecting the weighting functions to design the controller, the weight bounding the control command signal was equal to a single gain, penalizing the value

of the control command between the [0 -1] region. A new controller could be designed, taking in mind while selecting a weight for the control command signal, the dynamics of the valve actuator. This would be efficient in cases when the control process led the engine to instabilities. The control command would not be affected by possible instabilities and it would not produce a great control command immediately at the start of the process.

- As noted at the experimental remarks the rotational speed of the compressor is affected by the air injection process. A transfer function between the air injection command and the rotational speed of the turbocharger, could be defined with the intention of designing a feedback controller capable of keeping the rotational speed of the compressor to a suitable reference value.

Appendix A

Control Algorithm

In this chapter of the Appendices, the algorithm for the design of H_∞ controllers is described, in reference of the general control configuration problem described in figure A.1.
The generalized plant P of figure A.1 can be partitioned as in equation A.1.

$$P = \begin{bmatrix} P_{11} & P_{12} \\ P_{21} & P_{22} \end{bmatrix} \tag{A.1}$$

A state space realization of the generalized plant P is given by A.2.

$$P = \begin{bmatrix} A & B_1 & B_2 \\ C_1 & D_{11} & D_{12} \\ C_2 & D_{21} & D_{22} \end{bmatrix} \tag{A.2}$$

The signals in A.1 are :

- u the control variables
- v the measured variables
- w the exogenous inputs
- z the error signals to be minimized

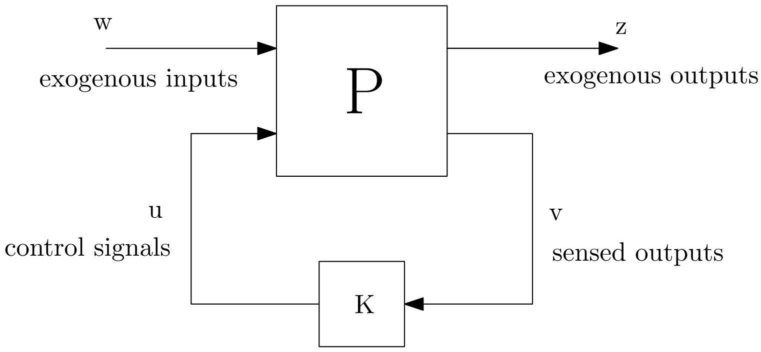

Figure A.1: The general control configuration.

The closed loop transfer function between z and w is given by the linear fractional transformation as in equation A.3

$$F_l(P,K) = P_{11} + P_{12}K(I - P_{22}K)^{-1}P_{21} \tag{A.3}$$

H_∞ control aims to minimize the infinity norm of $F_l(P,K)$. The assumptions described below are typically made for H_∞ design algorithms.

1. (A, B_2, C_2) is stabilizable and detectable.

2. D_{12}, D_{21} have full rank.

3. $\begin{bmatrix} A - j\omega I & B_2 \\ C_1 & D_{12} \end{bmatrix}$ has full column rank for all ω.

4. $\begin{bmatrix} A - j\omega I & B_1 \\ C_2 & D_{21} \end{bmatrix}$ has full column rank for all ω.

5. $D_{11} = 0$ and $D_{22} = 0$.

Based upon these assumptions, the object is to identify a stabilizing controller K minimizing the norm $||F_l(P,K)||_\infty$. The solution required is not always the optimal one. It is sometimes simpler, to define a suboptimal set of controllers. If γ_{min} is the minimum value of $||F_l(P,K)||_\infty$, then the proximity to the optimum solution can be defined by γ, where $||F_l(P,K)||_\infty < \gamma$, with $\gamma > \gamma_{min}$. This objective can be achieved using the algorithm of Doyle (1989). γ is iteratively reduced in order to reach the desired proximity to the optimal solution. The algorithm of Doyle is described below.

If assumptions 1-5 are valid, there exists a set of stabilizing controllers $K(s)$ such that

$$||F_l(P,K)||_\infty < \gamma$$

if and only if:

1. $X_\infty \geq 0$ is a solution to the algebraic Riccati equation

$$A^T X_\infty + X_\infty A + C_1^T C_1 + X_\infty(\gamma^{-2}B_1B_1^T - B_2B_2^T)X_\infty = 0 \tag{A.4}$$

with

$$Re\lambda_i[A + (\gamma^{-2}B_1B_1^T - B_2B_2^T)X_\infty] < 0, \forall i \tag{A.5}$$

2. $Y_\infty \geq 0$ is a solution to the algebraic Riccati equation

$$AY_\infty + Y_\infty A^T + B_1B_1^T + Y_\infty(\gamma^{-2}C_1^TC_1 - C_2^TC_2)Y_\infty = 0 \tag{A.6}$$

with

$$Re\lambda_i[A + Y_\infty(\gamma^{-2}C_1^TC_1 - C_2^TC_T)] < 0, \forall i \tag{A.7}$$

3. $\rho(X_\infty Y_\infty < \gamma^2)$

The set of controllers that satisfy the requirement $\|F_l(P,K)\|_\infty < \gamma$ are given by the linear fractional transformation $K = F_l(K_c, Q)$, where :

$$K_c(s) = \left[\begin{array}{lll} A_\infty & -Z_\infty L_\infty & Z_\infty B_2 \\ F_\infty & 0 & I \\ -C_2 & I & 0 \end{array}\right] \tag{A.8}$$

$$F_\infty = -B_2^T X_\infty \tag{A.9}$$

$$L_\infty = -Y_\infty C_2^T \tag{A.10}$$

$$Z_\infty = (I - \gamma^{-2} Y_\infty X_\infty)^{-1} \tag{A.11}$$

$$A_\infty = A + \gamma^{-2} B_1 B_1^T X_\infty + B_2 F_\infty + Z_\infty L_\infty C_2 \tag{A.12}$$

and Q is a stable proper transfer function that $\|Q\|_\infty < \gamma$. Typically

$$Q = 0$$

Thus

$$\boxed{K(s) = -F_\infty (sI - A_\infty)^{-1} Z_\infty L_\infty} \tag{A.13}$$

Appendix B

Stability Criterion Under the Presence of RHP Zeros

In this chapter, the stability criterion for the sensitivity function's weight is described. It is a requirement to secure that instability is avoided. RHP system zeros are a cause of concern, because the closed loop poles move towards the place of the RHP zeros especially when high control gains are required.
The theorem states that for each RHP-zero z of G(s) the sensitivity function S must satisfy B.1.

$$||wpS||_{\infty} \geq |w_P(z)| \prod_{i=1}^{N_P} \frac{|z + p_i|}{|z - p_i|} \tag{B.1}$$

In B.1 p_i signifies the N_p $RHP - poles$ of G(s). If G(s) has no RHP poles then B.1 simplifies to B.2

$$||w_P S||_{\infty} \geq |w_P(z)| \tag{B.2}$$

If no weighting function is included for the sensitivity function, then

$$||S||_{\infty} = M_s \geq \prod_{i=1}^{N_P} \frac{|z + p_i|}{|z - p_i|} \tag{B.3}$$

Appendix C

Simulation With Leakage

In this part of the appendixes the effect of the leakage manipulating method of the control command is described. The leakage method decreased the control command by a certain fraction of it while the curve on the compressor map approached a specific suge safety limit line.

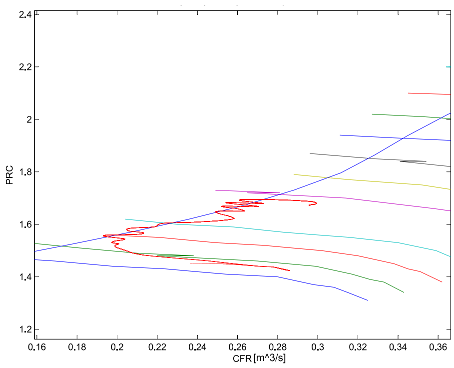

Figure C.1: The trajectory on the compressor map during the control process in simulation, having implemented the leakage method of manipulating the control command.

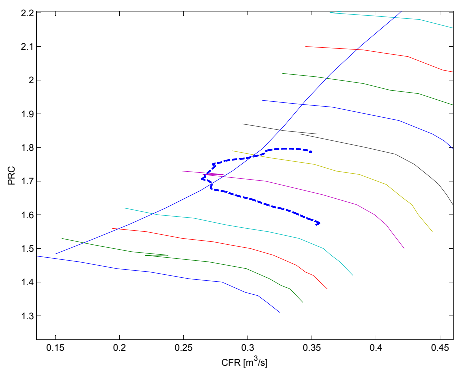

Figure C.2: The trajectory on the compressor map during the control process in simulation, without having implemented the leakage method of manipulating the control command.

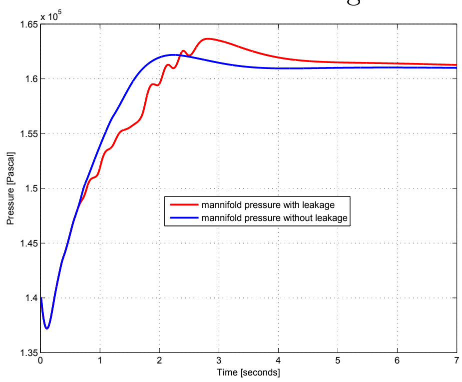

Figure C.3: The intake manifold pressure with and without implementing the leakage method of manipulating the control results.

Bibliography

[1] G. Papalambrou. *Operation control of marine propulsion Diesel engine during transient loading operation.* Doctoral Thesis, School of Naval Architecture and Marine Engineering, National Technical University of Athens, 2008.

[2] G. Zames. *Feedback and optimal sensitivity: Model reference transformations, weighted seminorms and approximated inverses.* Proc. 17th Allerton Conf. 1979.

[3] Ν. Κρικέλης. *Εισαγωγή στον αυτόματο έλεγχο.* 3η Έκδοση, Συμμετρία, 2000.

[4] S. Skogestad, I. Postlethwaite. *Multivariable Feedback Control: Analysis and Design.* 2nd edition Wiley, 2005.

[5] K. Zhou, J. C. Doyle. *Essentials of Robust Control.* Prentice Hall, 1999.

[6] D. W. Gu, P. Hr. Petkov, M. M. Konstantinov. *Robust Control Design with Matlab.* Springer, 2005.

[7] Ν. Κυρτάτος. *Ναυτικοί Κινητηρες Diesel.* Συμμετρία, 1993.

[8] Κ. Ρακόπουλος. *Αρχές Μηχανών Εσωτερικής Καύσης.* Φούντας, 1985.

[9] L. Guzzella, C. H. Onder. *Introduction to Modelling and Control of Internal Combustion Engine Systems.* Springer, 2006.

[10] L. Eriksson, I. Honder. *An Analytic Model for Cylinder Pressure in a Four Stroke S.I. Engine.* 2002-01-0371,Society of Automotive Engineers, 2002.

[11] M. Klein. *Single-Zone Cylinder Pressure Modelling and Estimation for Heat Release Analysis of SI Engines.* Linkoping Studies in Science and Technology, 2007.

[12] M. Jung. *Mean Value Modelling and Robust Control of the Airpath of a Turbocharged Diesel Engine.* Department of Engineering, University of Cambridge, Dissertation submitted for the degree of Doctor of Philosophy, 2004.

[13] J. T. Gravdahl, O. Egeland. *Compressor Surge and Rotating Stall: Modelling and Control.* London: Springer Verlag, 1999.

[14] F. A. Matekunas. *Modes and Measures of cyclic combustion variability.* SAE Technical Paper 830337, 1983.

[15] F. A. Matekunas. *Engine combustion control with ignition timing by pressure ratio management.* US Pat., A, 4622939, 1986.

[16] L. Eriksson. *Requirements for and a systematic method for identifying heat release model parameters.* Modeling of SI and Diesel Engines, SP-1330(SAE Techical Paper no.980626): 19-30, 1998.

[17] W. Z. Black. *Applied Thermodynamics.* Pearson Education Inc, 2008.

[18] J. C. Doyle. *Lecture Notes on Advances in Multivariable Control.* Minneapolis, USA, ONR, Honeywell Workshop, 1984.

[19] G. Balas, R. Chiang, A. Packard, M. Safonov. *Robust Control Toolbox: Getting Started Guide.* The MathWorks, October 2013.

[20] F. A. Williams. *Combustion Theory,Second Edition.* The Benjamin/Cummings Publishing Company.

[21] Googol Technology. *Inverted Pendulum Instruction Manual, Suitable for GLIP.* Series Second Edition, April, 2006.

[22] G. P. Theotokatos. *On Cycle Mean Value Modelling of Large Two-Stroke Marine Diesel Engine.* Proceedings of the Institution of Mechanical Engineers, Part M: Journal of Engineering for the Maritime Environment September 1, 2010 vol. 224 no. 3 193-205

[23] G. P. Theotokatos. *Ship Propulsion Plant Transient Response Investigation using a Mean Value Engine Model.* International Journal of Energy, Issue 4, Vol. 2, 2008.

[24] J. B. Heywood. *Internal Combustion Engines Fundamentals.* Mc-Graw Hill, 1998.

[25] R. B. Krieger, G. L. Borman. *The computation of apparent heat release for internal combustion engines.* ASME, 1967.

[26] E. N. Balles, K. M. Chun, F. E. Nelson, J. A. Echian, J. B. Heywood, J. A. Gatowski. *Heat release analysis of engine pressure data.* SAE paper No,841359, 1984

[27] M. Mladek. *Cylinder Pressure for Control Purposes of Spark ignition Engines.* PhD thesis, ETH, 2003.

[28] R. Ebrahimi. *Performance optimization of a Diesel cycle with specific heat ratio.* PhD thesis, Shahrekord University, 2009.

[29] Y. Yeliana, C. Cooney, J. Worm, D. J. Michalek, J. D. Naber. *Estimation of double-Wiebe function parameterts using least square method for burn durations of ethanol- gasoline blends in spark ignition engine over variable compression ratios and EGR levels.* Applied Thermal Engineering 31 2213-2220, Elsevier, 2011.

[30] G. Stiesch. *Modelling Engine Spray and Combsution Process.* Springer-Verlag, 2003.

[31] *http://www.lme.ntua.gr:8080/academic-info-1/prospheromena-mathemata/eisagoge-ston-automato-elegkho/files/lab_invpend_cs_2011.pdf*

[32] *http://www.mathworks.com/help/physmod/hydro/ref/needlevalve.html*

[33] http://www.spiraxsarco.com/resources/steam-engineering-tutorials/control-hardware-el-pn-actuation/control-valve-actuators-and-positioners.asp